AD NUMBER

AD913768

LIMITATION CHANGES

TO:

Approved for public release; distribution is unlimited.

FROM:

Distribution authorized to U.S. Gov't. agencies only; Test and Evaluation; 31 MAY 1973. Other requests shall be referred to Office of Naval Research, Arlington, VA 22203.

AUTHORITY

ONR ltr 8 Oct 1975

LINE ARRAY IMAGING TECHNIQUES

FINAL TECHNICAL REPORT

CONTRACT NO. N00014-72-C-0504

MAY 31, 1973

Electronics Research Division
Rockwell International
3370 E. Miraloma Avenue
Anaheim, California 92803

C72-1013/501

LINE ARRAY IMAGING TECHNIQUES

Final Report

31 May 1972

Prepared by

T. T. Kumagai

ARPA Order No. 1806, dated 9 Feb 1972, Amendment 2
Program Code No. 421
Contractor: Rockwell International Corporation
Electronics Research Division
Date of Contract: 1 June 1972
Amount of Contract: $54,098
Contract No. N00014-72-C-0504
Expiration Date: 31 May 1973
Principal Investigator: T. T. Kumagai (714) 632-3594
Program Manager: R. A. Brandewie (714) 632-3682

Scientific Officer: Dr. Fred Quelle, ONR, Boston
Contract Monitor: Dr. Fenner Milton, NRL, Washington, D.C.

This research was supported by the Advanced Research Projects Agency of the Department of Defense and was monitored by ONR under Contract No. N00014-72-C-0504.

DISCLAIMER:

The views and conclusions contained in this document are those of the authors and should not be interpreted as necessarily representing the official policies, either expressed or implied, of the Advanced Research Projects Agency or the U.S. Government.

UNCLASSIFIED

Security Classification

DOCUMENT CONTROL DATA - R & D

(Security classification of title, body of abstract and indexing annotation must be entered when the overall report is classified)

1. ORIGINATING ACTIVITY (Corporate author) ROCKWELL INTERNATIONAL 3370 Miraloma Avenue Anaheim, California 92803	2a. REPORT SECURITY CLASSIFICATION UNCLASSIFIED 2b. GROUP

3. REPORT TITLE

LINE ARRAY IMAGING TECHNIQUES

4. DESCRIPTIVE NOTES (Type of report and inclusive dates)

Final Technical Report

5. AUTHOR(S) (First name, middle initial, last name)

Tom T. Kumagai

6. REPORT DATE May 31, 1973	7a. TOTAL NO. OF PAGES 126 + Appendices	7b. NO. OF REFS
8a. CONTRACT OR GRANT NO. N00014-72-C-0504 b. PROJECT NO. ARPA Order No. 1806, dated 9 Feb. 1972 c. d.	9a. ORIGINATOR'S REPORT NUMBER(S) C72-1013/501 9b. OTHER REPORT NO(S) (Any other numbers that may be assigned this report)	

10. DISTRIBUTION STATEMENT

This document has been approved for public release and sale; its distribution is unlimited.

11. SUPPLEMENTARY NOTES Prepared for Office of Naval Research	12. SPONSORING MILITARY ACTIVITY Sponsored by Advanced Research Projects Agency

13. ABSTRACT

This optical design study determined the utility of mechanically-scanned transmitter techniques for a laser radar designed for fine-grained target imaging and tracking. Beam combiner techniques were studied to permit the laser radar to share large diameter optics with a high-energy laser. Beam combiners are not currently available; thus, the recommended optical design is based upon a dual aperture system. A survey of scanning techniques was performed to determine the most optimum scanner for a high efficiency system with 100 x 100 diffraction-limited resolution elements operating at 100 frames per second. Upon completion of the survey, concentrated effort was placed on the application of a multifaceted rotating scanner and a torsional oscillating scanner. The study included investigations in the following areas: Scanner distortion, offset angle correction, optical cross-talk, signal-to-noise, Doppler bandwidth, range accuracy requirements, optical design considerations, and numerous other related areas.

DD FORM 1 NOV 68 1473

UNCLASSIFIED

Security Classification

14 KEY WORDS	LINK A		LINK B		LINK C	
	ROLE	WT	ROLE	WT	ROLE	WT
LASERS						
OPTICS						
SCANNERS						
DETECTORS						
DETECTOR ARRAYS						
DETECTOR CROSS-TALK						
LINE ARRAY IMAGING TECHNIQUES						

ACKNOWLEDGMENT

The author wishes to acknowledge the contributions made by Dr. Fenner Milton, ONR, Washington, D.C., in providing the direction and interest in the contract.

In addition, the following Rockwell International personnel contributed to the contract:

Dr. Richard Shubert
Torsional Scanner Analysis

W. C. Davis
Optical Design

Dr. T. R. Waite
Consultant

ABSTRACT

This optical design study determined the utility of mechanically-scanned transmitter techniques for a laser radar designed for fine-grained target imaging and tracking. Beam combiner techniques were studied to permit the laser radar to share large diameter optics with a high-energy laser. Beam combiners are not currently available; thus, the recommended optical design is based upon a dual aperture system. A survey of scanning techniques was performed to determine the most optimum scanner for a high efficiency system with 100 x 100 diffraction-limited resolution elements operating at 100 frames per second. Upon completion of the survey, concentrated effort was placed on the application of a multifaceted rotating scanner and a torsional oscillating scanner. The study included investigations in the following areas: Scanner distortion, offset angle correction, optical cross-talk, signal-to-noise, Doppler bandwidth, range accuracy requirements, optical design considerations, and numerous other related areas.

TABLE OF CONTENTS

TABLE OF CONTENTS

ILLUSTRATIONS

ILLUSTRATIONS

I. INTRODUCTION AND SUMMARY

A. INTRODUCTION

The purpose of this optical design study is to determine the utility of mechanically scanned transmitter techniques to a laser radar designed for fine-grained target imaging and tracking. The base line requirement is for a high efficiency system with 100 x 100 diffraction limited resolution elements operating at 100 frames per second at 10.6 microns using either a single detector element or a linear array.

In order to maintain as large an aperture as possible, the study initially considered shared aperture with the high energy laser. Sharing one aperture would allow the use of 1 meter diameters permitting higher energy densities on the target and yielding higher signal-to-noise ratios for the laser radar signal returns. However, sharing aperture requires that the high energy beam and the laser radar beam be combined into a single outgoing beam in the transmit mode and that the received radar signal be adequately separated from the same optical channel.

During the study, two methods of beam combiner techniques were examined and discarded for near term use as being considered not "within the state-of-the-art." One method was the Brewster angle beam combiner in which the high energy laser beam is transmitted through a "window" at Brewster angle, and the laser radar beam is reflected off the outgoing side of the window to combine with the high energy beam.

This technique was eliminated based upon the lack of proper "window" material operating at high energy densities and considered not within the state-of-the-art.

The other technique examined is the diffraction grating beam combiner which could be designed to be as high as 95% efficient. However, even with this high efficiency, approximately 5% of the high energy would be scattered in various undetermined directions. Assuming that the scatter is uniform, the amount of energy which could be scattered into the laser radar receiver direction would be sufficient to damage the detector. Thus, the efficiency of the beam combiner would have to approach 100% before it could be considered viable for application in a shared aperture system.

As a result of the problems concerning the beam combiner, the study was directed to a dual aperture system in which the high energy is separately directed towards the target from the laser radar. In order to minimize the bore sighting problems using two apertures, both apertures share a common output primary lens by utilizing the separate halves of the output lens. Similarly, both beams are focused by the same secondary lens which permits automatic focusing of both beams at the target distance.

For the dual aperture study, 40 cm apertures were considered with a 10 cm separation between apertures. This size permits the use of a 1 m output aperture whose field is segmented into two 40 cm beams. In addition, this size permits the use of a 1 meter coelostat which can serve as the tracking mirror.

During the initial part of the study, a number of different types of scanners were surveyed for possible application in the system. The scanners surveyed were eventually reduced to two scanner types which were

investigated in detail. The two selected scanners were the multifaceted rotating scanner and the torsional sinusoidal scanner. The multifaceted rotating scanner is limited to applications where small beams are utilized. For this system application the use of a multifaceted rotating scanner limited the beam size to the order of a centimeter. Thus with a multifaceted scanner, a 40 power telescope is necessary to obtain a 40 cm output beam.

The torsional sinusoidal scanner can be used with larger beam sizes. Its limitation is primarily in the scan frequency. The study has indicated that a 10 cm beam can be scanned at rates of the order of 1 kHz without exceeding the distortion limits. However, since 10^4 lines per second are required to be scanned, the torsional scanner should be applied in a 10 resolution element fan beam system which would require only a 1 kHz scan rate.

A detailed discussion of the trade-off characteristics of the multifaceted scanner and the torsional scanner is given in Section IV.

In order to provide fine-grained target imaging of aircrafts at reasonable ranges, the laser radar transmitter power should be in the range of 1 to 5 KW. Single mode TEM_{oo} 10 micron lasers are available at output power levels of 1 KW. Within the near term, 5 KW lasers may be available. A power level of 1 KW is sufficient to permit fine-grained target imaging at ranges up to 6 to 8 KM depending upon the atmospheric losses. The lower range is under adverse weather conditions corresponding to approximately 2.5 dB/KM (light fog).

B. SUMMARY OF RESULTS

As a result of the study, two different systems designs were examined in critical detail. These were a two-beam multifaceted scanner (20 facets) and a ten resolution element fan sinusoidal scanner. A detailed discussion of the selected systems optical design is given in Section V. In this section, only a summary of the relative merits of each system is given.

Optical design layouts of each type of system are given in Figures I-1 and I-2. The salient features of both systems are given in Table 1. It is to be noted that the overall efficiency of both systems are comparable.

The design of the multifaceted system is limited to a maximum of two beams because of optical design reasons. With multiple beams utilizing a multifaceted scanner, in order to prevent an increase of beam area on the facet (giving rise to increased dead time), the multiple beams are required to overlay on the scanner face. As a result, the beams are diverging at the input to the first beam expander. Because of this divergence, the design of the beam expander telescope limits the number of beams for near diffraction limited operation. With a two-beam system, the beam expander system is required to operate one field width in one direction and one-half field width in the other direction.

With a multielement fan beam, the beam expander must be designed to operate nearly a full field width in both directions. Near the edges of the field, the fan beam through a beam expander optical train becomes distorted.

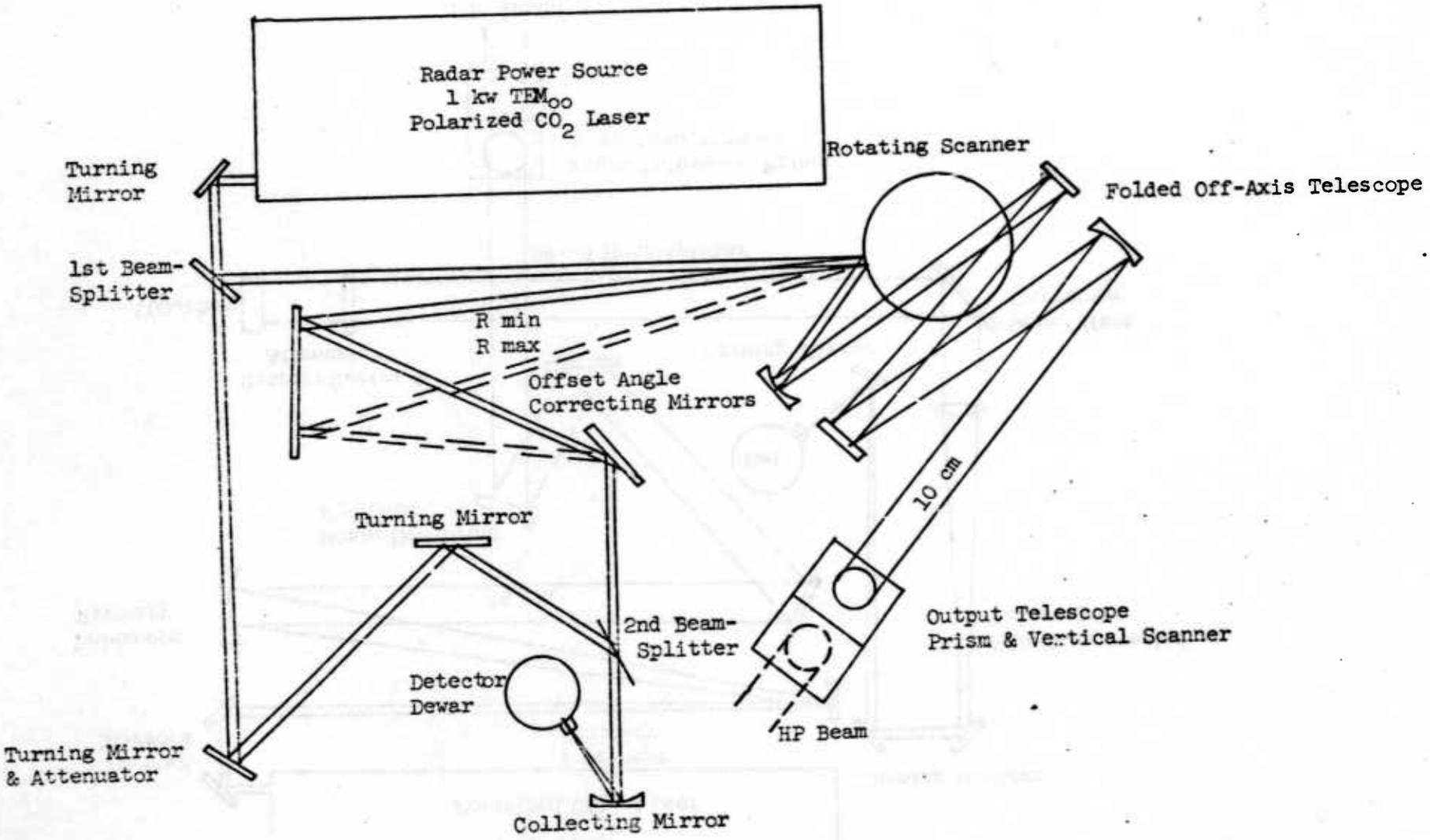

Figure I-1: Geometrical Layout of the Two Beam System

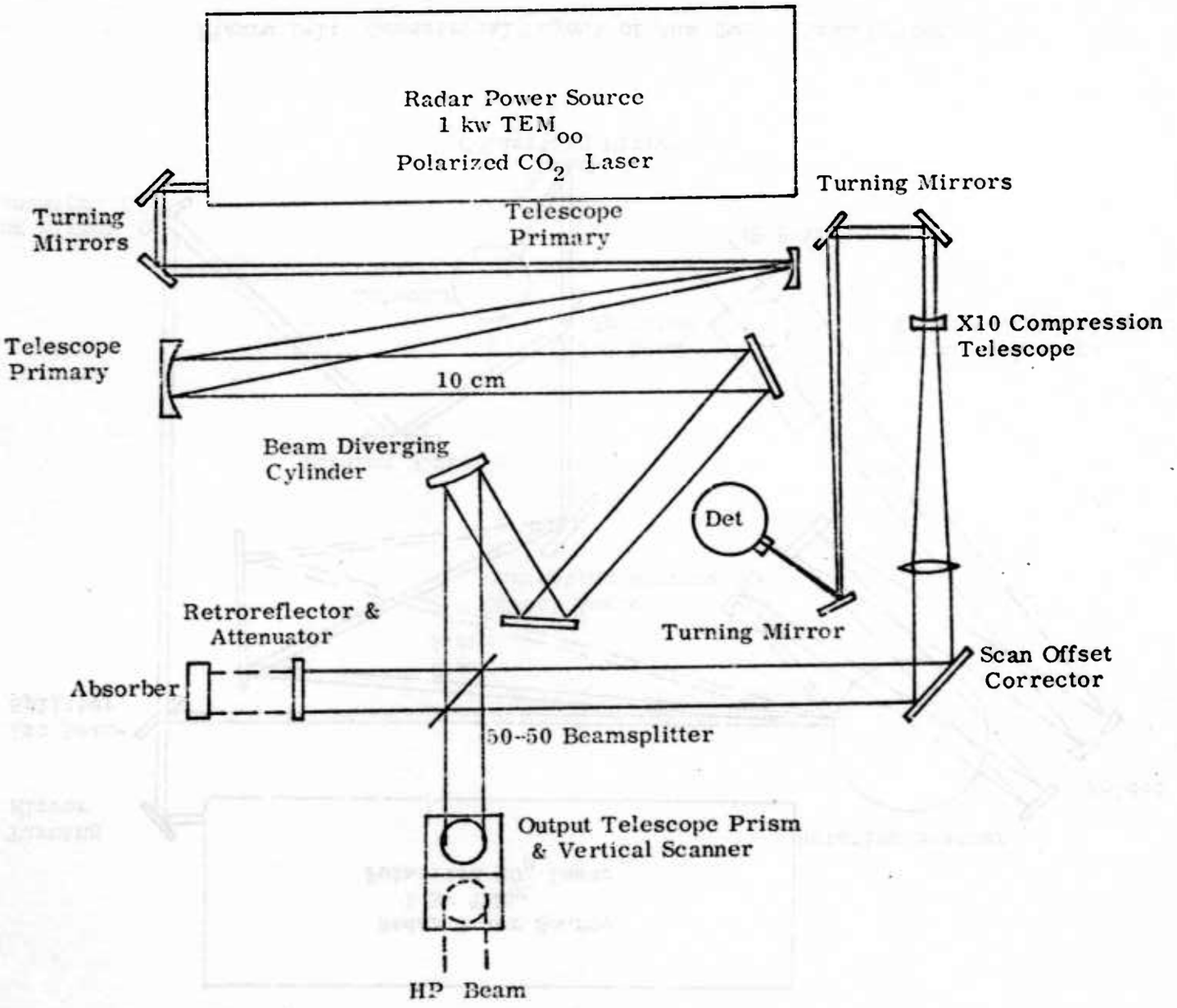

Figure I-2 Geometrical Layout of the Fan Beam System

TABLE 1 SYSTEM STUDY RESULTS

		Two Beam Rotating Scanner	10 Element Fan Sinusoidal Scanner
1.	Maximum Range	18 km	Unlimited
2.	Scanner Size	15 cm (radius)	10 cm x 14 cm face
3.	Beam Size at the Scanner	1 cm	10 cm
4.	Output Aperture	40 cm	40 cm
5.	Scanner Efficiency	$1/2\pi$	$1/\pi$
6.	Optical Efficiency (Excluding Scanner)	0.435	0.1
7.	Average Relative Signal for 50 Meter Range Accuracy	0.7 (peak)	~1 (peak)
8.	Overall Efficiency (Products of Items 5, 6, and 7)	0.048	0.032

Also, in the case of more than two beams on a multifaceted scanner, the beam divergence from the scanner is increased requiring that the beam expander operate over a greater field.

In the case of the ten-element fan sinusoidal scanner, the beam on the scanner is 10 cm. This results in a decrease in field size by a factor of 10 as compared to the required field size at the 1 cm multifaceted scanner. Thus, the optical design problems for a ten-element fan sinusoidal scanning system are reduced in comparison to a 1 cm multifaceted scanning system.

In addition to the trade-off characteristics given in Table 1, other considerations which were examined leading to the choice of the 10-element fan beam system include offset angle considerations, number of filter bins required for processing the received signal, range tracking requirements, and optical cross-talk rejection between adjacent detectors. Detailed analyses of each of these considerations are discussed in Section II. A summary is presented here.

1. Offset Angle Considerations

In a two-beam 20-faceted scanning system, the two-way time of flight for targets at ranges between 1 km to 20 km varies from 6.7 μ sec to 133 μ sec. Because of this time of flight, the high-speed scanner is displaced in angular position during the receive mode relative to the transmit mode. Compensation is required for this offset angle which varies from 0.02 radian to 0.4 radian. Compensation of such large variation in offset

correction can be achieved, but only with a high degree of complexity. The optical layout shown in Figure I-1 requires 60 cm offset angle correcting mirrors. This is to be contrasted with a sinusoidal scan offset corrector in the 10-element fan beam system.

In the 10-resolution element fan beam system, the variation in offset angle correction is from 2×10^{-4} radian to 4×10^{-3} radian corresponding to targets in the range 1 km to 20 km. The sinusoidal offset angle corrector does require amplitude and phase correction;whereas, the multifacted scanner requires only amplitude correction. However, since phase and amplitude can easily be controlled, the balance is in favor of the sinusoidal scanner.

2. Number of Processing Filters Required

It is shown in Section II-E that the number of processing filters required to process a Mach 2 target is

$$N_D = 79.6\, N_B^2$$

where

N_D = required number of resolvable Doppler discrimination bins, and

N_B = number of beams or its equivalent to cover the field.

Thus, the 10 resolution element fan beam requires a factor of 25($=10^2/2^2$) increase in the number of processing filters in comparison to the 2-beam system. In terms of the receiver processor complexity, the 2-beam system is favored.

3. Range Tracking Requirements

The range tracking requirements are determined by the amount of signal loss tolerance in the system. The optimum size detector to achieve maximum signal in bore-sighted operation is an Airy disc size detector; i.e., a detector whose radius corresponds to the radius of the first dark ring of the Fraunhofer pattern. The relative signal responses for various size detectors are given in Figure II-9 (Section IIF). In Section IIF, it is shown that if an average of 30% loss in signal is allowed in a 2-beam 20-faceted system, the corresponding range accuracy requirement is 50 meters. Increasing the detector size from an optimum Airy disc size allows an increase in the range gate requirements at the expense of a decrease in overall signal response throughout the range gate. This is illustrated in Figure II-9.

The 10-element fan beam scanner for the same system tolerances yields an allowable range gate of 467 meters, or a factor of 10 improvement over the 2-beam multifaceted system. Thus, the 10-element fan beam system is superior with respect to range tracking requirements.

4. Optical Cross-Talk Rejection

Optical cross-talk presents no problems in the 2-beam multifaceted system since the two beams are separated by a half field width or 50 resolution elements. (The scan field is 100 x 100 resolution elements.)

In Section IIG, a careful analysis of the optical cross-talk is presented with results relating to the 10-element fan beam system. In the fan beam system, the case of interest is where the fan beam is spread over a "glint" area of the target. Then the question arises as to the discrimination of a diffuse target reflected signal return from optical cross-talk from an adjacent glint resolution element return. In the case of a 10-element array of Airy disc size detectors whose center-to-center distance is also one detector size, the optical cross-talk coefficient is 5×10^{-4} between adjacent detectors. Therefore, for a 1% diffuse target reflector, the optical cross-talk from an adjacent glint point will not exceed the diffuse target signal until the effective "gain" from the glint point exceeds 2×10^{5}.

Using a bubble glint model, as described in Section IIB, the gain is given as

$$G = \frac{1}{2\left(1 - \cos \frac{\phi}{2}\right)} ,$$

where ϕ is the central angle of the bubble subtended by the beam. Letting $G = 2 \times 10^{5}$, the corresponding value of φ is $\varphi = 4.48 \times 10^{-3}$ radian. The corresponding radius of curvature of the bubble exceeds 100 meters. Thus, to achieve a gain of 2×10^{5}, the target surface is required to be virtually flat over the entire beam size on the target. This is highly unlikely; therefore, it is concluded that in the 10-element fan beam system, adequate discrimination can be performed between glint target returns and "non-reflective" ($\sim$1%) diffuse targets.

II. PARAMETRIC SYSTEMS ANALYSIS

A. INTRODUCTION

In considering an imaging radar system which is to cover a solid angle of 100 x 100 resolution elements, each equal to the diffraction limited beam size, there are a number of possibilities. The possibilities can be assembled into four groups: (1) place a 100 x 100 array of detectors in the image plane of the receiver telescope and illuminate the entire solid angle to be imaged; (2) place a 100-element linear array of detectors in the image plane, fan the beam into a 100 resolution element fan and use a scanning system normal to the fan direction; (3) place a reduced number of detector elements (for example, a 10-element detector array) in the image plane and raster scan a reduced fan beam (a 10-resolution element fan) over the 100 x 100 resolution element scan field; and (4) raster scan with a single or double (discrete) beam over the 100 x 100 resolution element scan field.

The first method listed of placing a 100 x 100 array of detectors in the image plane was eliminated from further consideration based upon not being within the detector state-of-the-art. The second method of using a 100-element linear array of detectors in the image plane is considered in the analysis but has been eliminated based upon the requirement of narrow processing filter bins and the exceedingly large number of filters required to perform the processing. Thus, the concentrated effort of the study has been devoted to the last two methods.

B. SIGNAL-TO-NOISE RATIO

The signal-to-noise ratio (S/N) for a coherent detection system can be expressed as

$$S/N = \frac{P_T \epsilon_o \epsilon_r e^{-2\alpha R} \eta A_R}{\pi R^2 h\nu B} \qquad (1)$$

for a target whose area is greater than the diffraction limited beam size on the target, where

P_T = Laser transmitter power

ϵ_o = Optics efficiency, transmit and receiver

ϵ_r = Target reflectivity

α = Atmospheric attenuation coefficient (km^{-1})

R = Target range

η = Detector Efficiency

A_R = Receiver Aperture area

$h\nu$ = Quantum energy

B = Bandwidth

For the case where the target size is less than the diffraction limited beam size, the S/N in equation 1 is multiplied by the ratio of the target area to the beam size, giving rise to a $1/R^4$ relationship in the signal-to-noise. For the study under consideration, the $1/R^4$ signal-to-noise is particularly important in glint tracking of aircrafts at longer ranges --- ranges at which there is insufficient signal-to-noise to perform high resolution image tracking.

In glint tracking, a particular glint return is chosen which is approximately independent of the target's orientation.

Thus, to adequately formulate a model for glint tracking, an appropriate gain factor is required in the S/N equation.

Glint Model:

The glint model chosen is a spherical bubble whose normal incident reflectivity is 0.7 which is attached to a nonreflective background as illustrated in Figure II-1. Consider a plane wave directed towards the segmented bubble whose radius is r. The reflected wave is specularly reflected over an angle 2ϕ where ϕ is the subtended angle of the bubble.

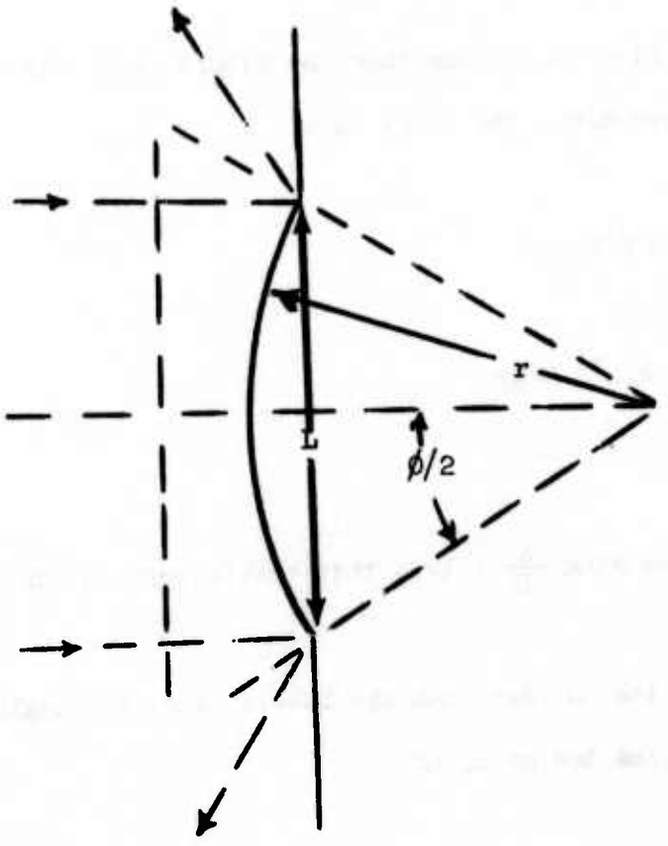

Figure II-1: Plane Wave Reflection on a Spherical Bubble Glint Model

To determine the gain, consider two different cases:

CASE I:

Focused beamsize $\frac{\lambda}{D}$ R greater than bubble vertical extent.

Where the beam size is greater than the bubble size, the bubble extent ($2r \sin \phi/2$) determines the gain. Let

$$2r \sin \phi/2 = L$$

or

$$\phi = 2 \sin^{-1} L/2r$$

CASE II:

Focused beam size $\frac{\lambda}{D}$ R less than bubble vertical extent.

Where the beam size is less than the bubble size, the angle subtended by the beam determines the gain, or

$$\phi = 2 \sin^{-1}\left(\frac{\lambda R}{2Dr}\right)$$

In addition when the vertical extent of the bubble is very large compared to the beam size, it is known that the reflected energy possesses a lob structure of a few degrees in extent. Thus, the effective gain angle of the bubble model is replaced by

$$\varphi' = \varphi + \Delta\varphi$$

where $\Delta\varphi$ represents the limiting lobe size when $2r >> \frac{\lambda}{D} R$.

Then the gain can be given as

$$G = \frac{\pi}{2\pi(1 - \cos \varphi/2)}$$

$$= \frac{1}{2(1 - \cos \varphi/2)}$$

For a glint bubble model, r = 1 meter radius and L = 30 cm which is scanned by a laser radar whose diffraction limited aperture is 40 cm operating at 10.6 micron, the gain is shown in Figure II-2. (A 5^{o} lobe size is used in the gain model.)

Thus, for glint model tracking

$$S/N = \frac{P_T \epsilon_o \epsilon_r e^{-2\alpha R} \eta A_R}{\pi R^2 h\nu B} G$$

for

$$\frac{\lambda}{D} R < L,$$

and

$$S/N = \frac{P_T \epsilon_o \epsilon_r e^{-2\alpha R} \eta A_R}{\pi R^2 h\nu B} G \frac{L^2}{(\frac{\lambda R}{D})^2}$$

for

$$\frac{\lambda}{D} R \geq L.$$

The signal-to-noise is shown in Figure II-3 for a 30 cm glint bubble target whose radius is 1 meter. Similarly, the signal-to-noise is shown for a 0.5% reflective target in Figure II-4. In both figures, the total transmitter power is 1 kw with a sinusoidal scanner bandwidth of 1.57 MHz. The optics efficiency is 6.25% based upon 75% beam splitter losses and other optical losses.

From the signal-to-noise results, it can be concluded that high resolution target imaging of aircrafts can only be performed at ranges less than 8 km under adverse weather conditions (attenuations in the range 1-2.5DB/km).

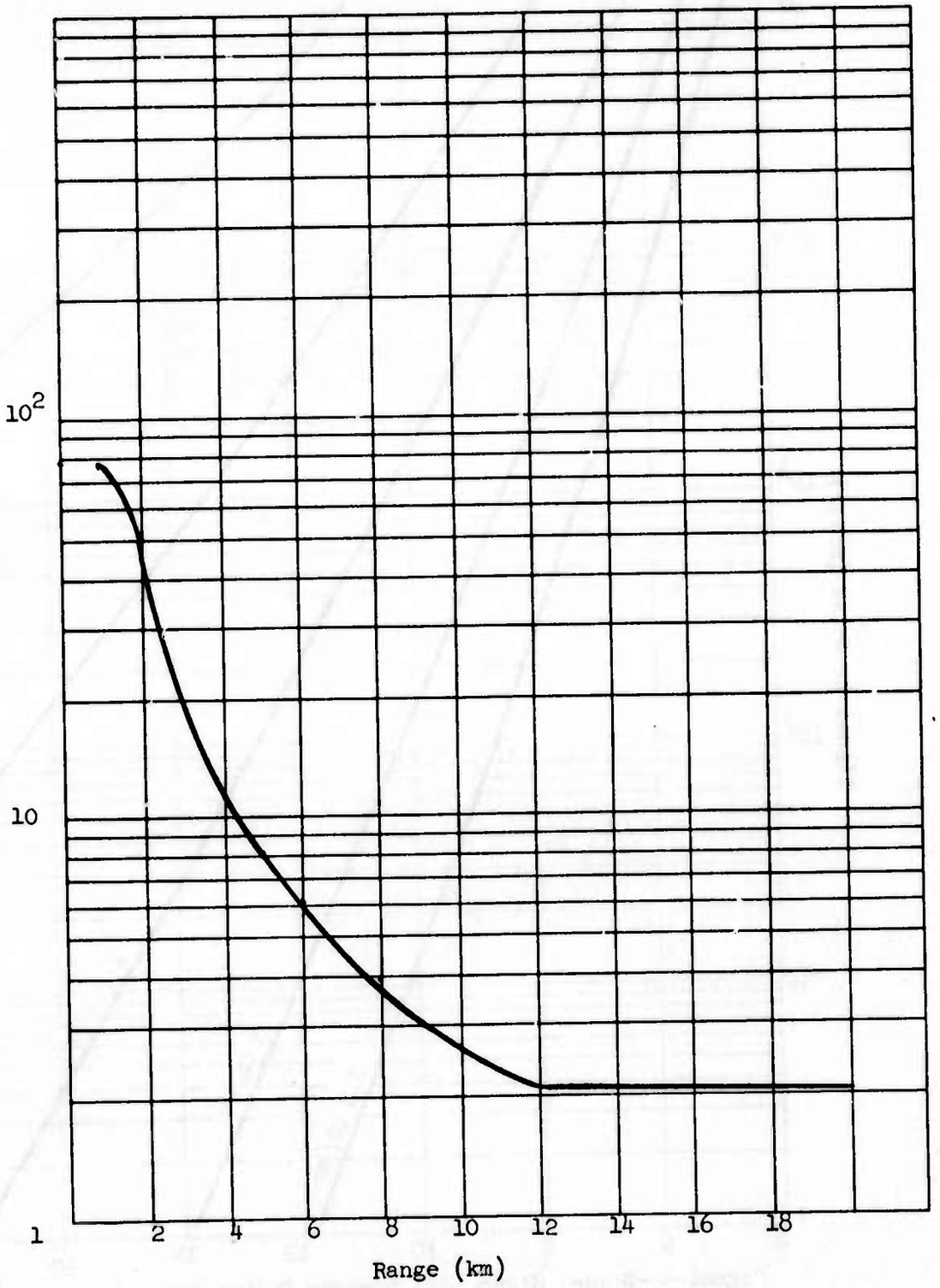

Figure II-2: Gain versus Range
(1 m Radius Bubble, 30 cm vertical extent)

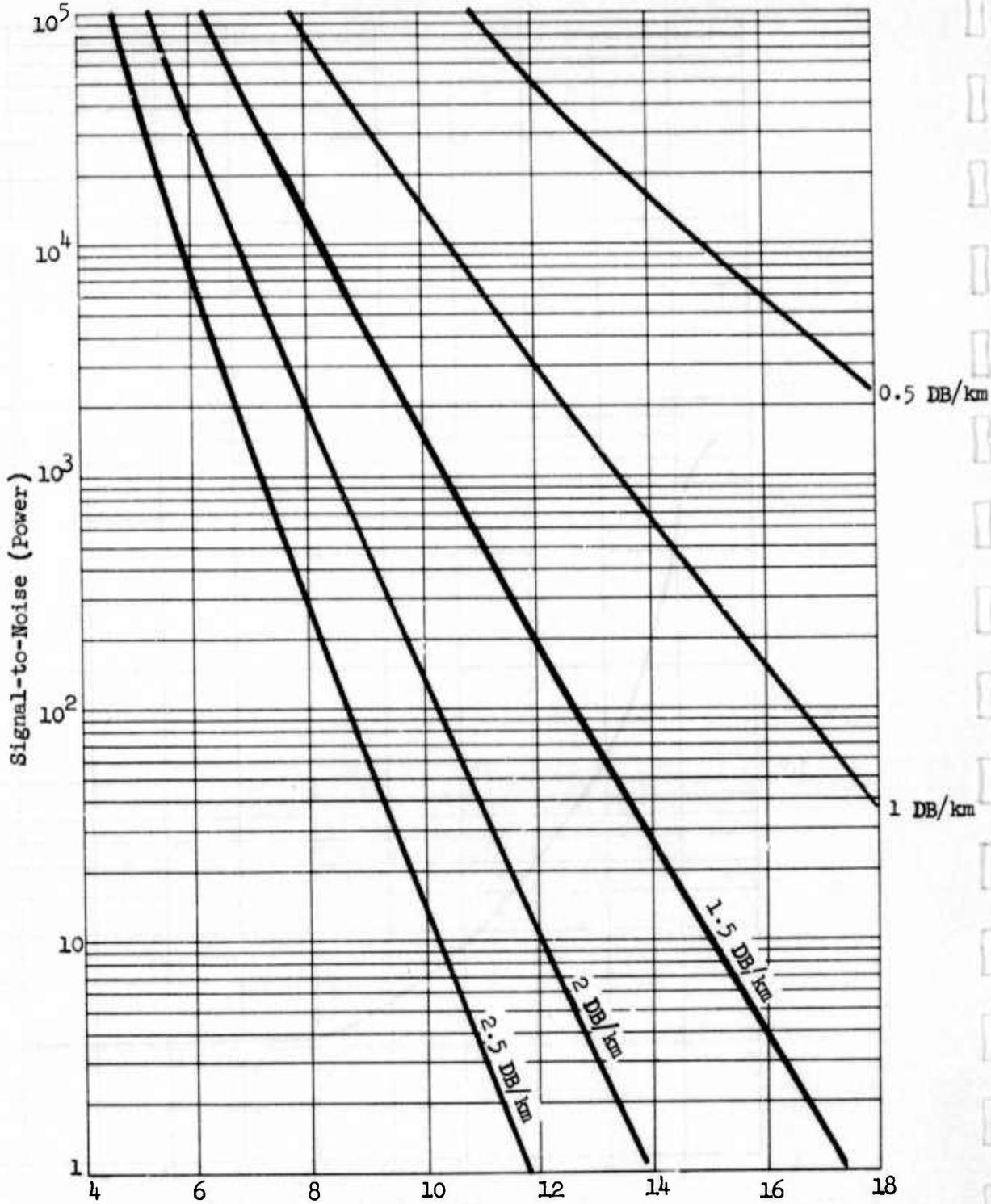

Signal-to-Noise, Sinusoidal Scanner Optics Efficiency = 0.06, 1000 watts in N Beams, Bandwidth = 1.57/N MHz Glint Model, 1 M Radius Bubble, 30 cm Target, Reflectivity = 0.7

Figure II-3.

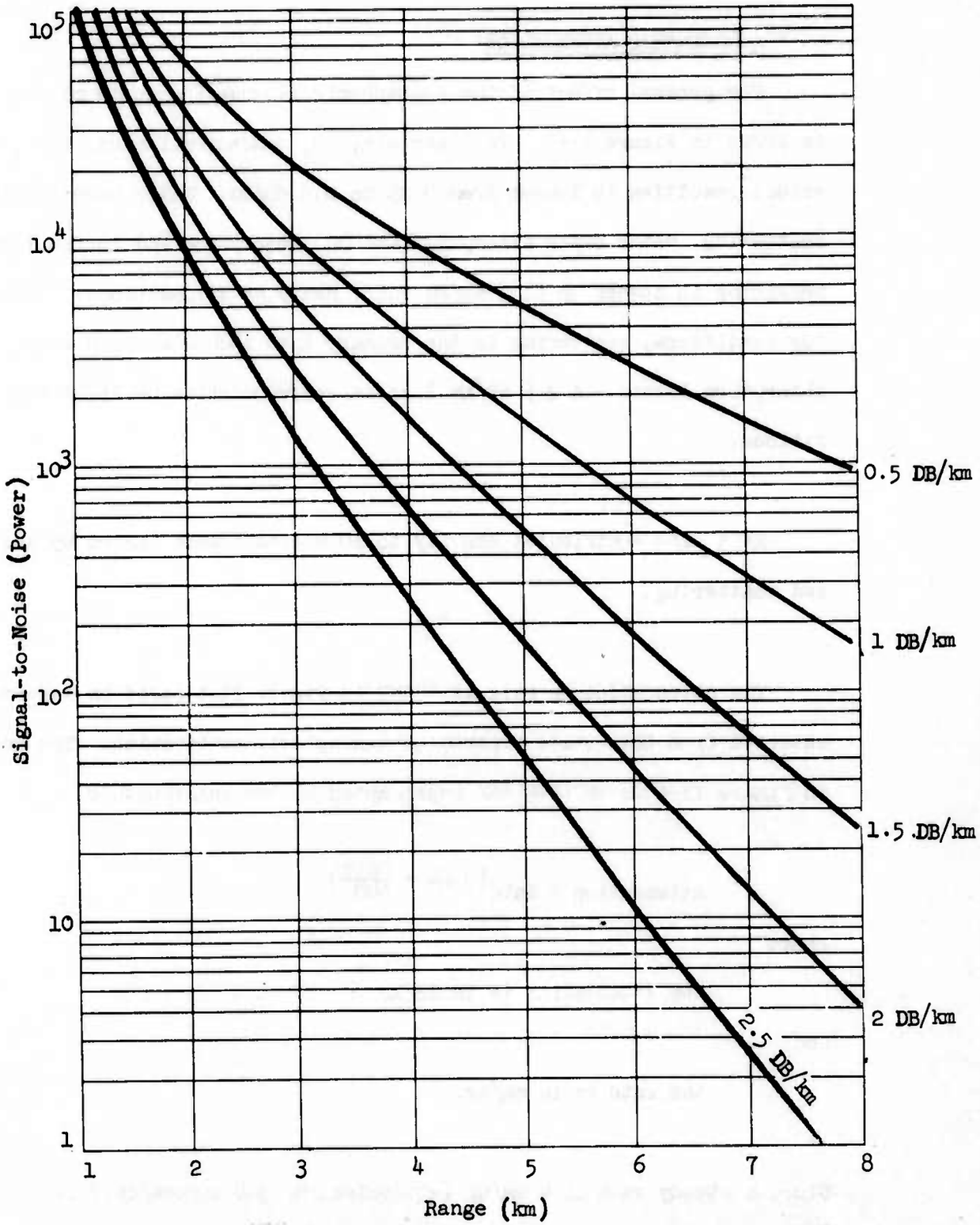

Signal-to-Noise 0.5% Reflective Diffuse Target Sinusoidal Scanner with Beamsplitter, Optics Efficiency = 0.0625, 1000 watts in N Beam fan Bandwidth = $1.57 \times 10^6/N$ Hz

Figure II-4

C. ATMOSPHERIC ATTENUATION

The general effect of the atmospheric attenuation on 10 micron beams is shown in Figure II-5. In clear air, CO_2 concentration has the greatest effect resulting in losses from 0.25 to 0.5 dB/km. Under haze conditions, scattering, water vapor absorption and CO_2 absorption add to the losses resulting in losses up to 2 dB/km under heavy haze conditions. Then, under fog conditions, scattering is the primary loss mechanism with water absorption losses. A 2.5 dB/km loss is representative of light fog conditions.

Rain also contributes heavily to 10 micron losses caused by absorption and scattering.

The attenuation in rain is shown in Figure II-6 based on information obtained from Ohio State reports on atmospheric attenuation. The curve in Figure II-6 is empirically represented by the relationship

$$\text{Attenuation} = \text{Rate}^{\left(0.64 + \frac{\text{Rate}}{600}\right)}$$

where

the attenuation is in dB/km

and

the rate is in mm/hr.

Since a steady rain of 4 mm/hr (equivalent to 3.8 inches/day) is a fairly high rain rate, 2.5 dB/km is approximately the maximum attenuation that would be expected under any type of adverse weather condition.

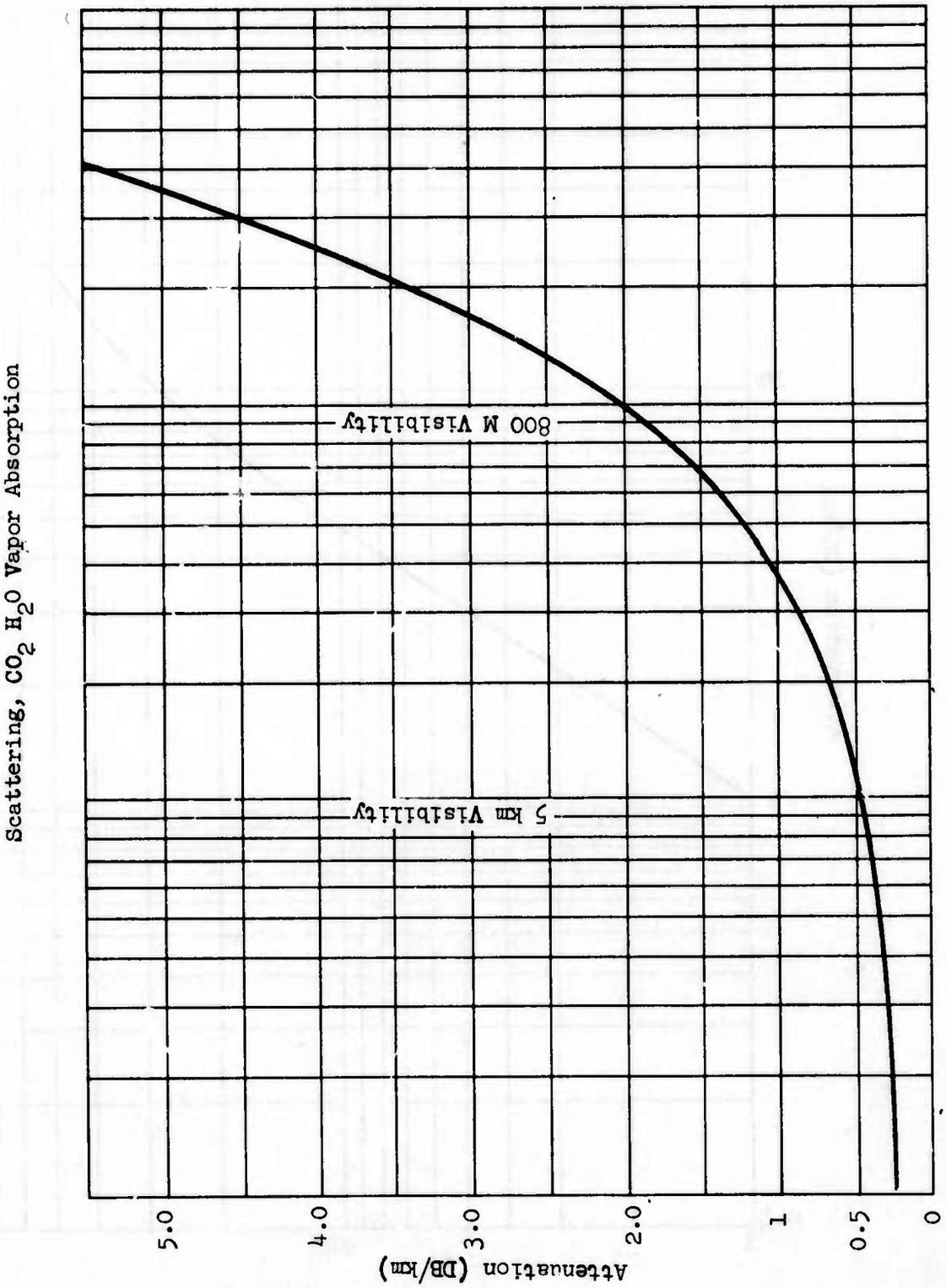

Figure II-5: Atmospheric Attenuation

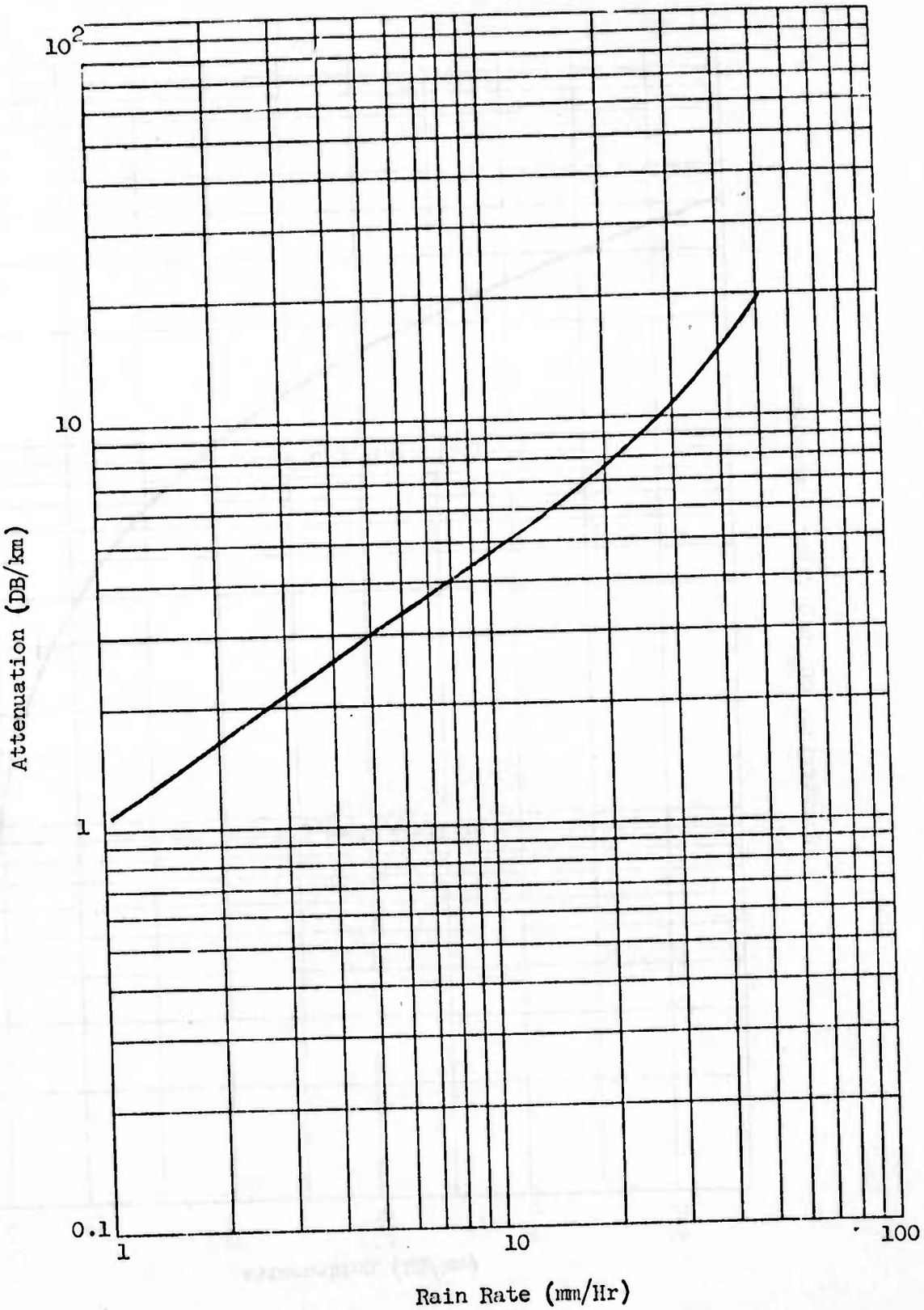

Figure II-6. Attenuation versus Rain Rate

D. BANDWIDTH AND SCANNER EFFICIENCY

Determining the bandwidth requires an examination of the time per resolution element. For a sinusoidal scanner, the bandwidth relationship to the time per resolution element was examined experimentally with a 10.6 micron laser radar (a linear raster scanner improves the bandwidth requirements by a factor π). In Technical Report AFAL-TR-69-360, "Coherent Imaging and Moving Target Detection at 10.6 Microns (U)," June 1970, the experimentally measured bandwidth is shown to follow the relationship

$$\Delta\nu_B = \frac{\sqrt{2}}{2} (D/\lambda)\, \omega(2\theta_{BD}), \tag{1}$$

where

$$\theta_B = \theta_{BD} \sin \omega t$$

and

$2\theta_{BD}$ is the full beam scan angle.

$\Delta\nu_B$ was measured to the full bandwidth measuring across the base on a <u>voltage</u> scale. Thus, the bandwidth at half voltage maximum is approximately

$$\Delta\nu_{\frac{1}{2}} = \tfrac{1}{2}\Delta\nu_B = \tfrac{1}{4}\sqrt{2}\,(D/\lambda)\, \omega(2\theta_{BD}). \tag{2}$$

Furthermore, assuming the distribution to be Gaussian, the voltage v is

$$v = v_o \exp\left[-(r/r_o)^2\right]$$

where

r is the radius from the center of the beam.

The power spectrum then would be of the form

$$p = p_o \exp\left[-2(r/r_o)^2\right].$$

The voltage at half maximum is

$$v_{\frac{1}{2}m} = v_o/2 = v_o e^{-(r/r_o)^2}$$

which results in a corresponding radius r

$$r = 4_o(\ell n2)^{\frac{1}{2}}.$$

Similarly, the power at half maximum occurs at the radius

$$r = \frac{r_o}{\sqrt{2}}(\ell n2)^{\frac{1}{2}}$$

from the relationship

$$p_{\frac{1}{2}} = p_o/2 = p_o e^{-(\sqrt{2}\, r/r_o)^2}.$$

In the experimental verification of equation (1), the variation in frequency from the center frequency was directly proportional to the distance from the beam center. Therefore, the bandwidth at half-power maximum may be obtained by dividing equation (2) by 2. The result is

$$\Delta\nu_{HP} = \tfrac{1}{4}(D/\lambda)\,\omega(2\theta_{BD}). \qquad (3)$$

The sinusoidal scanner gives rise to an angular displacement of the beam as

$$\theta_B = \theta_{BD} \sin \omega t.$$

Then

$$\Delta\theta_B = \theta_{BD}\, \omega \Delta t \cos \omega t.$$

For $\Delta\theta_B = \lambda/D$ and $\Delta t = \tau_m$ where τ_m is the minimum ($\cos \omega t = 1$) dwell time on a target resolution spot,

$$\lambda/D = \theta_{BD}\, \omega\, \tau_m$$
$$= (2\theta_{BD}) \frac{\omega \tau_m}{2} . \qquad (4)$$

Substituting equation (4) in equation (3) gives

$$\Delta\nu_{HP} = 1/2\, \tau_m$$

or

$$B = 1/2\, \tau_m .$$

The above analysis is given to show that from experimental data, the bandwidth relates to τ_m by

$$B = 1/2\, \tau_m$$

rather than

$$B = 1/\tau_m$$

where τ_m is the dwell time on the target of the beam measured across the half-power points corresponding to a beamwidth λ/D.

Since for a sinusoidal scanner, equation (4) gives

$$\tau_m = \frac{2(\lambda/D)}{\omega(2\theta_{BD})} ,$$

the bandwidth becomes

$$B = \frac{\omega(2\theta_{BD})}{4\ (\lambda/D)}$$

$$= \frac{\pi f(2\theta_{BD})}{2(\lambda/D)} \quad . \qquad (6)$$

The quantity $(2\theta_{BD})$ is the full azimuthal scan angle and f is the azimuthal scan frequency. In comparison, the bandwidth of an ideal linear scanner is

$$B_{ls} = f\,\frac{(2\theta_{BD})}{2(\lambda/D)}$$

which differs from the sinusoidal scanner by a factor π. Thus, since the signal-to-noise is proportional to 1/B, the efficiency of a sinusoidal scanner is $1/\pi$ relative to an ideal linear scanner.

In the case of a multifaceted scanner, the time per resolution element is

$$\tau_m = \frac{(\lambda/D)}{\dot{\theta}_{Beam}}$$

where

$$\dot{\theta}_{Beam} = 2\,\dot{\theta}_{Scanner}$$

$$\dot{\theta}_{Scanner} = \frac{2\pi f}{N_F}$$

N_F = number of facets

then the bandwidth

$$B_{ms} = \frac{1}{2\,\tau_m}$$

$$= \frac{2\pi f}{N_F(\lambda/D)}$$

for a multifaceted scanner. Since efficiency is inversely proportional to bandwidth, the relative efficiency of a multifaceted scanner (compared to the ideal linear scanner) is

$$\frac{B_{ls}}{B_{ms}} = \frac{N_F(2\theta_{BD})}{4\pi} \quad .$$

In the system under consideration, $2\theta_{BD} = 100(\lambda/D)$, and D=1 cm at the multifaceted scanner. Figure II-7 shows the variation in multifaceted scanner efficiency which equals the sinusoidal scanner efficiency for $N_F = 40$.

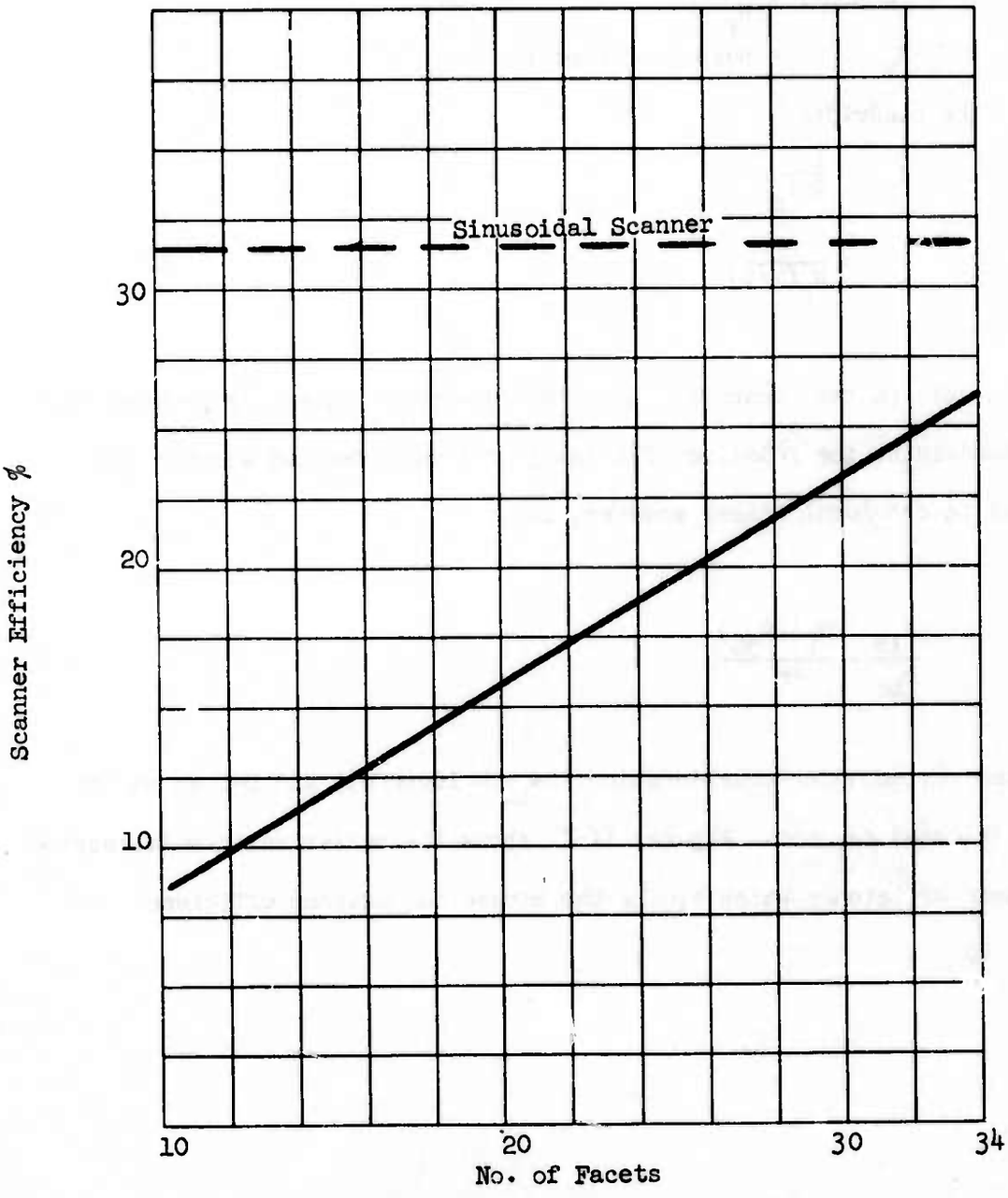

Multi-faceted Scanner Efficiency

Figure II-7

E. BANDWIDTH VERSUS NUMBER OF BEAMS

Although the signal-to-noise for a given transmitter output power is dependent only upon the total system bandwidth, equivalent to the bandwidth for a single beam raster scanning system, the number of beams or resolution elements in a fan affects the signal processing bandwidth. In order to track a Mach 2 target, the total Doppler span corresponding to a Mach 2 target must be provided in the electronic processor. Since a Mach 2 target yields a Doppler return of 125 MHz, the rquired number of resolvable Doppler discrimination bins is $N_D = \frac{125 \times 10^6}{B} N_B$ where B is the bandwidth corresponding to the time per resolution element and N_B is the number of resolution elements being scanned.

For a sinusoidal scanner which is required to scan 10^4 lines/sec

$$B N_B = 1.57 \text{ MHz}.$$

Whereas it will be shown that for a multifaceted scanner scanning 10^4 lines/sec

$$B N_B = \frac{\pi \times 10^7}{N_F}$$

where N_F = number of facets. For a 20 faceted rotating scanner

$$B N_B = 1.57 \times 10^6.$$

Thus, with either a sinusoidal scanner or a 20 faceted rotating scanner, the number of Doppler discrimination bins required is

$$N_D = \frac{1.25 \times 10^8}{1.57 \times 10^6} \; N_B^2$$

$$= 79.6 \; N_B^2.$$

In order to maintain a practical number of filter bins in the electronic processor,

$$N_B = 10$$

has been considered as a practical upper limit.

For a 20 faceted rotating scanner, the offset angle and the number of Doppler filter bins (N/D) are given in Figure II-8 versus the number of beams. The beam offset angle is shown for a 10 km range target which for a 2 beam system corresponds to an offset angle of 0.2 radians. Since the range of targets is from 1 km to approximately 20 km, a 2 beam 20 faceted rotating scanner system is required to correct the beam offset angle from 0.02 rad to 0.4 radians.

In the design of the two-beam multifaceted scanner system, advantage is taken of this large offset angle to eliminate the requirement of a beamsplitter.

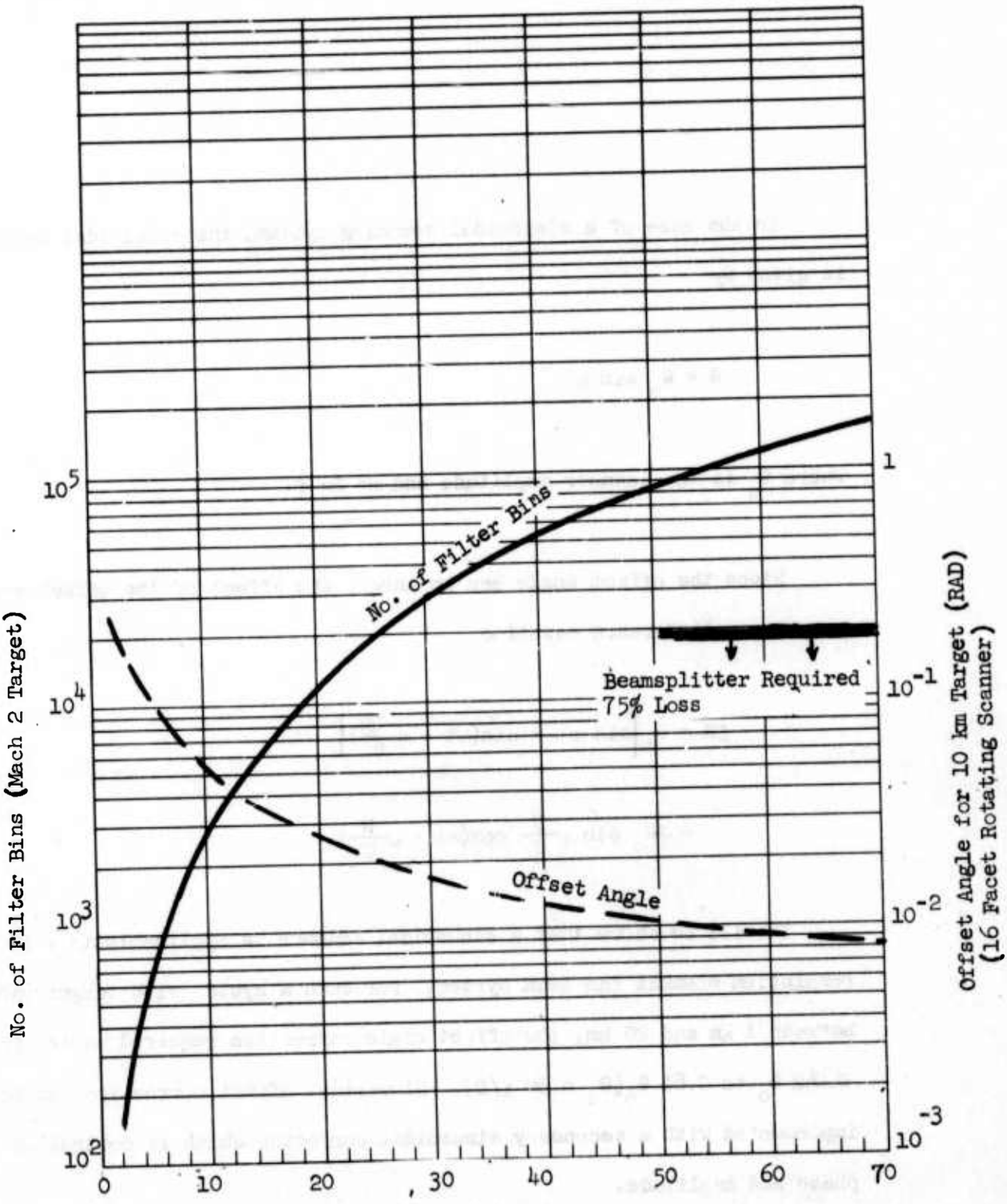

Comparison of No. of Filter Bins Required
and Offset Angle Versus No. of Beams

Figure II-8

In the case of a sinusoidal scanning system, the sinusoidal scanned angle is given by

$$\theta = \theta_o \sin \omega t$$

where θ_o is the scanner amplitude and $\omega = 2\pi f$.

Since the offset angle can be large, the effect of the offset angle requires a difference equation

$$\Delta\theta = \theta_o\left[\sin \omega t - \sin(\omega t - \omega\frac{2R}{C})\right]$$

$$= 2\theta_o \sin \omega\frac{R}{C} \cos(\omega t - \omega\frac{R}{C})$$

It will be shown that a sinusoidal scanner is applicable to a 10 resolution element fan beam system. For such a system with target ranges between 1 km and 20 km, the offset angle correction required varies from $0.042\,\theta_o$ to $0.81\,\theta_o(\theta_o = 50\,\lambda/D)$. Sinusoidal offset correction can be implemented with a secondary sinusoidal corrector which is controlled in phase and amplitude.

F. RANGE TRACKING REQUIREMENTS

The range tracking requirements are compared for a two-beam multi-faceted scanner system and a 10-resolution element sinusoidal fan beam system. The range accuracy required is determined by the requirement in tracking the offset angle for each system.

1. Multifacet Scanner Range Requirements

In a multifaceted scanner system, the offset angle is

$$\Delta\theta = \frac{8\pi 10^4}{N_F N_B} \text{ R/C}$$

which for a 2-beam 20 faceted system is

$$\Delta\theta = 2\pi 10^3 \text{ R/C}$$

This can be written in the form

$$\delta\theta = 2\pi 10^3 \delta R/C$$

where

$\delta\theta$ = angular tolerance of the received signal, and

δR = system range accuracy.

The value of $\delta\theta$ requires an examination of the detector response for variations in $\delta\theta$. The case of coherent detection of a focused Fraunhofer beam with variations in displacement relative to the detector center is analyzed in Appendix A. Figure II-9 and II-10 indicate the variation in signal as the relative position of the beam center changes with respect

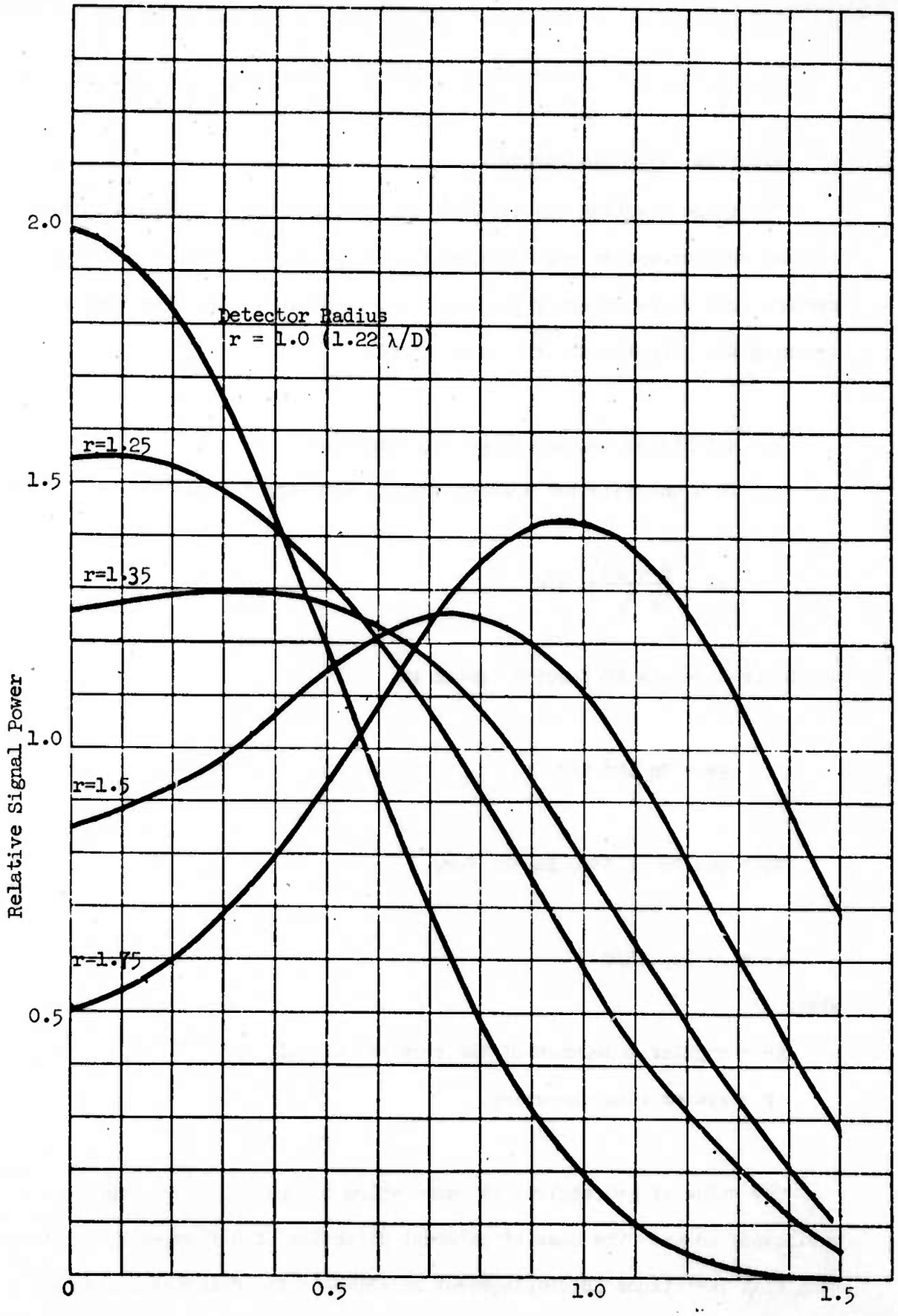

Figure II-9: Signal Power in Heterodyne Detection with Beam Center Displacement

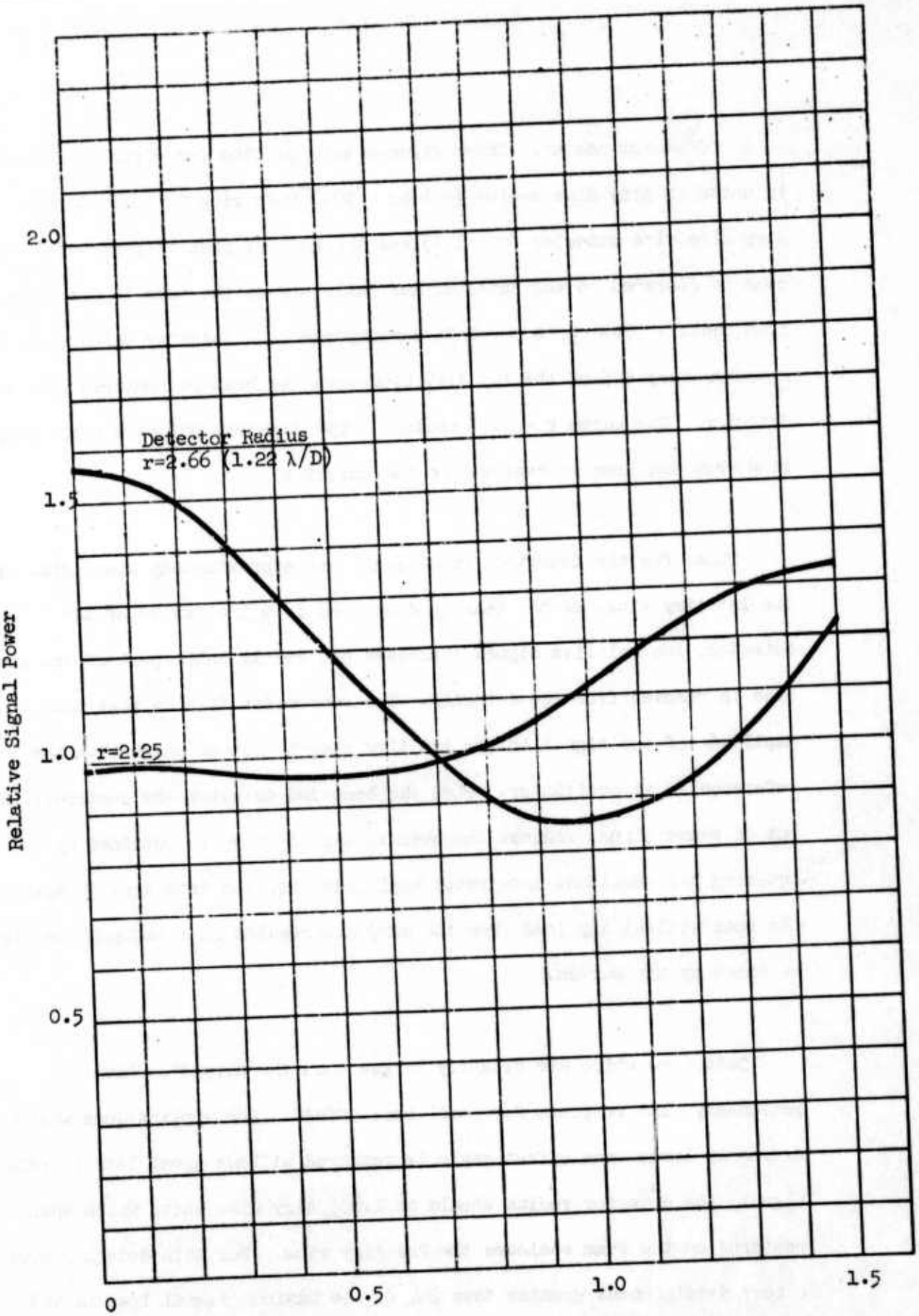

Figure II-10: Signal Power in Heterodyne Detection with Beam Center Displacement

to the detector center. These figures were plotted for circular detectors in units of Airy disc radius (= 1.22 λ/D). Referring to these curves, the Airy disc size detector (r = 1.0) has the highest peak response when the beam is centered on the detector and falls off as the beam is displaced from center. The curve r = 1.35 corresponds to a detector which encloses approximately 40% of the 1st Airy ring when the beam is centered upon the detector. The curve r = 1.75 encloses approximately 90% of the 1st Airy ring when the beam is centered on the detector.

Thus, for the detectors whose radii are approximately the radius of the 1st Airy ring, as the beam is displaced from the center of the detector, the relative signal increases noticeably until part of the Airy disc is removed from the detector. The reason for this is that the amplitude of the signal in the 1st Airy ring is out of phase with the reference local oscillator. When the beam and detector are centered, the out of phase signal reduces the overall signal which is obtained by squaring the resultant integrated amplitude over the detector. Displacing the beam without any loss from the Airy disc results in a net gain in signal as shown by the curves.

Detectors which are slightly larger than the Airy disc have a reasonably flat response for small beam offset. For applications where extremely large beam offset angle is required without great loss in relative signal, the detector radius should be 2.655 Airy disc units which when centered on the beam encloses the 2nd Airy ring. For this detector over a beam displacement greater than 2 λ/D, the maximum signal loss is 43% relative to the beam centered position.

However, increasing the detector size compensates for beam offset tolerance at the expense of target resolution. Thus, with a high speed multifaceted scanner, a qualitative tradeoff must be made by weighing the range requirements with target resolution.

The relative signal for various size detectors with the beam centered on the detector varies as

$$\left[1 - J_o(r)\right]^2$$

as shown by W. T. Cathey (IEEE Proceedings, 56, 1968) where r is the detector radius and a plane wave reference is used as the local oscillator.

The function $\left[1 - J_o(r)\right]^2$ is shown in Figure II-11. Thus, although the detectors which are slightly larger than the Airy disc are less sensitive to angular offset, the selection of the detector size depends upon the most probable angular offset error for the application.

For example, assume that the multifaceted scanner system is to operate with a range accuracy of 50 meters. Then the worst case angular offset of the return signal beam with respect to the detector center is

$$\delta\theta = 2\pi 10^3 \times 50/3 \times 10^8$$

$$= 1.05 \times 10^{-3} \text{ radians.}$$

For a 1 cm beam on the scanner, $\lambda/D = 1.06 \times 10^{-3}$ radians, and the Airy

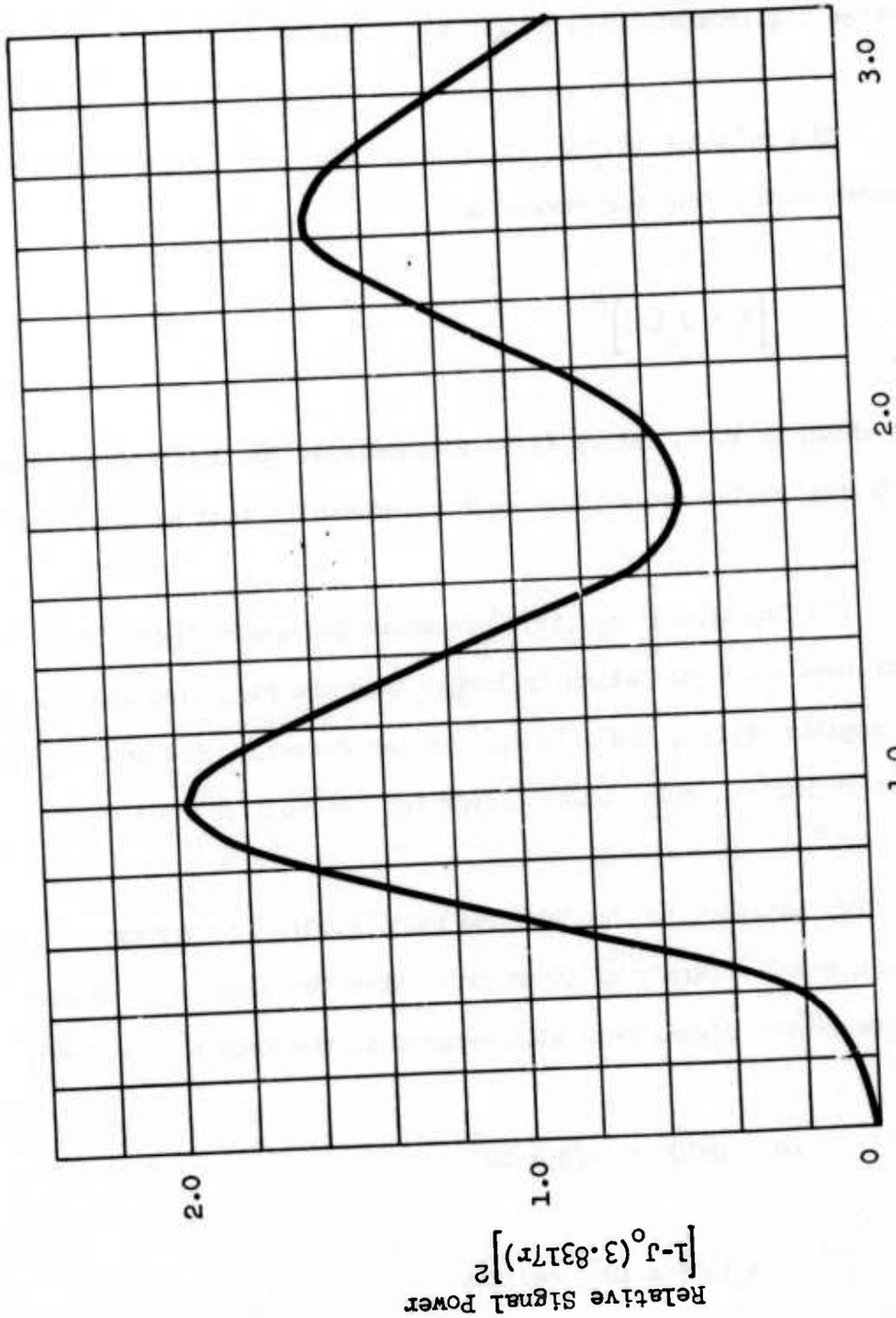

Figure II-11: Signal Power with Beam Centered on Detector

disc is $1.22\ \lambda/D = 1.3 \times 10^{-3}$ radians. Thus, a 50 meter range accuracy corresponds to a worst case relative displacement of the beam on the detector of 1.05/1.3 = 0.8 Airy disc units. Then, over the range of uncertainty, from 0.0 to 0.8 Airy disc units assuming that the error in beam offset angle is equally weighted to the relative signal over the range, and the relative signal is averaged, the following results are obtained.

Detector Size (Airy disc units)	Average Relative Signal
1.0	1.3546
1.25	1.3432
1.35	1.1790
1.5	1.1238

Thus, using an equal probability distribution (for the sake of simplicity), the Airy disc size detector is the optimum detector size for a system with 50 meter range accuracy. With 50 meter range accuracy, the average signal response is down only 30% compared to the peak signal response when the beam is perfectly centered.

In practice, however, the beam offset error is more likely Gaussian distributed which would tend to increase the average signal response for the Airy disc size detector which would increase the choice of this size detector.

2. Ten Element Fan Beam Scanner

Now let us examine the range requirements for a 10 element fan beam scanner. For this system, the required offset angle correction is

$$\Delta\theta = \theta_o\left[\sin \omega t - \sin(\omega t - \omega\, 2R/C)\right]$$

$$= 2\theta_o \sin \omega R/C \cos \omega(t - R/C)$$

where

$$\theta_o = 50\ \lambda/D \text{ (amplitude of the beam scan angle).}$$

The offset angular error corresponding to the range accuracy is then obtained by differentiating $\Delta\theta$ with respect to range,

$$\frac{d\Delta\theta}{dR} = 2\theta_o \frac{\omega}{C} \cos \omega(t - 2\,R/C)$$

or the maximum error is

$$\delta\theta = 2\theta_o \frac{\omega}{C} \delta R$$

where δR is the range accuracy.

For a ten element fan beam system,

$$\omega = 2\pi f$$

$$= 2\pi 10^3$$

and

$$\delta\theta = 2 \times 50 \frac{\lambda}{D} \times \frac{2\pi 10^3}{3 \times 10^8} \delta R$$

$$= 2.09 \times 10^{-3} \frac{\lambda}{D} \delta R.$$

To compare this with the multifaceted scanner (for a 50 meter range accuracy)

$$\delta\theta = 0.105\ \lambda/D$$

$$= 8.6 \times 10^{-2} \text{ Airy disc units.}$$

Thus, a 50 meter range accuracy requirement for a 10-element sinusoidal scanner would be almost equivalent to maintaining the beam on the center of the detector with the system operating near peak response.

Another comparison is to allow the beam to be offset by 0.8 Airy disc units or $0.8 \times 1.22 \lambda/D$. Then the corresponding range accuracy is

$$\delta R = 467 \text{ meters.}$$

Thus, for a sinusoidal scanning system, there would be no problems with respect to correcting the offset angle.

G. DETECTOR CONSIDERATIONS

1. Optimum Local Oscillator Power

The laser radar detector must be sheltered from spurious light from sources other than the target signal and the local oscillator. Whether that light comes from backscatter or other sources, it contributes to noise currents and heating in the detector.

All spurious light which produces direct current in the detector also produces shot noise current of the order of $2eIB$ where e is the charge on the electron, I is the current, and B is the detector bandwidth. A heterodyne detector is usually operated so that shot noise induced by the D.C. current generated by the local oscillator light dominates all other noise. In fact, the local oscillator power is usually increased as high as possible to get the maximum heterodyne amplification of the received signal without other detrimental effects such as heating the detector.

When the spurious light due to backscatter or other sources equals the local oscillator power in magnitude, it will have doubled the shot noise and perhaps carry the total power on the oscillator above the threshold for catastrophic failure due to heating.

If one expects backscattered light to be a problem, he should bring the local oscillator power up to about half the total light power the detector can tolerate without detrimental effects. Consequently, the tolerable backscattered light will be approximately equal to the local oscillator power. If the local oscillator power were made much lower, the backscattered light could at best be doubled before catastrophic

failure and at lower levels it would already be significantly affecting signal-to-noise ratio by increasing the shot noise relative to LO shot noise.

With this conclusion, the determination of tolerable backscatter is reduced to the problem of finding the maximum tolerable L.O. power and dividing by two.

2. Maximum Tolerable Backscatter

The previous section pointed out that the maximum tolerable backscatter of spurious light is about half the maximum tolerable local oscillator power. This varies from detector to detector depending on the type of detector and its size. The same factors influence frequency response so that one might expect a trade-off between frequency response and scatter tolerance.

Some of the larger, photoconducting mercury doped germanium detectors could tolerate local oscillator powers of the order of 100 milliwatts. However, these had the disadvantages of liquid helium cooling and narrow bandwidth (few tens of megacycles) frequency response.

The more modern diode detectors fabricated from mercury cadmium telluride or lead ten telluride have much higher frequency response (at liquid nitrogen temperatures), much smaller size and much lower tolerance for light power. A typical 5 mil by 5 mil lead tin telluride detector will have nearly a gigahertz bandwidth but will tolerate only about five milliwatts or less of local oscillator power. Although large diodes are rarely used in todays systems, increase of the diode size would increase the tolerance to local oscillator power. For example, at 20 mil by 20 mil, a diode made from the best available lead ten telluride material would have a cutoff frequency of the order of 150 megahertz allowing direct detection of Doppler shifted signals from Mach 2 vehicles.

Increasing the diode size from 5 to 20 mils should increase the tolerance for local oscillator power from 4 to 12 times depending on the diode thickness and heat sink electrode structure. The increase in size would, of course, require that the F number of the lens in the heterodyne system be correspondingly increased to fit the Airy disc to the detector. It would appear, however, that a local oscillator power of 50 milliwatts could be tolerated corresponding to a tolerance for about 25 milliwatts of backscattered light in a well-designed system.

3. Detector Cross-Talk

One problem which was considered in the systems application of the Line Imaging Array Techniques is the possibility of cross-talk between adjacent detectors for signals in the 100 - 500 MHz range. These frequencies are generated by the Doppler return relative to the local oscillator (LO) signal. The upper end of the range is established as the worst case systems application for two aircrafts approaching each other at high speeds. The Doppler return signal is approximately 60 MHz per 1000 ft/sec relative closing rate. Thus in ground-to-air or air-to-air applications the Doppler return signal would likely be within the 100 to 500 MHz range.

At 10.6 microns the size of the main lobe of the return signal measured across the first dark ring is determined by the relationship:

$$d = f_{number} \times 2.44 \times 1.06 \times 10^{-3} \text{ (cm)}$$

$$= f_{number} \times 2.44 \times 1.06 \times 10^{-3}/2.54 \text{ (inch)}$$

$$= 1.02 \times f_{number} \text{ (mils)}$$

Thus as a good approximation, the detector size required in mils is the detector lens f_{number}. For an f-30 system as the detector focusing optics the detector size is 30 mils (0.030"). For calculation purposes, let us consider an f-25 to f-30 detector system.

An array of 25 mil detectors would require decoupling of the transmission leads with 25 mil center-to-center spacings. Conventional contacts to the detectors at signal frequencies in the 100 to 500 MHz range would cause cross-talk between leads. With coaxial cable, the point of contact to the

detector is not shielded; therefore, at the point of contact, there would be cross-talk.

To eliminate the cross-talk, the frequency band is within the band of frequencies for which either microstrip line or strip line technology is applicable.

Consider an array of lead tin telluride detectors. Each detector is a diode with a planar ohmic contact at the base. The top of each diode has a transparent (at 10.6 micron) ohmic contact. The total thickness of the diode is approximate 0.020 inch with a dielectric coefficient of the order of 150. Each detector is essentially a current source with a shunt capacitance of about 6 pf. Thus assuming a 50 ohm transmission line from the detector, the RC time constant based upon the 50 ohm load impedance would limit the bandwidth. Applying microstrip technology, increasing the line width to gap ratio minimizes coupling in the microstrip portion where the gap is determined by the substrate thickness separation from the ground plane. Thus since the detector is 0.020 inch in thickness, with a microstrip substrate 0.020 inch then for a line width of 0.004 inch, the line-width to gap ratio is

$$w/h = 0.2$$

Finally, for an array of detectors with 0.025 in center to center spacing the coupling can also be reduced and virtually elminated by bringing lines from adjacent detectors out from the opposite sides since the coupling is also dependent upon the line width to line spacing ratio.

One rule of thumb is that if the spacing between lines is twice the line width, the cross-coupling is down 60 db. A particular known example of a 20 db cross coupling between microstrips is the following example:

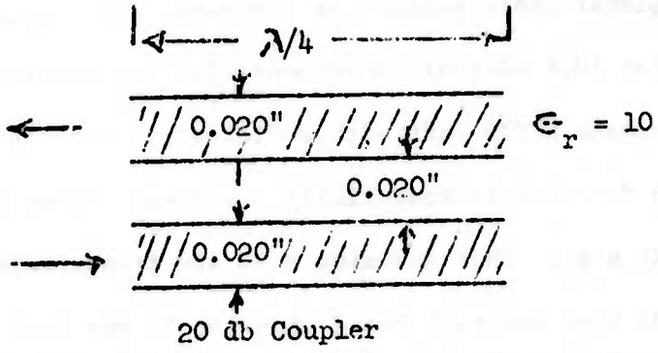

In the above example λ is the wavelength of the transmission frequency and ϵ is the dielectric constant of the substrate.

Thus it could be concluded that microstrip lines spaced 0.05 in center-to-center separation with a line width of 0.004 inch should virtually eliminate cross-coupling. In addition fanning out the microstrip line removes any possible coupling between transmission lines.

A computer program is available within Rockwell International to determine the actual cross-coupling for any given microstrip configuration.

One might also pose the question pertaining to the operation of microstrip line detectors at 77°K relative to the variance in the expansion coefficients of the different materials. The technology is available within Rockwell International to solve this problem since the same technology is utilized in cooled parametric amplifiers to reduce the noise figure.

In addition to detector lead cross-talk, for detectors closely packed in a linear array, the detectors must be electromagnetically shielded from adjacent detectors. Airborne Instrument Laboratories have developed detectors operating at 10 micron which are copper-shielded. The main disadvantage of this technique is the requirement of high F-numbers in the detector focusing lens. F-numbers required range from F-90 to 300.

H. OPTICAL CROSS-TALK

In either heterodyne or non-heterodyne operation, it is the function of the receiver optical system to collect energy, reflected from the target, onto a designated detector.

To determine the extent to which this collecting system allows energy, intended for this designated detector to fall upon adjacent detectors (cross-talk) is the subject for analysis in this section. To make this determination it is necessary to analyze the distribution of energy in the focal plane of the collecting system, which is also the plane in which the detectors are placed.

The collecting system under study may be made up of any number of optical elements provided they have a definable end focal plane. For example, a telescope-focusing lens combination may be treated as a single collecting lens with proper considerations for telescope aperture and magnification, and the assumption that the focusing lens has sufficient aperture to accept the beam relayed to it by the

telescope. Thus, we may concern ourselves only with a collecting aperture D and the amplitude distribution in its focal plane.

In a coherent heterodyne detection system, the distribution of energy is not in accord with the well known expression

$$I = \left[2\frac{J_1(r)}{r}\right]^2 I_o \qquad (1)$$

where

I = intensity

I_o = intensity incident upon the aperture

r = radial distance from geometrical center of the pattern, and

J_1 = Bessel function of the first kind and first order.

As Cathey[1] has shown, because the signal mixes with the reference signal, the energy is determined by integrating the amplitude over a given area and squaring the result.

The amplitude distribution is given by $2J_1(r)/r$ for a Fraunhofer pattern. Thus, to determine the effect of optical cross-talk on adjacent detectors, the amplitude

$$2A_o\int\frac{J_1(r)}{r}\ r\ dr\ d\theta \qquad (2)$$

must be integrated over the space occupied by the adjacent detector.

---

[1] IEEE Proceedings, 56, 1968.

Since it is extremely difficult to even set the limits of integration of the field in the above integral, the coordinate system was transformed to the center of the detector resulting in an integral of the form

$$A = 2A_o \int_o^{2\pi} \int_o^{R_o} \frac{J_1(r)}{r} \, R \, dR \, d\theta \qquad (3)$$

where R is the radial distance of an element on the detector from the center of the detector. The total energy on the detector is then given by A^2.

The integral in (3) was numerically computed using the method given in Appendix A for various detector center-to-center spacings using the optimum detector size whose radius is $1.22 \lambda/D$.

The effect of cross-talk on adjacent detectors is shown in Figure II-12 for detectors with diameters $2.44 \lambda/D$. It is to be noted that the cross-talk normalized signal power is maximum (6.2×10^{-4}) when detectors are arrayed with center-to-center spacing of $2.44 \lambda/D$ (edges of detectors touching). With detector spacings less than $2.84 \lambda/D$ (center-to-center), the cross-talk reduces sharply as the detector separation is increased. (The resultant amplitude on the detector undergoes a sign change at a center-to-center spacing of $2.84 \lambda/D$). If the spacing between detectors is 10% of the detector diameter, the cross-talk is down 40 dB. Thus, cross-talk should not present a detector problem in linear arrays.

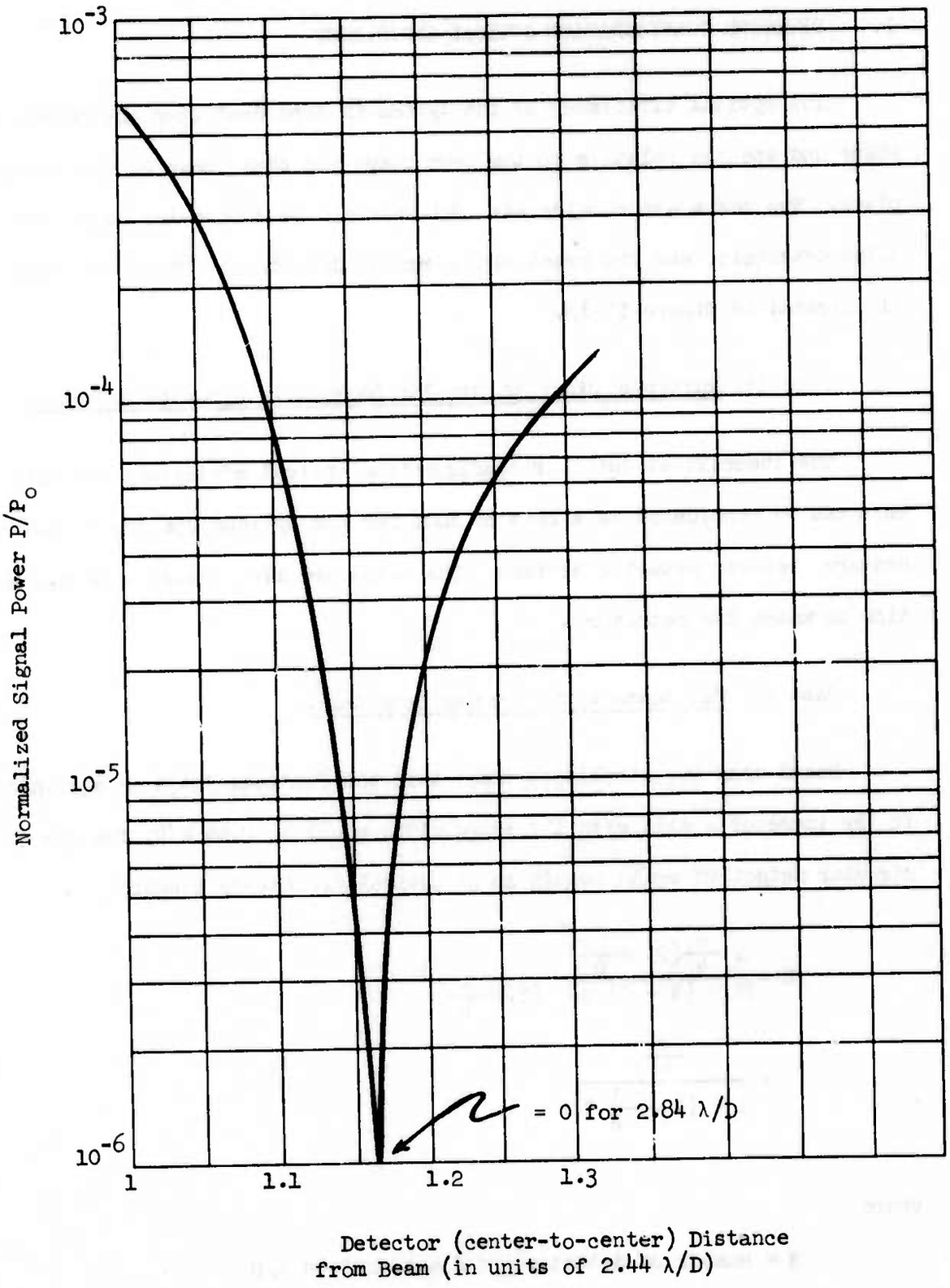

Figure II-12: Optical Cross-Talk on Adjacent Detector.

Detector size = 2.44 λ/D
(P_o = Signal power with detector at beam center.)

I. DETECTOR CONFIGURATION OPTICAL EFFICIENCY

The optical efficiency of the system is dependent upon the detector shape and spacing relative to the beam shape and beam image on the detector plane. Two cases are considered: Multiple discrete circular beams with circular detectors, and fan beams with circular detectors. These two cases are illustrated in Figure II-12.

Case 1: Multiple Discrete Circular Beams with Circular Detectors

The theoretical detector configuration optical efficiency for this case can be considered as a base of 100% for the optimum spacing of $2.84\ \lambda/D$ measured between detector centers. The beams are also spaced with this separation to match the detectors.

Case 2: Fan Beams with Circular Detectors

Based upon the simplified model that the fan beam image is equivalent to the image of a slit with the image width equal to $2.44\ \lambda/D$, the use of circular detectors would result in an optical efficiency E where

$$E = \frac{N \frac{\pi}{4} \left(2.44 \frac{\lambda}{D}\right)^2}{[N + (N - 1)\, S]\ \left(2.44 \frac{\lambda}{D}\right)^2}$$

$$= \frac{\frac{\pi}{4}}{1 + \left(1 - \frac{1}{N}\right) S}$$

where

N = number of detectors of diameter $2.44\ \lambda/D$

S = relative edge-to-edge spacing between the detectors.

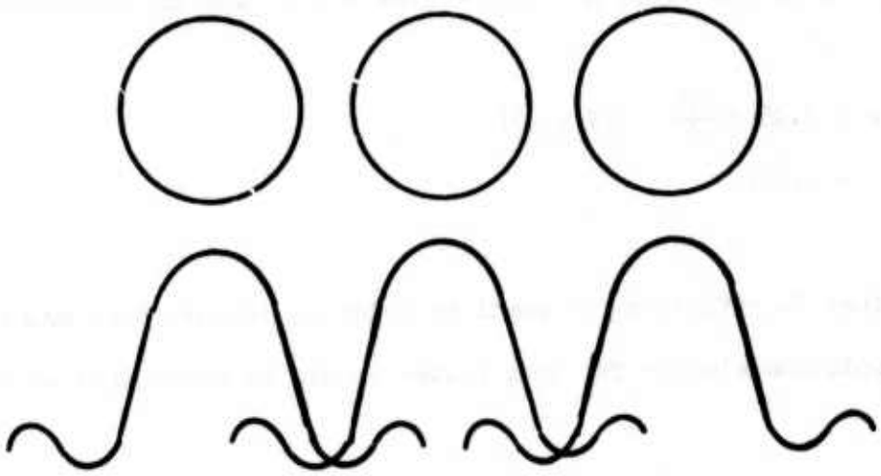

A. Multiple Discrete Beams with Matched Detectors
The $J_1(x)/x$ function is shown below detectors.

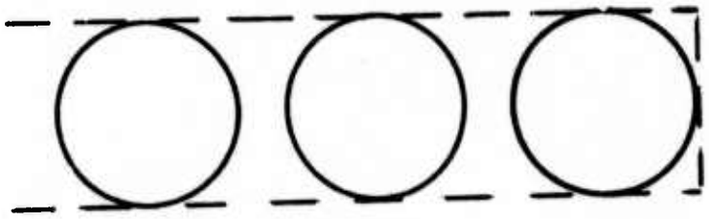

B. Fan Beam Image with Circular Detectors

Figure II-13: Detector Configuration to Illustrate Optical Efficiency

Thus, the optimum spacing is S = 0 which results in an efficiency

$$E = \frac{\pi}{4} .$$

For the case in which the cross-talk is minimum; i.e., a detector center-to-center spacing of 2.84 λ/D, S = 2.84 - 2.44 = 0.4, and the efficiency is

$$E = 0.96 \times \frac{\pi}{4} \quad (N = 10)$$
$$= 0.75.$$

Since the loss in efficiency is small in order to achieve zero cross-talk, the ten resolution element fan beam system should be configured in this manner.

III. REVIEW OF SCANNING TECHNIQUES

A. INTRODUCTION

The most severe scanning problem arises for the raster scan. In the present case, we are interested in scanning 100 x 100 resolution elements 100 times a second, or 10^6 resolution elements per second. For a one meter diameter beam of ten micron radiation, the diffraction angle (resolution element) is 10^{-5} radians. The scan rate, therefore, is only $10^{-5} \times 10^6 = 10$ radians per second. If the beam diameter is reduced by a factor of ten, the scanner angular rate is still only 100 radians per second. The angular rate poses no difficulty even for the simpler scanners.

The real problem in scanning the field proposed here is turn-around time. The raster scan requires that one scan 10^4 lines per second and 10^2 frames per second. Turning the beam around at the end of the line or the end of the frame is the difficult problem. The result of poor turn-around is inefficiency in scanning. For example, the sinusoidally-driven oscillating mechanical mirror must be slow enough when pointed at the center of the field to give a dwell time long enough to accumulate a satisfactory signal. This means that it spends too much time inefficiently on the rest of the field where the mirror is moving more slowly. This nonuniformity in the signal over the image field must be removed and this is done by inefficiently attenuating the signal over most of the field.

If one attempts to drive an oscillating mirror in a sawtooth scan, he finds all of his troubles at the extremities of the scan when he must apply large forces to reverse the mirror motion. In general, the mirror does not stop and reverse instantaneously. There is a non-zero turn-around time which produces corresponding inefficiencies. Although the sawtooth scanning mirror

uses radar power more efficiently, it may actually be cheaper and easier to waste the laser power and use the simpler sinusoidal scan.

Reflecting a beam from a multifaceted rotating mirror is another well known method of scanning. Here again there is a wasted turn-around time. Whenever the beam overlaps the edge between two mirror facets, the beam is split into two parts pointing to opposite edges of the field. Any signal is ambiguous and is therefore wasted. This, too, is an inefficiency that can be compensated with greater transmitter power.

A number of other constraints limit the devices which can be considered for a scanning system. The most significant are: beam size, scan amplitude, scan cycle frequency, and scan uniformity (linearity and turn-around time). There is a trade-off between scan amplitude and beam size. Beam size can be reduced by an optical system which produces a corresponding increase in scan amplitude. This otherwise linear trade-off is limited by aberrations in the optics as angular deviation from the optical axis increases. In the shared aperture case, we are dealing with a one meter diameter beam with about 10^{-5} radian divergence to be scanned over a 10^{-3} radian field every 10^{-2} seconds. A scanner for the one meter beam at these frequencies is totally out of the question. Reduction of the beam diameter to 10 cm increases the scan field to 10^{-2} radians (0.6 degree); reduction to one cm requires a 10^{-1} radian (6 degree) scan field. In order to obtain scan frequencies of 100 sec^{-1} or faster, the scanner aperture size must be of the order of 10 cm or less because of mechanical frequency limitation or availability of optical quality materials for electro-optic or acousto-optic devices. To avoid detrimental aberration of off-axis rays, the scan half angle for mirror systems must be less than three degrees so that a minimum beam size is about 1.0 cm.

Another limitation on beam size may result from power density. A 5 kilowatt beam on a 1 cm diameter scanner or even a lens can be devastating if there is a few percent absorption of beam energy.

It would appear, therefore, that we are restricted to scanners with aperture diameters in the 1 cm to 10 cm range. For the large diameters, mechanical frequencies and availability of materials make the task very difficult. For the smaller diameters, power density and aberrations of off-axis beams make the task difficult or impossible.

B. Electro-Optic Scanners

In principle, it should be possible to scan a beam by passing it through a prism whose index of refraction can be varied by application of a field. Attempts to achieve this, however, have not been highly successful even in the visible where high quality, transparent electro-optic materials are readily available. Among other problems, small nonuniformities in the applied field and material destroy the coherence of the scanned beam. In the 10 micron wavelength range, the available electro-optic materials are much more limited and the use of electro-optic crystals as scanners for the present task is at best a remote possibility. One could avoid the prism design if a controlled field gradient could be produced but this is even more difficult and has met with little practical success.

C. Acousto-Optic Scanners

Acousto-optic scanners are becoming increasingly popular for very high frequency scanning in the visible. They function by causing the light beam to undergo Bragg reflection from an acoustic wave in a transparent fluid

or crystal with a high piezo-optic constant. The reflection angle changes as the frequency (wavelength) of the acoustic wave is changed.

The efficiency of such devices falls off with increasing scan angle because the intensity of the first order reflected beam is high only when both incoming and outgoing light beams meet the acoustic wave at the Bragg angle. This is possible only at one scan angle unless the direction of propagation of the sound wave is changed with frequency and scan angle. A number of techniques have been attempted to overcome this difficulty. One crude method is to use an acoustic wave with a curved wave front (e.g., a spherical wave). The light wave is propagated across the region of the sound wave, meeting different portions of the sound wave at different angles. It is reflected efficiently only from that portion of the wave which it meets at the Bragg angle. As the acoustic frequency and Bragg angle are changed, maximum reflection occurs from a different region where the light wave meets the sound wave at the new Bragg angle. At best, this results in more uniform deflection efficiency with more loss at the zero scan angle and a little less at the larger angles.

Rockwell International, on an earlier contract (WPAFB Contract No. F33615-69-C-1230) developed an acousto-optic deflector for 10 micron radiation using a germanium crystal as the acousto-optic medium. The device quite efficiently deflected the beam into the first-order Bragg reflection when set at the Bragg angle. It has proven exceedingly valuable as a means of obtaining a fixed frequency shift from the transmitted beam for use as a local oscillator for a radar receiver. However, deflections deviating from the Bragg angle drop rapidly in intensity. Generation of the acoustic wave in the germanium crystal from a phased array of line source piezo-electric transducers made it

possible to steer the acoustic beam to maintain the Bragg angle throughout the scan. However, it proved impractical to drive the phased array with the very high acoustic powers and phase control required for effective scanning.

Although acousto-optic scanners are a possibility at ten microns, apertures of more than a centimeter with modest efficiency over a few degrees scan angle are at the limit of the present state-of-the-art. A system design incorporating such a scanner for use with a 5 kilowatt beam would be a high risk design and would require extensive scanner development work.

D. Oscillating Galvonmeter Mirrors (Sinusoidal and Sawtooth)

Oscillating galvonmeter mirrors with torsion bar suspension are the most thoroughly proven scanners for beam apertures of a few centimeters at frequencies up to a kilocycle per second. Section IV contains a complete analysis of such a mirror scanner. If sine wave scanning in this beam size and frequency range is desired, the scanner is "state-of-the-art."

If a sawtooth scan linear in time is desired, the task is more difficult. The sawtooth curve may be represented as an infinite Fourier series which contains the harmonics of the basic sine wave. The problem differs from that described in Section IV in that the mirror is driven at a frequency well below resonance with several harmonics. Although considerably more power is required to drive the "sawtooth" mirror, apertures of a few centimeters at frequencies of the order of a hundred cycles are possible with relatively small turnaround times and not unreasonable power requirements.

E. Bender-Bimorph Mirror Scanners

The bender-bimorph consists of two flat rectangular pieces of piezo-electric material bonded together with a thin conductive paste.

Together they form a thin laminated beam. The outer surfaces are coated with a conductive layer. By means of the three conductive electrodes formed by the outer coating and the bond, the piezo-electric slabs can be driven. The slabs are poled so than an electric field applied across one of them causes it to lengthen along the beam length. The result is a bending of the beam. A mirror can be attached to the beam end and its orientation controlled by the field applied to the bimorph.

Autonetics has conducted extensive analyses and experiements with these devices. With these devices, it is possible to achieve apertures of greater than two centimeters and closed loop tracking frequencies greater than 400 Hz. For a resonant frequency scanner, the bender bimorph technique (considering the present state-of-the-art) would be limited to about 1 kHz rate and scan angles of about 1 degree for an aperture of approximately 1 cm.

F. ROTATING MULTIFACETED MIRRORS

A multifaceted mirror with mirror faces parallel to the axis of rotation reflecting a beam in the plane normal to the axis of rotation can give quite high scan rates. In principle, scan rates as high as $2\pi\,\omega$ radians per second are possible where ω is the rotation rate in cycles per second. Rotation rates as high as 60,000 rpm are possible with small mirrors. However, a number of complications arise. The most restrictive is the fact that the beam is divided into two parts when it overlaps a mirror facet edge. This creates a dead time due to misdirected beam or ambiguity in beam direction.

The dead time due to transitions from one facet to another can be reduced by creating the multifaceted mirror from a larger diameter rotor with sides flattened to give the rotor the cross section of a regular polygon. If there are n faces (n sided polygon), the dead time is approximately $\frac{nd}{C}$ where d is the beam diameter and C is the circumference of the circle circumscribing the polygon. A detailed analysis of choosing the number of facets and the radius is given in Section IV.

G. ROTATING WEDGE PRISM

By rotating a wedge prism around the axis of the incoming beam the outgoing beam can be caused to move in a conical scan. By fanning the beam by passing it through a cylindrical lens prior to the rotating wedge, the conical scan is replaced by a rotation of the fan so as to sweep out a circle. With a linear array of detectors, the circle could be imaged. However, there would be a nonuniform intensity over the circle requiring a correction in the display.

By means of two synchronized counter-rotating wedges, the beam can be caused to undergo a linear scan sinusoidal in time. This is equivalent to the sinusoidally oscillating mirror scanner. Although rotation rates for small wedges might be as high as a thousand cycles per second, a pair of synchronized counter-rotating wedges would be limited to, at most, a few hundred cycles per second.

H. ROTATING MIRRORS (MIRROR NORMAL TO AXES OF ROTATION)

By reflecting a light beam from a mirror placed nearly normal to the axis of rotation, the outgoing beam can be caused to undergo a conical scan whose angle is the angular deviation of the mirror from perpendicular with respect to the axis of rotation. This conical scan can be used in the same way as that achieved from rotating wedges. Similar speeds can be achieved with greater ease.

I. MULTIPLE REFLECTION MOVING MIRROR SYSTEM

When scanning rates required are too high to achieve by a moving mirror, the effective angular scanning rate of a mirror can be increased by a factor of N if the light beam can be caused to reflect off of the same mirror N times before passing out of the system. A number of such optical systems have been devised. Most use a cylindrical or spherical mirror which keeps returning the beam back to the same point occupied by the moving mirror. However, at the same time these change the divergence or convergence of the beam which must be compensated.

In the present problem, angular scan rate poses no difficulty for the one-dimensional scan associated with a fanned beam and linear array. If the total scan angle is θ, the scan frequency is f cycles per second and the system output beam diameter is A times the beam diameter at the scanner, then the angular scanning rate at the scanner is $Af\theta$. The most extreme numbers for the present system are

$$A = 100$$

$$f = 100 \text{ sec}^{-1}$$

$$\theta = 10^{-3} \text{ radians}$$

so that the rate at the scanner is only 10 radians per second. For a two-dimensional raster scan with two one-dimensional scanners, the angular rate at the slow scanner is still $Af\theta$ but at the fast scanner is $RAf\theta$ where R is the number of lines in the raster or resolution elements in the one-dimensional scan angle θ. In the present problem, R = 100 so that the scan rate is 1000 radians per second.

A very fundamental problem arises in the multiple reflection systems. Although the angular rate is multiplied by the number of reflections, the number of times the beam is turned around and entered into a new cycle is not increased.

The amplification of scan angle and scan rate can be applied successfully if the basic scanner already provides fast enough turn-around. Consider a 10,000 Hz tuning fork with one end polished to a mirror finish. Such a high frequency tuning fork is limited to a fairly small angular amplitude (for reasonable forces and energies). If, however, one can put this vibrating mirror into a multiple reflection system or use N such tuning fork mirrors in a row, it is possible to amplify both the angular amplitude and angular rate by N.

In addition to the multiple reflection systems designed and built by Autonetics, a number of others have been reported. In particular, Leo Beiser of CBS Laboratories has described a periodic scan enhancement system. The near-confocal optical scan amplifier which he described at the 1972 Spring meeting of the Optical Society of America has many similarities to the multi-reflection scan amplifier described here.

An analysis of this type of scanner for an active imaging system presented the problem of compensating for the offset angle. In addition, this technique was abandoned because of the high-power densities on the mirrors. These problems and others associated with the scan amplifier are discussed in Appendix B. A brief discussion of a scan amplifier developed under contract is given in Appendix C.

IV. SELECTED SCANNER ANALYSES

A. INTRODUCTION

After the completion of a review of scanner techniques, a concentrated study was performed on the two most promising types of scanners: (1) multifaceted rotating scanner; and (2) torsional sinusoidal scanner. The basic limitations which are imposed on both types of scanners are distortion limits. The study was based upon a distortion limit of 1/8 wave at 10 microns.

For a single beam system required to raster scan 10^4 lines/sec., distortion limits the maximum target range to approximately 6.5 km using a tool steel multifaceted scanner. Beryllium increases the usage of a single beam raster scan system to approximately 10 km. Thus, to achieve ranges exceeding 10 km, a minimum of two beams is required.

With a multifaceted scanner, in order to minimize the dead time, determined by the beam size on the scanner, the smallest beam size considered reasonable is 1 cm which is of the order of the beam output from kilowatt lasers. However, with this small beam size since the scanner is required to scan the beam over 100 resolution elements, 100 λ/D at 10.6 microns is 106 mrad, or 6.07°. This large angle of scan places a stringent requirement upon the beam expanding telescope to operate diffraction limited over an input field of $\pm 3^\circ$. The optical design study has indicated that this requirement is reasonable for a two-beam system, but would impose great difficulties for more than two-beams.

Thus, the multifaceted scanner application is limited to a two-beam system. From the results of the range accuracy requirement to perform offset correction (30% signal loss to obtain 50 m range accuracy), a 10-resolution element fan beam system was studied using a sinusoidal scanner. With a sinusoidal scanner, the beam size can be increased to 10 cm. Increasing the beam size to 10 cm reduces the beam scan angle for 100 resolution element scan to $100\ \lambda/D = 10.6$ mrad or 0.6°.

The scanner analysis given in this section shows that a 10 cm beam scanner can scan the 0.6° field at the rate of 1 kHz to provide 10^4 lines/sec with a 10-resolution element fan beam.

B. MULTIFACETED SCANNER ANALYSIS

The application of a multifaceted scanner to the Line Array Imaging problem requires an analysis of the interdependence upon the target range to the number of facets, radius of the scanner, number of scanning beams and the beam size on the scanner. For a given target range and beam size, the radius of the scanner increases as the number of facets increase. As a result, tensile stress on the scanner increases. In addition, a limiting speed is reached when the deformation exceeds the optical limit to maintain a 1/8 wave flatness on the surface.

1. Scanner Equation

Prior to the derivation of a suitable stress equation, a basic governing relation is given in which the inscribed angle of one face is defined in terms of the sum of three parameters. (1) scanner dead time, (2) scanner transmit time, and (3) transmit/receive time of flight. For purposes of this analysis, a restriction is imposed that the received signal must be received during the time that the same scanner face is in operation. Problems concerning the reception of the return signal on two adjacent faces have not been examined.

Referring to Figure IV-1 the basic scanner equation can then be given as:

$$\theta = \alpha + K\frac{\lambda}{D} + \delta\,\theta \qquad (1)$$

where

α = dead time angle

$K\frac{\lambda}{D}$ = scanner angular motion for 2K resolution elements of beam size D

$\delta\,\theta$ = offset angle.

From Figure IV-1, it can be shown that if a D is the beam size on the scanner face, the dead time angle is

$$\alpha = \tan^{-1}\left[\frac{\cos\frac{\theta}{2}}{\frac{r}{aD} - \sin\frac{\theta}{2}}\right]$$

The value for 2K is 100; therefore, for D = 1 cm at 10.6 μ

$2K\,\lambda/D = 0.106$ radians (6.07^{o}).

The offset angle $\delta\theta$ is given by

$$\delta\theta = \dot{\theta}\ 2\ R/C$$

where

$2\ R/C$ = two-way transit time with target at range R,

C = velocity of light

$$\dot{\theta} = \frac{\theta\ 10^{4}}{N_B}$$

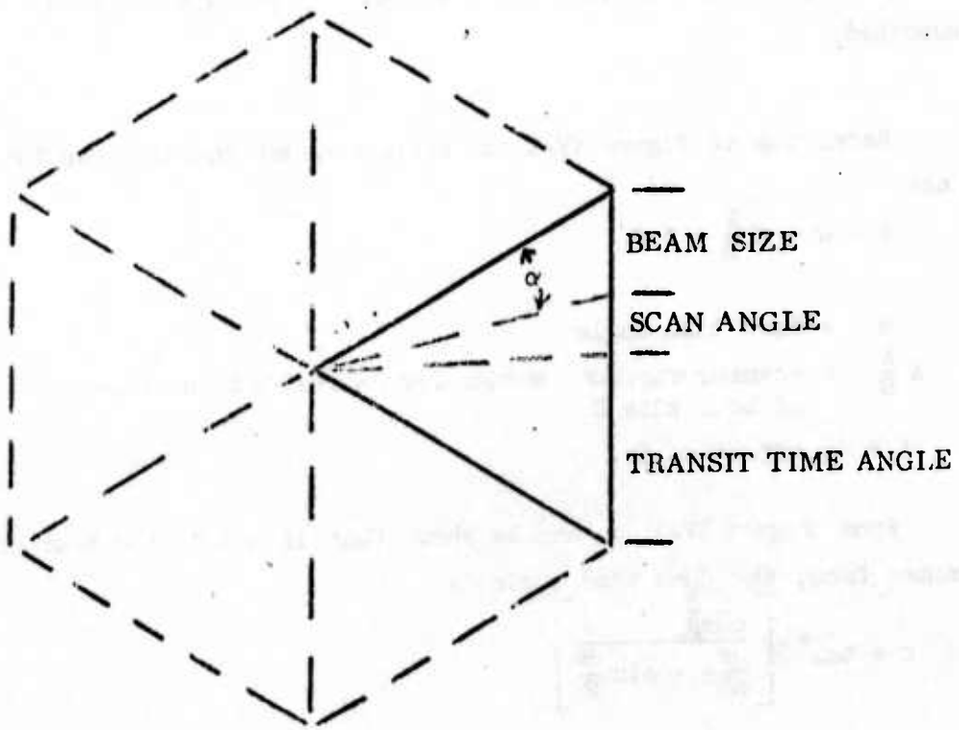

$$\frac{2\pi}{N_F} = \alpha + 50\ \frac{\lambda}{D} + \frac{2\pi 10^4}{N_F N_B}\ \cdot\ \frac{2R}{C}$$

FIGURE IV-1
DUTY CYCLE FOR
MULTIFACETED SCANNER

$$\theta = \frac{2\pi}{N_F N_B} 10^4$$

N_F = number of faces

N_B = number of beams

then

$$\frac{2\pi}{N_F} = \frac{\alpha}{r} + \frac{100}{2}\frac{\lambda}{D} + \frac{2\pi}{N_F N_B} 10^4 \, 2 \, R/C \qquad (2)$$

which is the basic scanner equation.

2. Stress Analysis

To evaluate equation (2) at the maximum allowable rate of the scanner, a stress analysis is required to obtain a relationship between the number of faces N_F and the radius r of the scanner.

Consider Figure IV-2 which is a diagram of the stresses and strains upon an unfinitesimal elemental volume of the cylinder in the radial direction. To determine the forces in the radial direction the stresses σ's are multiplied by the areas upon which they act. Considering a unit length normal to the stress direction and noting that the tangential stresses have a component along the radial direction, the sum of the forces radially is:

$$\sigma_r \, r \, d\theta + 2\sigma_t dr\left(\frac{d\theta}{2}\right) - (\sigma_r + d\sigma_r)(r+dr)\, d\theta = dm \, r\omega^2$$

the term $dm \, r\omega^2$ is the centrifugal force causing the stresses..

Since

$$dm = \rho r \, d\theta \, dr$$

where ρ= density. Upon simplifying

$$\sigma_t - \sigma_r - r\frac{d\sigma_r}{dr} = \rho \, r^2\omega^2 \qquad (3)$$

This equation has two unknown stresses σ_t and σ_r. To reduce the problem

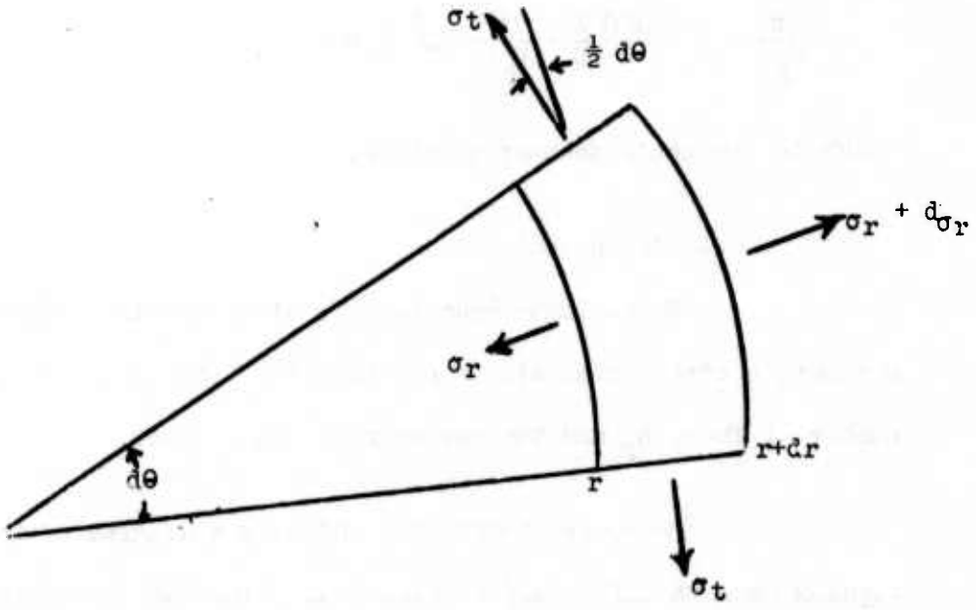

Figure IV-2: Stresses on Elemental Volume

to one unknown, a transformation is performed in terms of the deformations and material properties. The deformations of an element are described by its strains in the radial and tangential directions.

If u represents the radial displacement of a cylindrical surface at radius r, u + du is the corresponding radial displacement of the cylindrical surface at r + dr. Then the strain ϵ_r of an element in the radial direction is

$$\epsilon_r = \frac{(u + du) - u}{dr} = \frac{du}{dr}$$

Similarly the tangential strain on the element is

$$\epsilon_r = \frac{2\pi(r+u) - 2\pi r}{2\pi r} = \frac{u}{r}$$

From the properties of materials, the stresses and strains are related by

$$\sigma_r = \frac{E}{1-\mu^2} (\epsilon_r + \mu \epsilon_t)$$

$$\sigma_t = \frac{E}{1-\mu^2} (\epsilon_t + \mu \epsilon_r)$$

where E is Young's modulus and u is Poisson's ratio.

Upon substituting

$$\epsilon_r = \frac{du}{dr} , \quad \epsilon_t = \frac{u}{r}$$

$$\sigma_r = \frac{E}{1-\mu^2}\left(\frac{du}{dr} + \mu\frac{u}{r}\right)$$

$$\sigma_t = \frac{E}{1-\mu^2}\left(\frac{u}{r} + \mu\frac{du}{dr}\right)$$

which upon substituting into equation (3) yields a differential equation

$$r^2\frac{d^2u}{dr^2} + r\frac{du}{dr} - u = \rho\omega^2 r^3$$

A general solution to this equation is

$$u = \frac{\mu^2-1}{8E}\rho\omega^2 r^3 + a_1 r + \frac{a_2}{r} .$$

To evaluate this equation, the elemental displacements are not known at any radius, but the stress is known resulting from the rotational forces. The radial stress is then

$$\sigma_r = -\frac{(3+\mu)}{8}\rho\omega^2 r^2 + \frac{Ea_1}{1-\mu} - \frac{E}{1+\mu}\frac{a_2}{r^2} .$$

Since the solution must be valid for all values of r and be finite, $a_2 = 0$; otherwise, there is a discontinuity at the center. Furthermore, the a_1 term merely contributes as a constant addition to the stress and would only be significant if there is external pressure. (This term is independent of rotational rates.) Thus, at zero speed, imposing the condition that $\sigma_r = 0$ for $\omega = 0$, $a_1 = 0$. Or,

$$\sigma_r = -\rho\frac{\omega^2 r^2}{8}(3+\mu) .$$

It is significant to note that σ_r is independent of Young's modulus except through Poisson's ratio.

For Cordin tool steel, the design tensile stress limit is 100,000 psi. In comparison, beryllium has a tensile stress limit of the order of 450,000 psi. Based upon a stress limit of 100,000 psi and 450,000 psi for tool steel and beryllium, respectively, the maximum peripheral velocity allowable for each material is:

Tool Steel: $V = 4.6 \times 10^4$ cm/sec (max)

($\rho = 7.85$ gm/cc, $\mu = 0.3$)

Beryllium: $V = 2.1 \times 10^5$ cm/sec (max.)

($\rho = 1.854$ gm/cc, $\mu = 0.03$)

For application of high-speed diffraction limited scanners, the critical factor is not the design stress limit velocity, but rather the surface deformation.

3. Surface Deformation

In the above stress analysis, it has been shown that the displacement u of a surface at radius r is

$$u = \frac{\mu^2 - 1}{8E} \rho \omega^2 r^3$$

where

μ= Poisson's ratio

E= Young's modulus

ρ= density

ω= angular rotational rate.

(In the above equation, positive displacement is measured inward.)

Since u is a displacement in the radial direction, the component of u normal to the facet surface is a measure of the surface flatness. The flatness criterion utilized in the analysis is that the difference in the normal component of u can not exceed 1/8 wave between any two points of a facet which are within a beam size of eachother. The results are indicated in the next section which describes the minimum radii required to scan targets at various ranges.

4. Scanner Radius

The required scanner radius is determined from the equation

$$\theta = \tan^{-1}\left[\frac{\cos \theta/2}{\frac{r}{ad} - \sin \theta/2}\right] + 50\,\frac{\lambda}{D} + \dot{\theta}\, 2\, R/C$$

where

$\theta = \frac{2\pi}{N_F}$

r = radius

a = $1/\cos \varphi$ (φ = angle of incidence of the beam)

D = beam diameter

$\dot{\theta} = \frac{2\pi 10^4}{N_F\, N_B}$

N_F = number of facets

N_B = number of beams

R = target range

C = velocity of light

Based upon this equation using a 1 cm beam at an incidence angle of 30°, the required scanner radii are given in Figures IV-3 and IV-4 for a one beam and two beam system as a function of the number of facets and target ranges. The scanned field is 100 resolution elements with a line scan rate of 10^4 lines/sec corresponding to a frame size of 100 x 100 resolution elements and a frame rate of 100 frames/sec.

The one beam system exceeds the distortion limit for 6.5 km range using tool steel or 11 km range using beryllium. Within a range of 20 km, the two-beam system is primarily limited in radius by the manufacturer's fabrication limit of 15 cm.

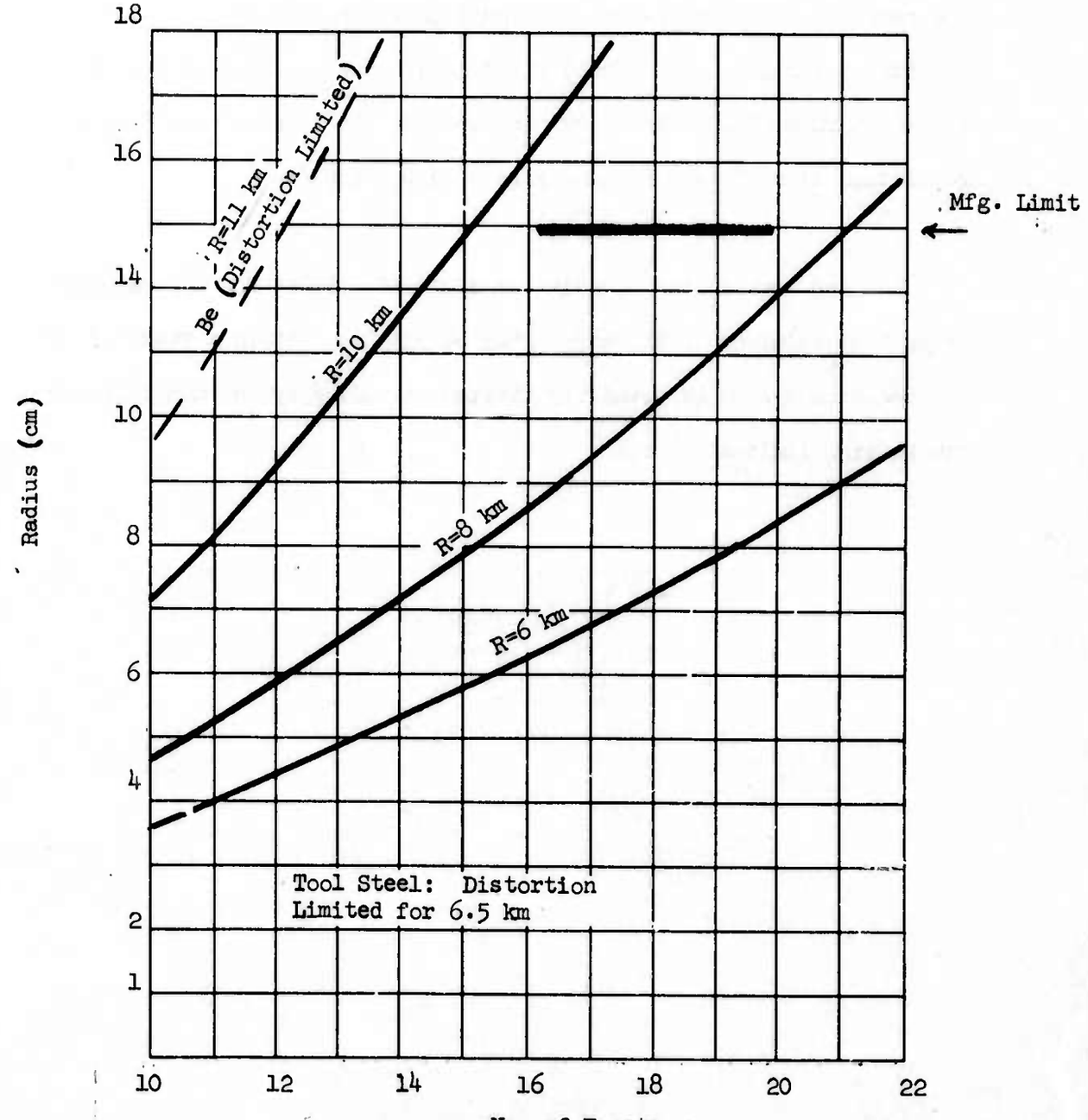

Scanner Radius Required for one-beam multifaceted system

Figure IV-3

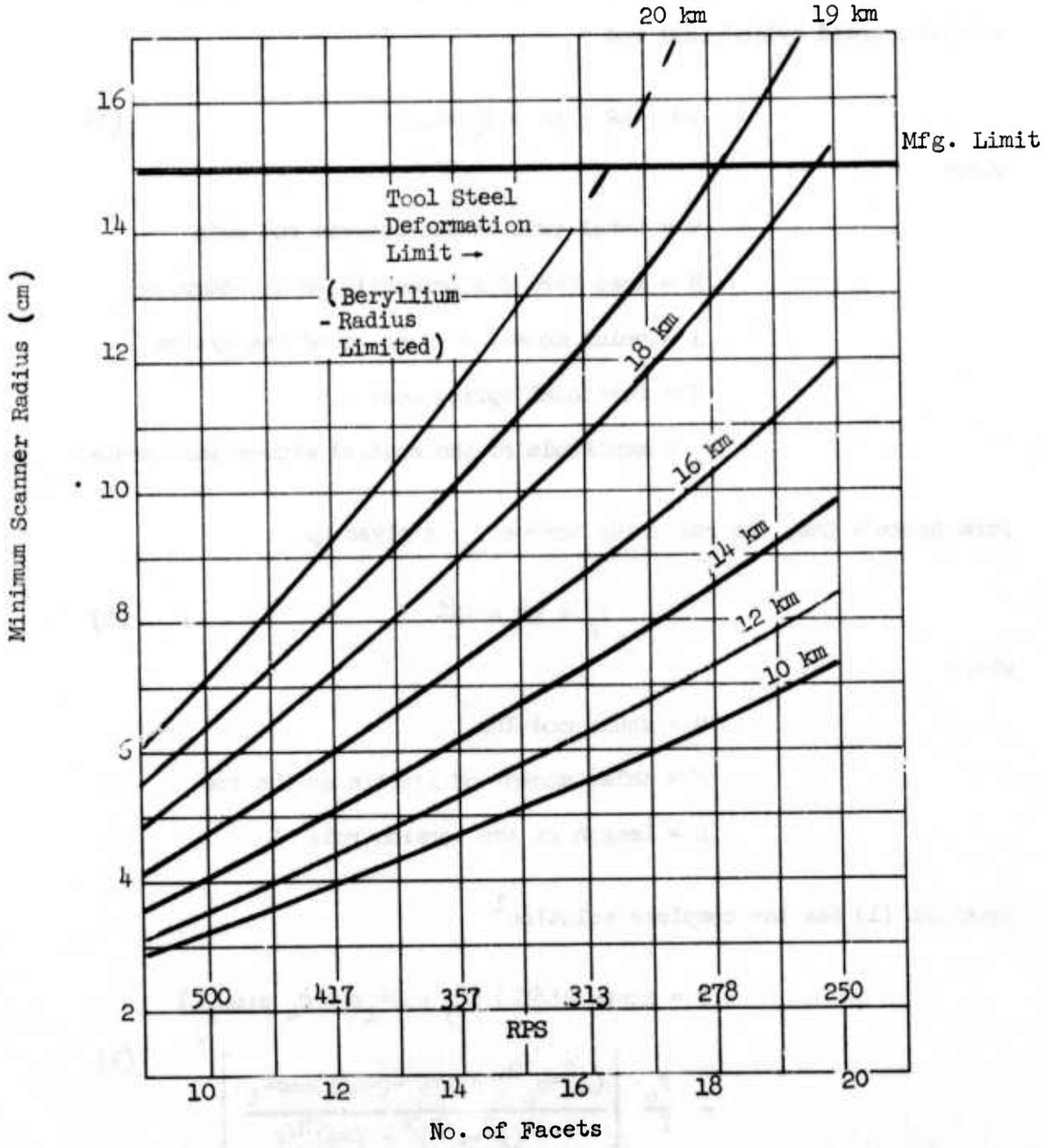

Required scanner radius to achieve indicated target range with 2-beam system scanning 10^4 lines/sec

Figure IV-4

C. TORSIONAL OSCILLATING SCANNER ANALYSIS

1. Equations of Motion

Consider the inhomogeneous torque equation for the torsional motion a solid cylindrical rod

$$I\ddot{\theta} + B\dot{\theta} + K\theta = T_o \sin\omega t \qquad (1)$$

where

θ = total twist angle between rod ends

B = loss term due primarily to air damping

I = polar moment of inertia of the system

K = torsional spring constant

T_o = amplitude of the applied sinuosidal torque.

From Hooke's Law, the restoring torque T_s is given by

$$T_s = K\theta = \frac{GJ\theta}{L} \qquad (2)$$

where

G = shear modulus

J = polar moment of inertia of the rod

L = length of the torsion rod.

Equation (1) has the complete solution[1]

$$\theta = \exp(-Bt/2I)\,(C_3 \cos\omega_1 t + C_4 \sin\omega_1 t) - \frac{T_o}{I}\left[\frac{(\omega^2-\omega_o^2)\sin\omega t - (\omega B/I)\cos\omega_t}{(\omega^2-\omega_o^2)^2 + (\omega B)^2/I}\right] \qquad (3)$$

[1] Shames, I. H., "Engineering Mechanics," Prentice-Hall, 1960, p. 354-358.

where the first term of (3) represents transient solutions, and the second term the steady-state forced solution and

$$\omega_1 = \left[K/I - (B/2I)^2\right]^{\frac{1}{2}}$$
$$\omega_o = (K/I)^{\frac{1}{2}} . \tag{4}$$

If we take

$$\theta_f(t) = \theta_m \sin(\omega t + \varphi) \tag{5}$$

then the maximum torque, T_o, from the steady-state solution in (3) can be derived as

$$T_o = \theta_m I\left[(\omega^2 - \omega_o^2)^2 + (\omega B/I)^2\right]^{\frac{1}{2}}. \tag{6}$$

The average power expended in the system may be computed from the relation

$$P_{av} = \frac{1}{T}\int_{-T/2}^{T/2} T_o \sin\omega t\ \dot{\theta}_f(t)\ dt \tag{7}$$

$$= \frac{1}{2}\ \theta_m \omega T_o \sin\varphi \tag{8}$$

where T is the period of the oscillation and θ is the phase angle between the applied torque and the scanner motion. Equations (6) and (8) then yield an expression for the drive power required

$$P_{av} = \frac{1}{2} B\theta_m^2\omega^2 \left[\left(1 - \frac{\omega_o^2}{\omega^2}\right) Q^2 + 1\right]^{\frac{1}{2}} \sin\varphi \tag{9}$$

where

$$\varphi = \tan^{-1}\left[Q(1 - \omega_o^2/\omega^2)\right]^{-1} \tag{10}$$

and the Q-factor is given by

$$P_{av} = \frac{1}{2} B\theta_m^2\omega_o^2 \tag{11}$$

It may be observed that at resonance $\omega = \omega_o$

$$Q = \omega I/B. \tag{12}$$

and the torque necessary to sustain oscillation is at a minimum given by

$$T_o = \theta_m\omega_o B. \tag{15}$$

2. Air Damping Coefficient

The air damping coefficient (B) may be derived by calculating the net drag force on a plane surface element moving through air at a velocity v and integrating all such forces over the surface of the torsionally resonant mirror shown in Figure IV-5.

For a plate area dA moving in a medium of density ρ, the net change in momentum of the gas molecules by the plate in some short time interval dt is

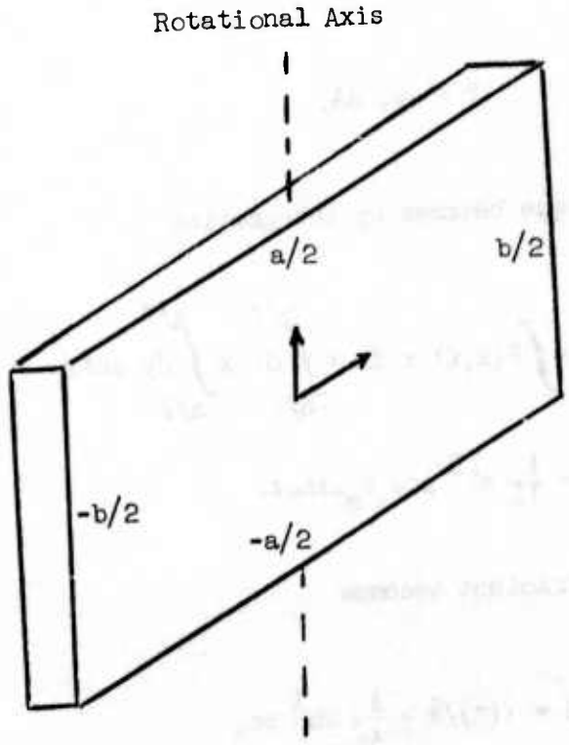

Figure IV-5. Geometry of the Resonant Scanner

$$dp = mdv = \frac{1}{2}\rho v(2v_{th}+v)dAdt \tag{14}$$

where v_{th} is the average thermal velocity of the gas atoms and may be taken to be approximately c, the velocity of sound in air. As long as $v \ll c$, the drag force on the moving element may be approximated by

$$F \cong \rho vc\, dA, \tag{15}$$

and the total drag torque becomes by integration

$$T(t) = \int F(x,t)\, x\, dx = \int_{-b/2}^{b/2} dx\, x \int_{-a/2}^{a/2} dy\, \rho c\dot{\theta}x \tag{16}$$

$$T(t) = \frac{1}{12} ab^3 \rho c\omega_o\theta_m \sin\omega t. \tag{17}$$

Hence, the damping coefficient becomes

$$B = T(t)/\dot{\theta} = \frac{1}{12} ab^3 \rho c, \tag{18}$$

and from (12) the required average power is

$$P_{av} = \frac{1}{24} \rho cab^3\theta_m^2\omega_o^2 \tag{19}$$

where

$$\rho = 1.135 \times 10^{-3}\ g/cm^3$$

$$c = 3.3 \times 10^4\ cm/sec.$$

Figure IV-6 illustrates the variation of average power required to sustain oscillation as a function of both the resonant frequency and peak mirror angle Θ_m for a specific mirror geometry. These theoretical results include only losses expected due to air damping. Generally, the true power drive requirements will be somewhat higher for practical systems.

3. Torsion Rod Parameters

Using the conditions of resonance and the defining equation for the moment of inertia for a circular cross section, the relation of the torsion rod radius (r) and L may be fixed. Using (4) and the expression

$$J = \frac{\pi}{2} r^4 \tag{20}$$

the equation

$$r^4 = \left(\frac{2I\omega^2}{\pi G}\right) L \tag{21}$$

is obtained as a constraining relation between the rod radius and its length.

An additional constraint relating r and L obtains from shear stress limits imposed on the torsional shaft. Using the expression for shear stress at the periphery of a shaft of radius r related to torque T

$$S = \frac{Tr}{J} \tag{22}$$

and defining S_s as the maximum shear stress at the edge of the rod and Se as the corresponding safe upper limit, we have

$$Se \cong \frac{S_s}{2}^2, \tag{23}$$

2 Moleev, Machine Design, p. 25

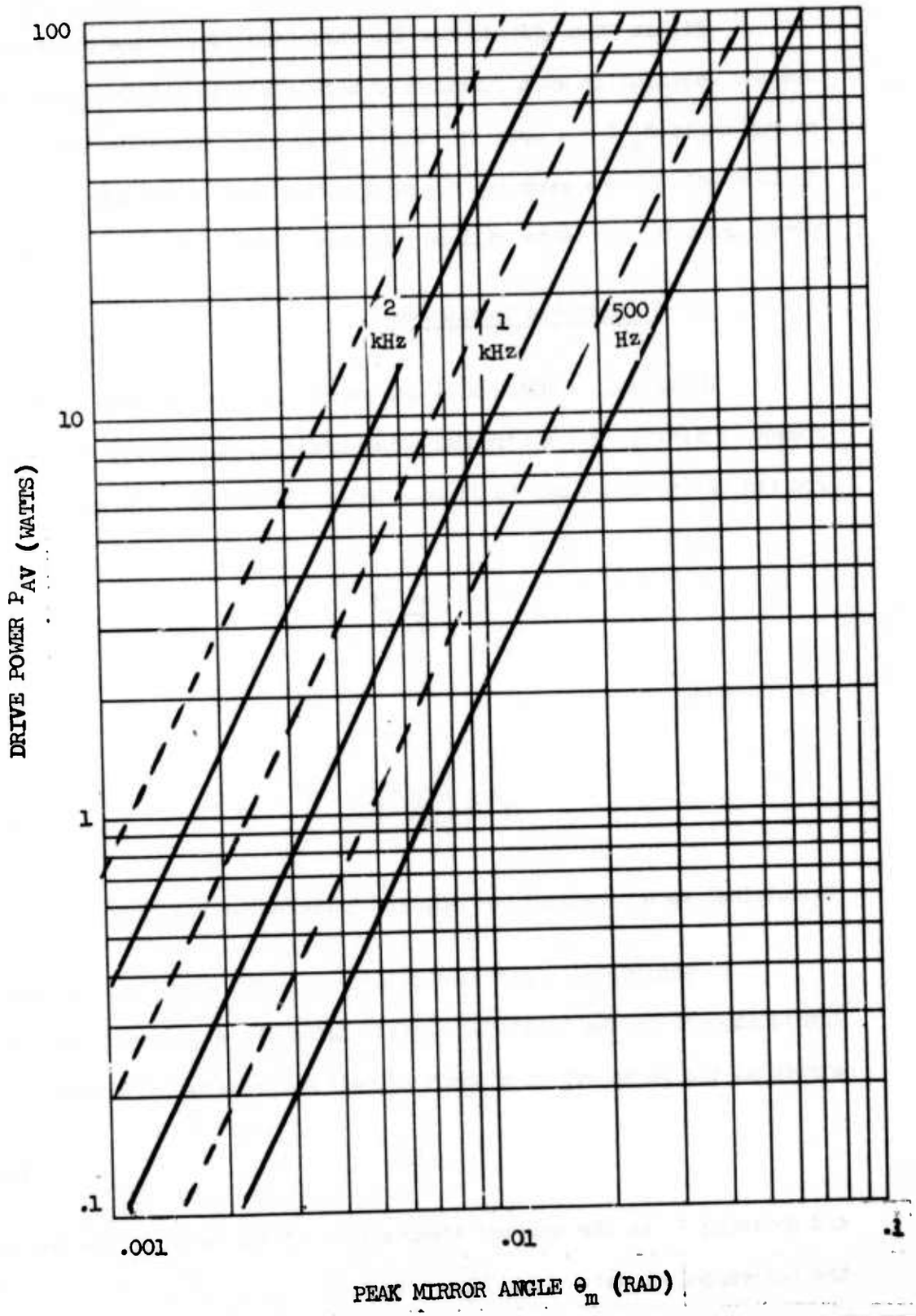

FIGURE IV-6. AVERAGE DRIVE POWER REQUIRED TO OVERCOME AIR DAMPING FOR b = 14 CM, a = 10 CM (DASHED LINES), AND b = 10 CM, a = 14 CM (SOLID LINES).

Therefore, the imposed constraint becomes

$$\frac{Tr}{J} = \frac{Gr}{L}\,\theta_m \leq \frac{S_s}{2} \qquad (24)$$

or

$$r \leq \frac{S_s}{2G\theta_m}\,L.$$

Equations (21) and (24) together specify a minimum rod thickness as

$$r \geq (4\theta_m I\omega^2/\pi S_s)^{\frac{1}{3}} \qquad (25)$$

for 7075-T6 aluminum alloy:

$$S_s = 1.29 \times 10^9 \text{ dynes/cm}^2$$
$$G = 2.66 \times 10^{11} \text{ dynes/cm}^2.$$

From the specification of the required scan angle, which is 4 times the peak angular mirror deflection θ_m, the moment of inertia of the mirror I, and the resonant frequency ω, (21) and (24) specify the rod radius and length, r and L.

4. Mirror Distortion Characteristics

A crucial factor determining the thickness of the mirror, d, is its dynamic deformation strength which must limit the maximum allowable mirror surface deflection γ to

$$\gamma \leq \lambda/8 \tag{26}$$

where λ is the optical wavelength. Brosens[3] has calculated the maximum distortion for a rectangular mirror to be

$$\gamma = 0.03438\, b^2 \omega^2 \theta_m I \frac{(1-\nu)}{Gd^3 a} \tag{27}$$

where υ is Poisson's ratio for the mirror material, we may compute the mirror inertia to be

$$I = \int r^2 dm = \frac{a\rho m}{12} (b^3 d + d^3 b) \tag{28}$$

so that with the values for aluminum

$$\rho m = 2.7 \text{ g} \cdot \text{cm}^3$$

$$\nu = .33$$

(27) reduces to

$$\gamma = 11.945 \times 10^{-14}) \omega_o^2 \theta_m b^5/d^2. \tag{29}$$

Equations (26) and (29) together determine the minimum mirror thickness for a specific aperture size.

---

[3]Brosens, P. J., "Dynamic Mirror Distortions in Optical Scanning." Applied Optics, Vol. 11. No. 12, p. 2987-2989 (1972).

Although a solid rectangular aluminum mirror has been considered here for simplicity, various hollow section designs may be utilized to greatly reduce mirror inertia without appreciably affecting deformation strength. These types of mirror modifications will not be considered here except to indicate the available flexibility in the design.

Figure IV-7 illustrates the maximum mirror distortion γ for a scanner operating at 1000 Hz with a peak mirror angle of 2.5 mrad as a function of the mirror width b. The dotted line represents the one-eight-wavelength limit imposed on the distortion and the curves are plotted for constant mirror thickness d.

5. Scanner Design Considerations

The previous sections present the basic equations for the design of torsional resonant scanners. In this section, we apply these design criteria to derive scanner parameters such as torsion rod dimensions, mirror thickness, electrical power and peak torque requirements given both scan angle and frequency. For a N-beam scanning system, the peak mirror scan angle θ_m is

$$\theta_m = \frac{\alpha}{4N} \tag{30}$$

where α is the full-scan angle. Taking the sample values

$$\begin{aligned} \alpha &= 42° \\ N &= 5 \\ \omega &= 2\pi(226) = 1420 \text{ sec}^{-1} \\ \theta_m &= .0366 \text{ rad} \end{aligned} \tag{31}$$

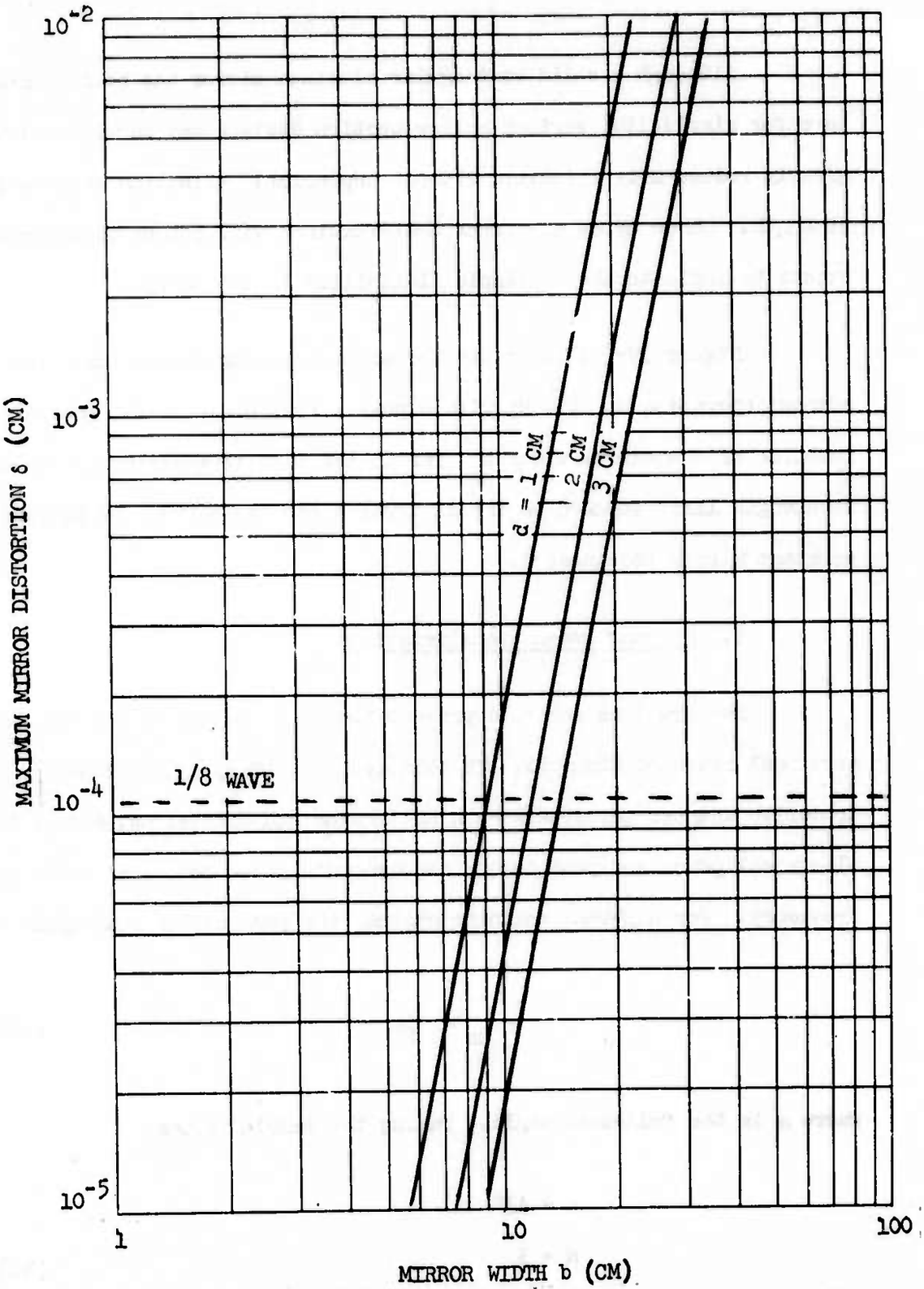

FIGURE IV-7. MAXIMUM MIRROR DEFORMATION δ FOR SINUSOIDAL SCANNER OPERATING AT 1000 Hz AND PEAK MIRROR ANGLE θ_m = 2.5 MRAD. THE CURVES ARE DRAWN AT CONSTANT MIRROR THICKNESS d.

and utilizing a rectangular mirror for which a = 4 cm, b = 9 cm, the average power required by the scanner to overcome air damping is from (15)

$$P_{av} = \frac{1}{24} \rho c a b^3 \theta_m^2 \omega^2 \tag{32}$$

$$P_{av} = 1.23 \text{ watts.}$$

Similarly, the peak torque required may be computed from (9) as

$$T_{pk} = \frac{2 P_{av}}{\theta_m \omega} \tag{33}$$

Since the oscillating mirror is subjected to high dynamic torques which cause distortion in a plane perpendicular to the rotation axis, the minimum mirror thickness required to limit the maximum distortion to one-eighth-wavelength is obtained from (21) and (24) as

$$d \geq 1.25 \times 10^{-5} \omega (\theta_m b^5)^{\frac{1}{2}} \tag{34}$$

$$d \geq 0.825 \text{ cm.}$$

As may be observed from (22), the mirror distortion is linearly related to its moment of inertia, so that the required mirror thickness may be reduced by 20% if the unused mirror corners are rounded. Therefore, the mirror thickness may be safely specified to be approximately

$$d = 0.66 \text{ cm.}$$

This results in a total system inertia from (23)

$$I \cong 0.8 \frac{a\rho m\, b^3 d}{12}$$

$$I = 347 \text{ g cm}^2 \tag{35}$$

where the numerical factor accounting for rounding of the mirror corners has been included. Equations (16) and (19) may now be used to determine a relationship between the torsion rod radius r and the rod length L. To limit the maximum shear stress to a safe value (19) requires

$$r \leq 2.42 \times 10^{-3}\, L/\theta_m$$

$$r \leq .066L. \tag{36}$$

For resonance (16) stipulates

$$r^4 = \frac{(2I\,\omega^2)}{\pi G} L \tag{37}$$

$$r^4 = 1.675 \times 10^{-3}\, L.$$

By combining (36) and (37), lower limits for r and L may be obtained from (20) and (36) to be

$$r \geq .294 \text{ cm}$$

$$L \geq 4.45 \text{ cm}.$$

Minimizing the rod length gives the dimensions

$$r = .2937 \quad (.116 \text{ in})$$
$$L = 4.445 \text{ cm } (1.75 \text{ in})$$

The sample design parameters determined from this section are enumerated for reference in Table (1).

$\alpha = 42°$	$f = 226$ Hz
$N = 5$	$P_{av} = 1.23$ watts
$\theta_m = .0366$ rad	axbxc = 4.0 x 9.0 x .66 cm
$T_{pk} = 4.73 \times 10^5$ dyne-cm (43 oz-in)	$r = .2937$ cm
	$L = 4.445$ cm

Table 1. Sample design parameters of the torsional scanner system.

V. SHARED VS DUAL APERTURES

A. INTRODUCTION

The shared aperture has the basic advantage over the dual aperture system in achieving increased power densities in the high-energy beam. The increase is proportional to the square of the relative diameters. In a dual aperture system, the output optics is limited to approximately 40 cm; whereas the shared aperture system permits output optics of 1 m diameter. Thus, the net gain in power density is 6.25 for a shared aperture system.

However, the shared aperture system requires a beam combiner to combine the high-energy beam with the laser radar scanned beam. The two methods of beam combining which were considered during the study were the Brewster angle beam combiner and the diffraction grating combiner.

The Brewster angle beam combiner requires a solution to the high-power density "window" problem. Thus, this method was discarded early in the study.

The diffraction grating beam combiner was investigated and is discussed in this section. However, it was also discarded for reasons that the efficiency required is not within the state-of-the-art.

In addition, the effect of backscatter is compared for the dual aperture and shared aperture systems. Since the required local oscillator (LO) power on the detector must be at least a factor of 2 greater than all of the noise power, the backscatter from the high-energy beam is an important parameter in determining the required LO power.

B. BEAM COMBINER

Two possible methods exist for the design of the beam combiner. The first is the Brewster angle beam combiner using candidate materials such as gallium arsenide. This type of beam combiner is illustrated in Figure V-1.

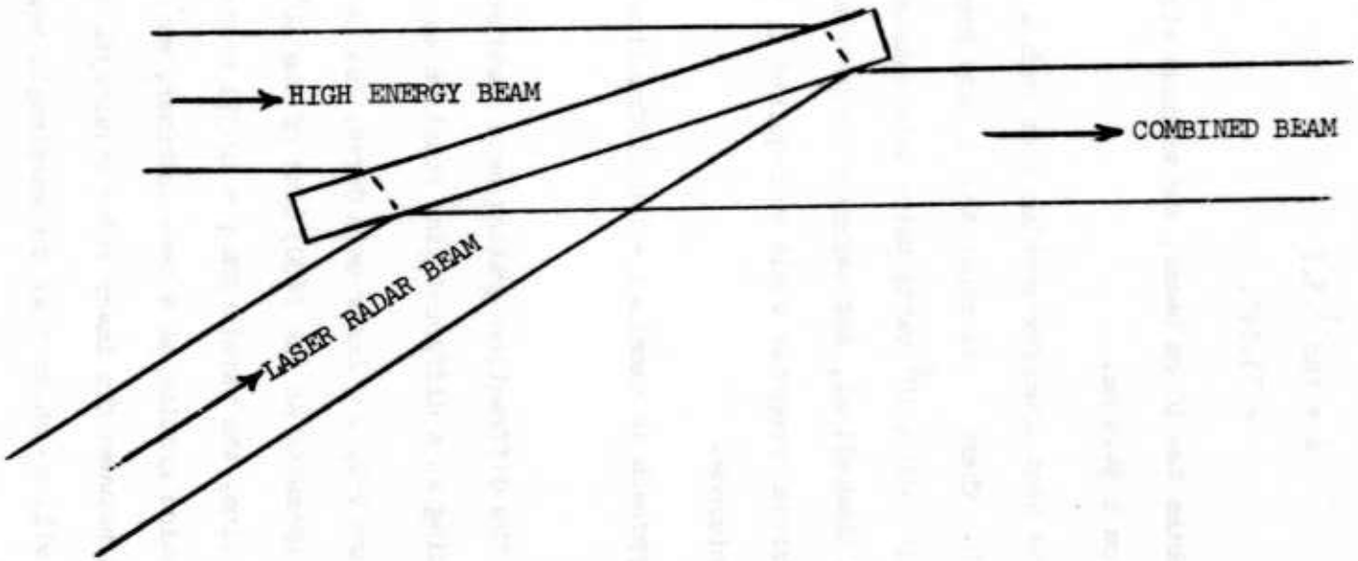

FIGURE V-1: BREWSTER ANGLE BEAM COMBINER

For GaAs whose index of refraction is 3.3, the Brewster angles is

$$\beta = \tan^{-1} 3.3$$
$$= 73.14°.$$

Then, in order to combine two 10 cm beams, the minimum size GaAs Brewster plate required is 10 cm x 34.5 cm.

An analysis of the heat transfer problem from such a beam combiner is given in Appendix D. There it is shown that a GaAs Brewster plate 1 cm thick could transmit 2.08×10^6 watts using thin channel cooling. However, this is only theoretical, and before a Brewster angle beam combiner can be recommended, further progress would be required in the high-energy window problem at 10 microns.

Thus, a second approach is examined - the diffraction grating beam combiner.

The principle of the diffraction grating beam combiner is to have the laser radar operating at a different line relative to the high-energy beam.

Referring to Figure V-2, CO_2 Laser Gain Curve, let us assume that the high-energy laser operates at the P(20) line of the $00^0 1 - 10^0 0$ vibrational band. For this P(20) line, the wavelength λ = 10.591 microns. Then in order to utilize the diffraction grating as a beam combiner, wavelength separation would be required between the laser radar wavelength and the high-energy laser wavelength. It will be shown that the wavelength separation should be as large as possible.

Thus, choosing the maxima of the various gain profiles, candidate wavelengths for the laser radar would be in the neighborhood of these

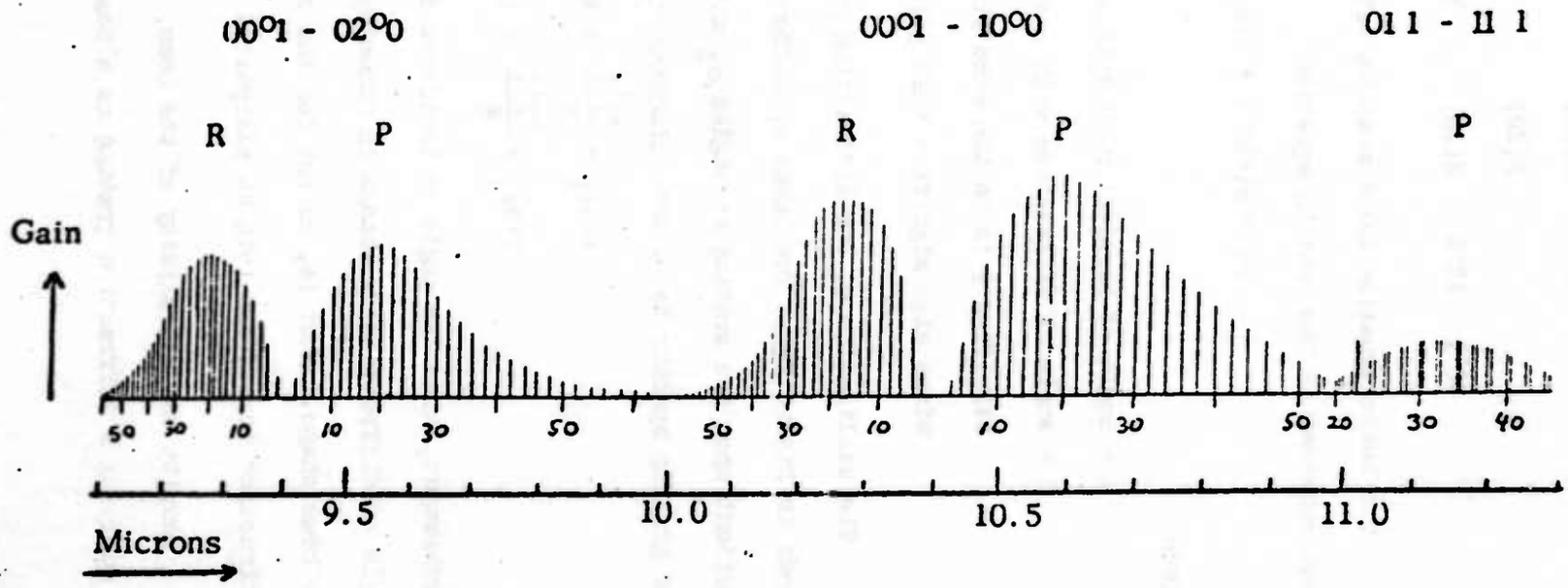

FIGURE V-2. - CO_2 Laser Gain Curve

maxima which are

00°1 - 02°0	R(20)	9.271 microns
	P(20)	9.552
00°1 - 10°0	R(20)	10.233

The basic equation which must be satisfied in a diffraction grating beam combiner is the grating equation

$$m\lambda = a(\sin\alpha \pm \sin\beta)$$

where

α = angle of incident rays with respect to the normal to the grating, and

β = angle of diffraction with respect to the normal. The plus sign signifies β is on the same side of the normal as α, while the minus sign signifies that β is on the opposite side.

The utilization of the diffraction grating as a beam combiner is shown in Figure V-3. Two beams of different wavelengths λ_1 and λ_2 are incident upon the grating at angles α_1 and α_2, respectively. Then, letting the grating spacing be a, the following equations must be satisfied:

$$\sin\alpha_1 = \frac{m_1\lambda_1}{a} + \sin\beta$$

$$\sin\alpha_2 = \frac{m_2\lambda_2}{a} + \sin\beta.$$

Furthermore, when the angle of incidence differs appreciably from the angle of diffraction, a change in geometry takes place with respect to the beam shape. That is, except for the zero order, a circular beam after diffraction transforms into an elliptical beam.

Despite the elliplicity of the beam, let us examine possible methods of applying a diffraction grating as a beam combiner. First, consider the

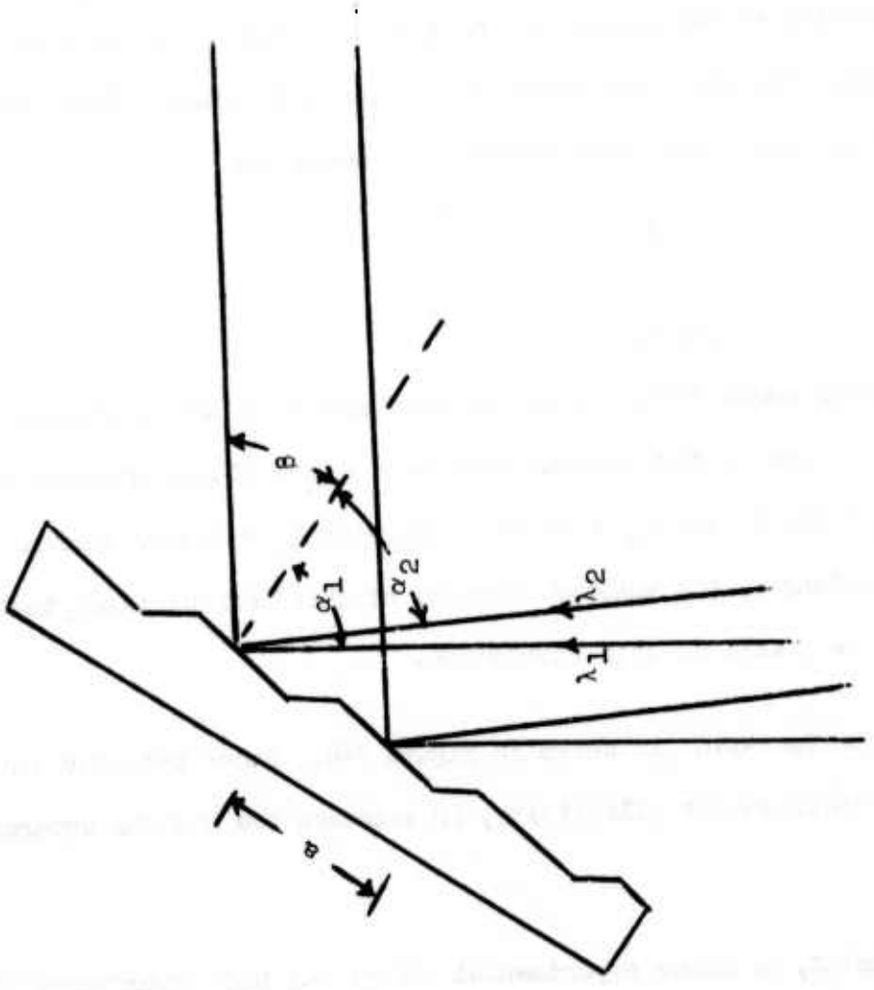

FIGURE V-3. GRATING GEOMETRY

grating equation

$$\sin i \pm \sin \theta = m \frac{\lambda}{a} .$$

To form a beam combiner, two beams at different wavelengths λ_1 and λ_2 are incident on the grating at two angles i_1 and i_2. The grating is designed to maximize diffraction into the first order (m = 1 for both beams. Thus, the grating equations for the first order diffraction beams are

$$\sin i_1 + \sin \theta = \frac{\lambda_1}{a}$$

$$\sin i_2 + \sin \theta = \frac{\lambda_2}{a} .$$

A number of different possibilities exist as combination of the different parameters, θ and a. One of the combinations is $a = \lambda_1 = 10.591$ microns, and $\theta = 35^\circ$. There $i_1 = 25.24^\circ$ and $i_2 = 17.57^\circ$. Choosing $\lambda_1 = 10.591$ microns as the high energy wavelength, the maximum transfer of this beam dictates that the grating should be blazed at this wavelength.

This configuration is shown in Figure V-4. Other possible configurations either increase the elliplicity, or decrease the angular separation of the beams.

At present, no known experimental effort has been undertaken to utilize a diffraction grating as a beam combiner at high energy densities. Many practical problems exist in such an application. Among these is the transfer efficiency of a diffraction grating into the first order. Although diffraction gratings can be designed to achieve as high as 95% efficiency, the 5% loss is divided between the zero order direction and scattering in other undetermined directions.

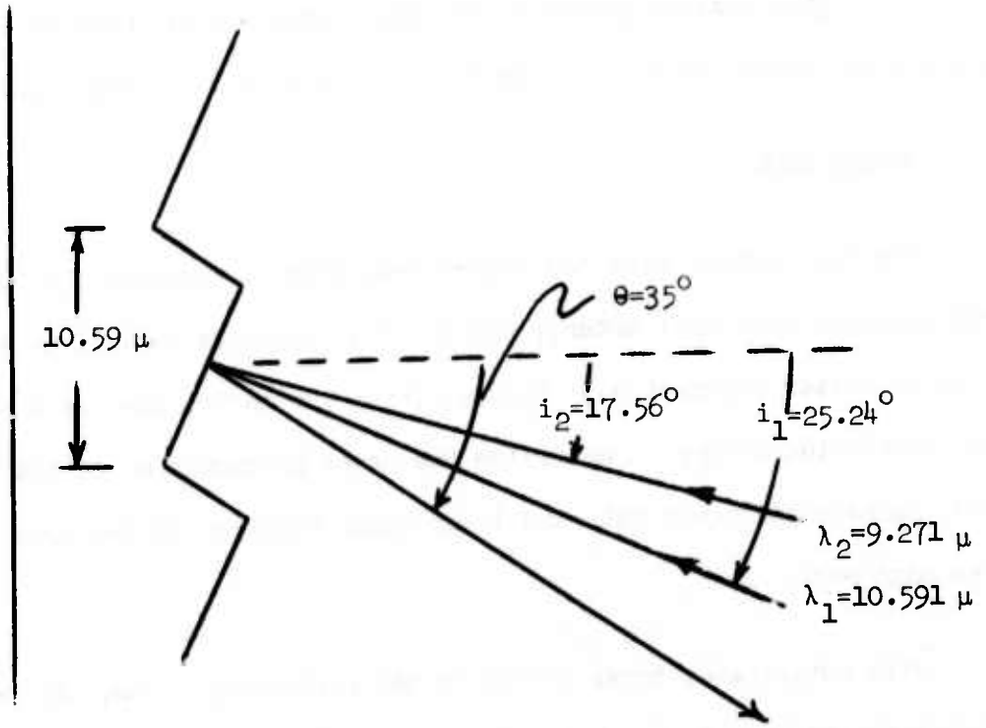

FIGURE V-4. DIFFRACTION GRATING BEAM COMBINER

If a significant part of the loss is scattering caused by the imperfections, a portion scattered energy would seriously affect the laser radar receiver detector response. In addition, slight variations in the grating pattern would give rise to "ghosts" resulting in effective loss of energy.

Other systems problems are also present which require further investigation before utilizing a diffraction grating as a beam combiner.

C. BACKSCATTER

The backscatter from the high-energy beam is examined for the shared aperture case (D=1 meter), and the dual aperture case (D=40 cm with 50 cm center separation.) Figures V-5. The curves are based upon single scattering theory to determine the order of magnitude of the anticipated backscatter power into the laser radar receiver system from the high-energy beam.

With anticipated power levels in the high-energy beam, the backscatter into the shared aperture system is of the order of milliwatts. In comparison, the backscatter into the dual aperture system is an order of magnitude less.

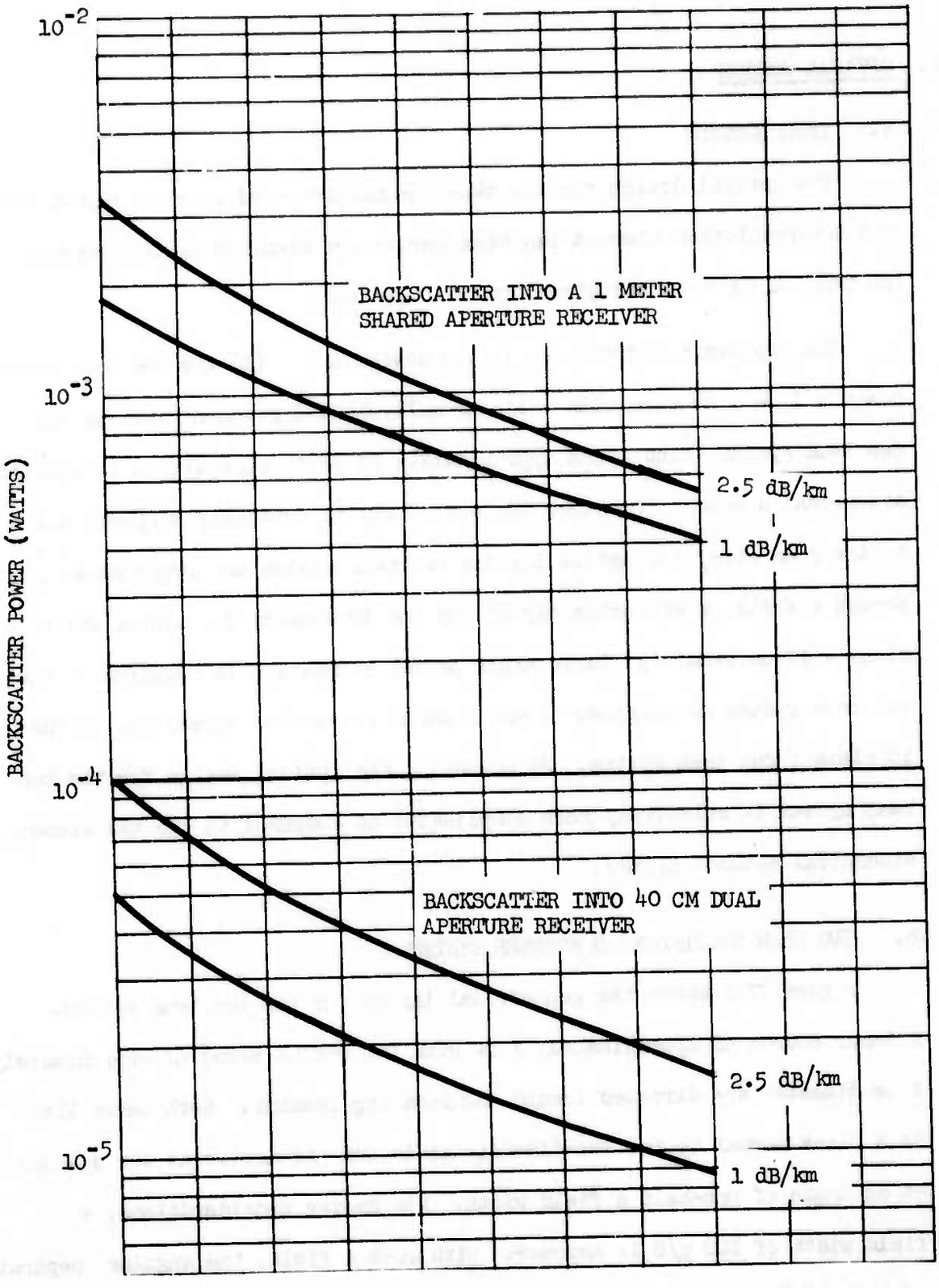

FIGURE V-5: COMPARISON OF RECEIVED BACKSCATTER FOR 1 METER SHARED APERTURE AND 40 CM DUAL APERTURE

VI. OPTICAL DESIGN

A. INTRODUCTION

The optical design for the two-beam multifaceted scanner system and the ten resolution element fan beam system are examined in this section. Geometrical layouts are given for each system.

The important differences in the design are: (1) the two beam system scans a 1 cm size beam with a linear multifaceted scanner; whereas the fan beam system scans a fan approximately 10 cm in size with a torsional sinusoidal scanner; (2) since the scan field is inversely proportional to the beam size, the optics for the two beam system are required to accept a field of approximately 6° for the 10 element fan system which scans a 10 cm beam; (3) large angle offset correction is required in the two beam system as compared to small angle sinusoidal correction in the 10 element fan beam system. As a result, the optical design for the two beam system is relatively more complicated as compared to the ten element sinusoidal scanner system.

B. TWO BEAM MULTIFACETED SCANNER SYSTEM

Figure VI-1 shows the geometrical layout for the two beam system. A laser source of approximately 1 kw with two output beams of approximately 1 cm diameter are directed toward the rotating scanner. Both beams lie in a plane normal to the two-dimensional layout and arrive at the scanner at an angle of one-half a field width. For design considerations, a field width of 100 λ/D is assumed. With such a field, the angular separation of the two beams is 50 λ/D = 53 mrad for λ = 10.6 microns and D = 1 cm.

In order to maintain a reasonable size for the 10:1 folded off-axis telescope, the two beams are superimposed on the scanner surface. With

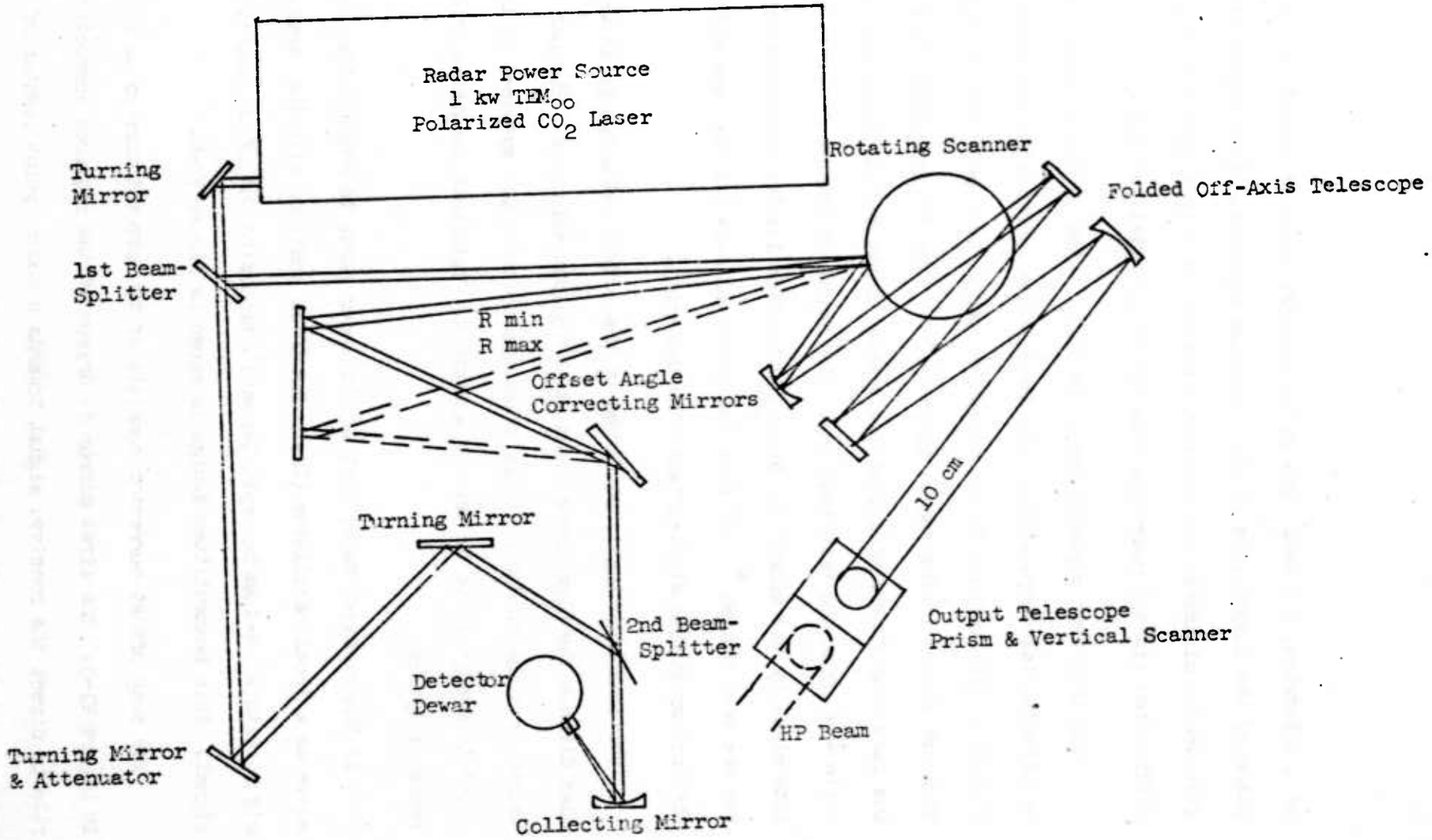

Figure VI-1. Geometrical Layout of the Two Beam System

as a criterion, the beam size in the scanner plane is imaged in the plane of the output lens of the 10:1 beam expander. (See Figure VI-2). This design minimizes the aperture size of the output lens with near-diffraction limited operation over the entire field of 100 λ/D.

The 10:1 beam expander design is illustrated in Figure VI-3. In an off-axis telescope system, the aberrations increase in the radial direction with respect to the telescope axis. Two beams with 3° separation are placed in the radial plane ($\pm$ 1.5° from the principal ray). The fast scan (horizontal scan) is normal to the radial plane over an angle $\pm$ 3° from the principal ray. The length of the telescope is then determined by the elngth for which diffraction limited operation exists for the beam placed $\pm$ 1.5° from the principal axis (or the beam with the maximum radial displacement from the axis).

Vertical scanning is performed by the output telescope prism which also directs the high-energy beam ot the output telescope. The path length from the folded off-axis telescope to the input eyepiece of the ouput telescope is to be kept to a minimum. This path length is of the order of 130 cm.

In the receiver path, part of the laser power is beamsplitted to serve as a local oscillator (LO). The LO is combined with the received signal with a low-loss beamsplitter which transmits 98% of the received signal. This beamsplitter design is shown in Figure VI-4.

The scan offset corrector consists of two pivoted mirrors as shown in Figure VI-5. The first mirror is driven at the required correction rate to direct the received signal towards a common point (center of rotation of the second correction mirror). The second mirror directs the received signal to the detector.

FIGURE VI-2:

TELESCOPE MULTIFUNCTION

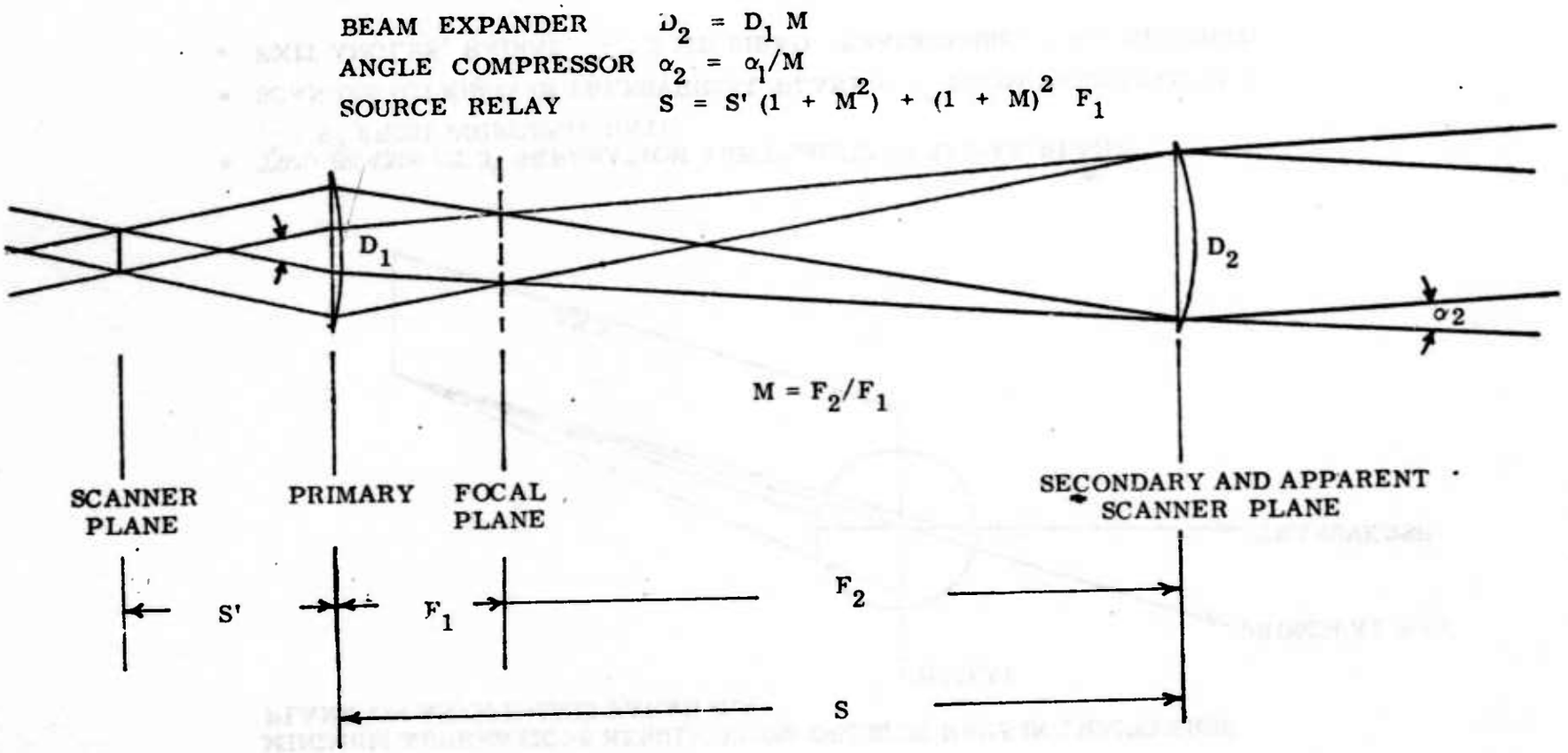

FIGURE VI-3: TWO SINGLE RESOLUTION ELEMENT BEAM SYSTEM INTERMEDIATE TELESCOPE DESIGN

MINIMUM ABERRATIONS RESULT FROM OBLIQUE RAYS IN TRANSVERSE PLANE ON AN OFF-AXIS PARABOLA

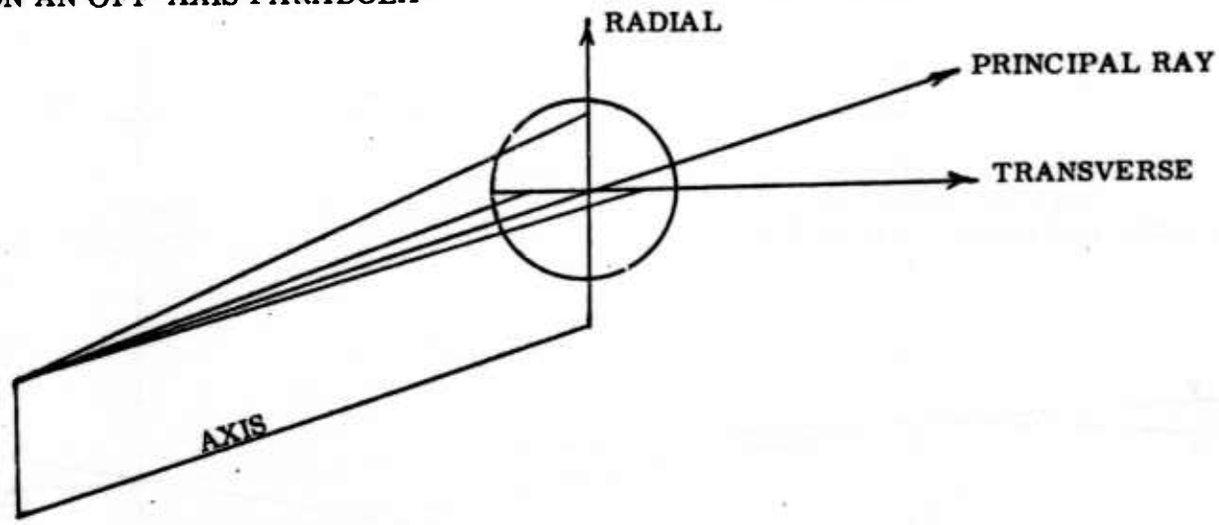

- TWO BEAMS AT 3^{o} SEPARATION ARE PLACED IN RADIAL PLANE ($\pm 1.5^{o}$ FROM PRINCIPAL RAY)
- SCAN DIRECTION IS IN TRANSVERSAL PLANE ($\pm 3^{o}$ FROM PRINCIPAL RAY)
- EXIT ANGLES, RADIAL: $\pm$ 2.5 MILLIRAD; TRANSVERSE: $\pm$ 5.0 MILLIRAD

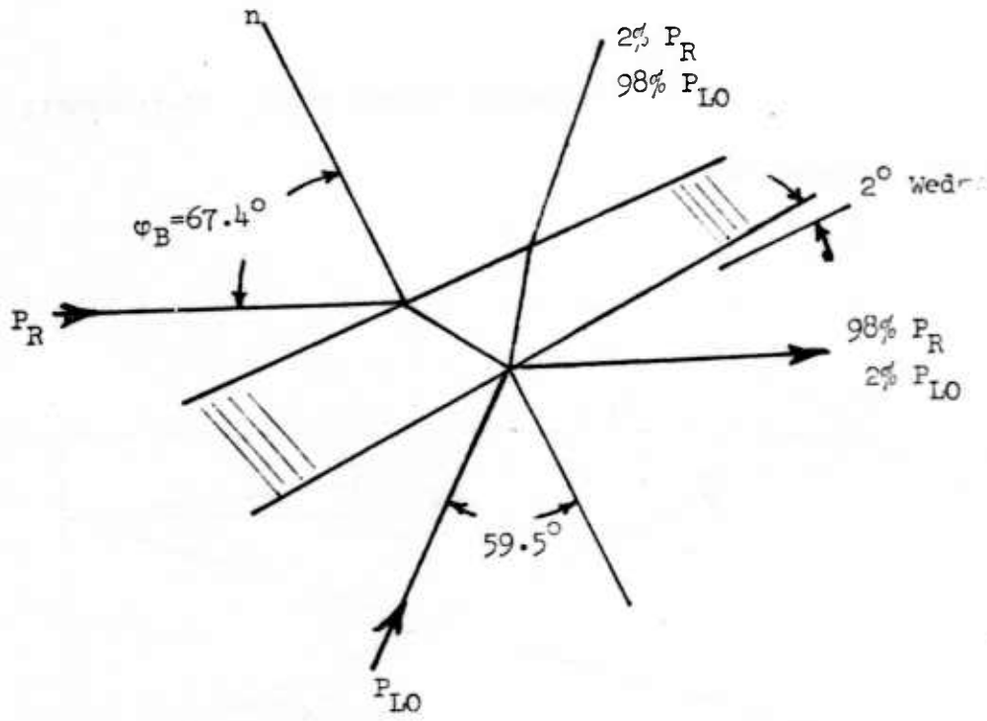

Low Loss Receive Power Mixing Beam Splitter Material:
ZnSe (n = 2.404 @ 10.6μm)

FIGURE VI-4: RECEIVER LOW LOSS BEAMSPLITTER

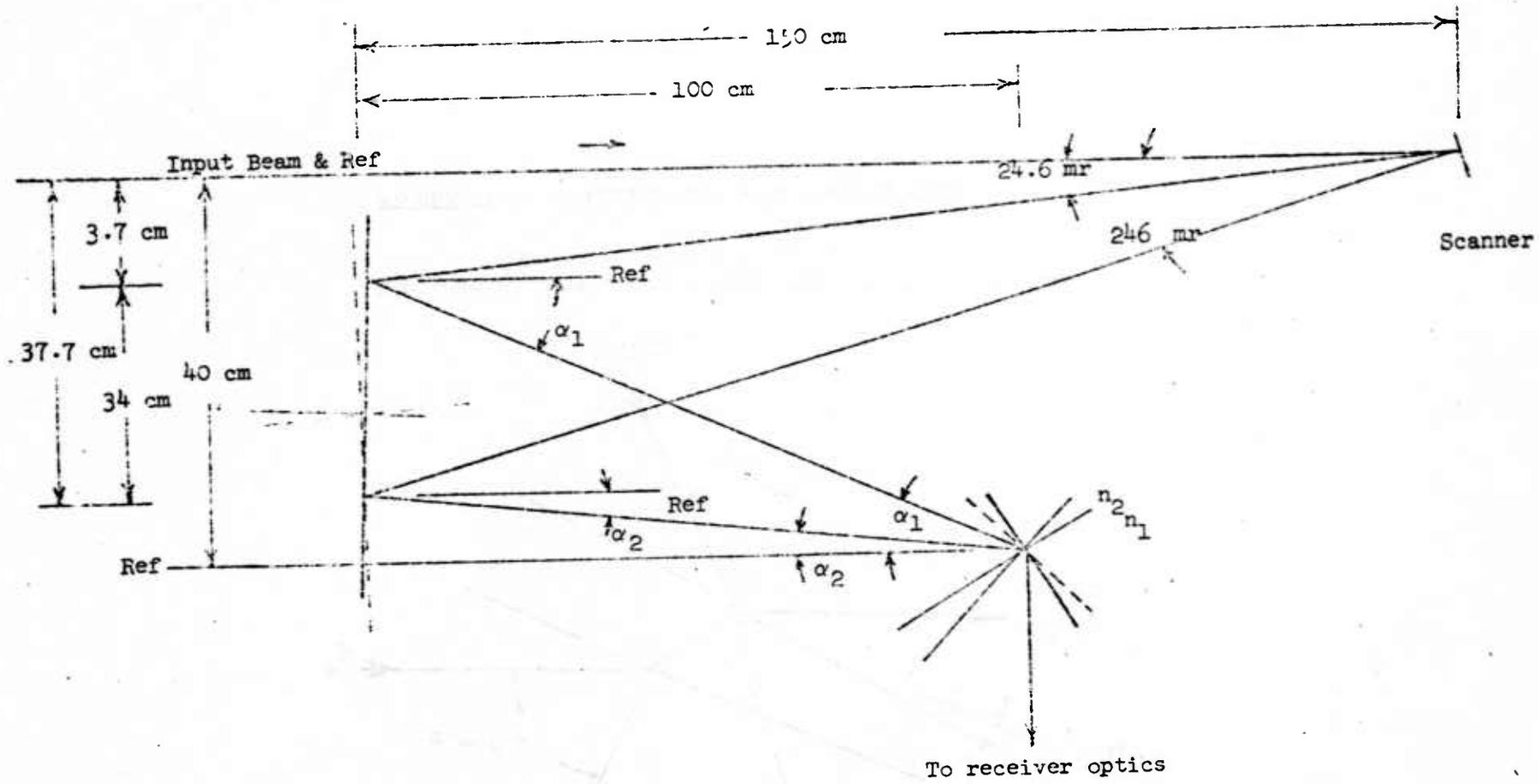

Figure VI-5: Scan Offset Corrector

The offset corrector design shown is based upon a minimum target range of 1 km and a maximum target range of 10 km. At the minimum target range, the offset correction required is approximately 20 mrad which eliminates the requirement of a beamsplitter to separate the transmit signal from the receive signal.

C. TEN-ELEMENT FAN BEAM SYSTEM

The basic design of the ten-element fan beam system is shown in Figure VI-6. In this system, the output of the laser is expanded to a 10 cm beam where it is fanned over ten resolution elements by a cylindrical diverging lens. The fan beam is then directed to the output telescope prism through a 50-50 beamsplitter. The output telescope prism also functions as a combined horizontal and vertical scanner. The 50-50 beamsplitter is the principle element in the development of the receiver interferometer. The receiver collection system is designed to meet the requirements of a ten-element detector array.

The ten power telescope used in this system can be designed easily since there is no field angle coverage problem involved in the design of this telescope. Its overall length can be as low as 50 cm and still maintain diffraction-limited operation.

The fan angle produced by the diverging lens (one plane only) for a ten resolution element fan is approximately one milliradian. This angle is sufficiently small as to have no adverse effects at the beamsplitter and to not produce a significant increase in beam size at the output prism. Upon arriving at the output prism-scanner, a scan pattern is produced as shown in Figure VI-7. In order to have 100% field coverage, the fast scanner operates at 1 KHz and the slow scanner operates at 50 Hz. This provides 100 frames/sec by scanning each frame in reverse order relative to the slow direction of the preceding frame.

During the retrace of each fast scan cycle, a partial overlay of the preceding scan occurs. The overlay pattern results in covering each resolution element of the field twice.

The received signal is reflected from the beamsplitter and mixed with the local oscillator beam. The mixed beam is directed towards the scan offset corrector and then through the beam reducing and image forming optics to the ten-element detector array. The requirements of the scan offset angle correction varies from 0.2 mrad to 4 mrad. Since the scan offset correction is a sinusoidal correction

$$\Delta\theta = 2\theta_o \sin \omega \frac{R}{C} \cos(\omega t - \omega \frac{R}{C})$$

(where $\theta_o = 50\ \lambda/D$, the beam scan amplitude), the offset corrector is controlled in phase and amplitude at the 1 KHz frequency of the main scanner.

The refracting telescope is designed in the receiver instead of a reflecting telescope because of the requirement of a very large F-number collecting lens for use with array element detectors. F-numbers required are in the range F-90 to 300. In the receiver section, the transmitted power is low (maximum 0.1 watt); thus, germanium or GaAs lens would be suitable, eliminating the necessity of complex off-axis telescope in this section.

D. OUTPUT TELESCOPE

The same output telescope design is applicable for both designs, the two-beam and fan beam system. The laser radar beam and the high energy beam ($\sim$ 10 cm) are directed toward the secondary of a 4-power Cassegrain telescope as shown in Figure VI-8. The primary output is directed into a 1 meter aperture tracking Coelostat.

This type of design was selected to provide automatic focusing of both beams at the target range by appropriate motion of the secondary lens.

A conventional design 4 power Cassegrain telescope serves as the output telescope with separate halves of the telescope being used for either the high energy beam or the laser radar.

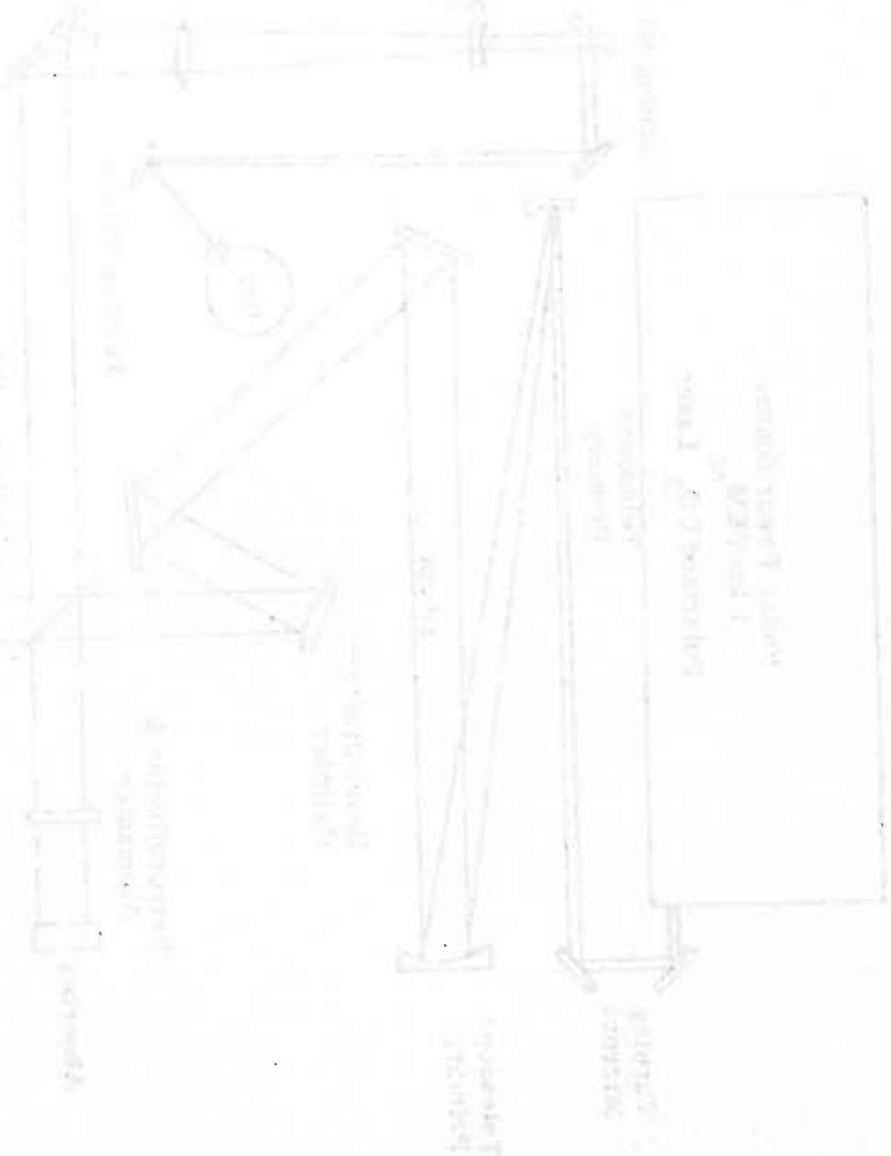

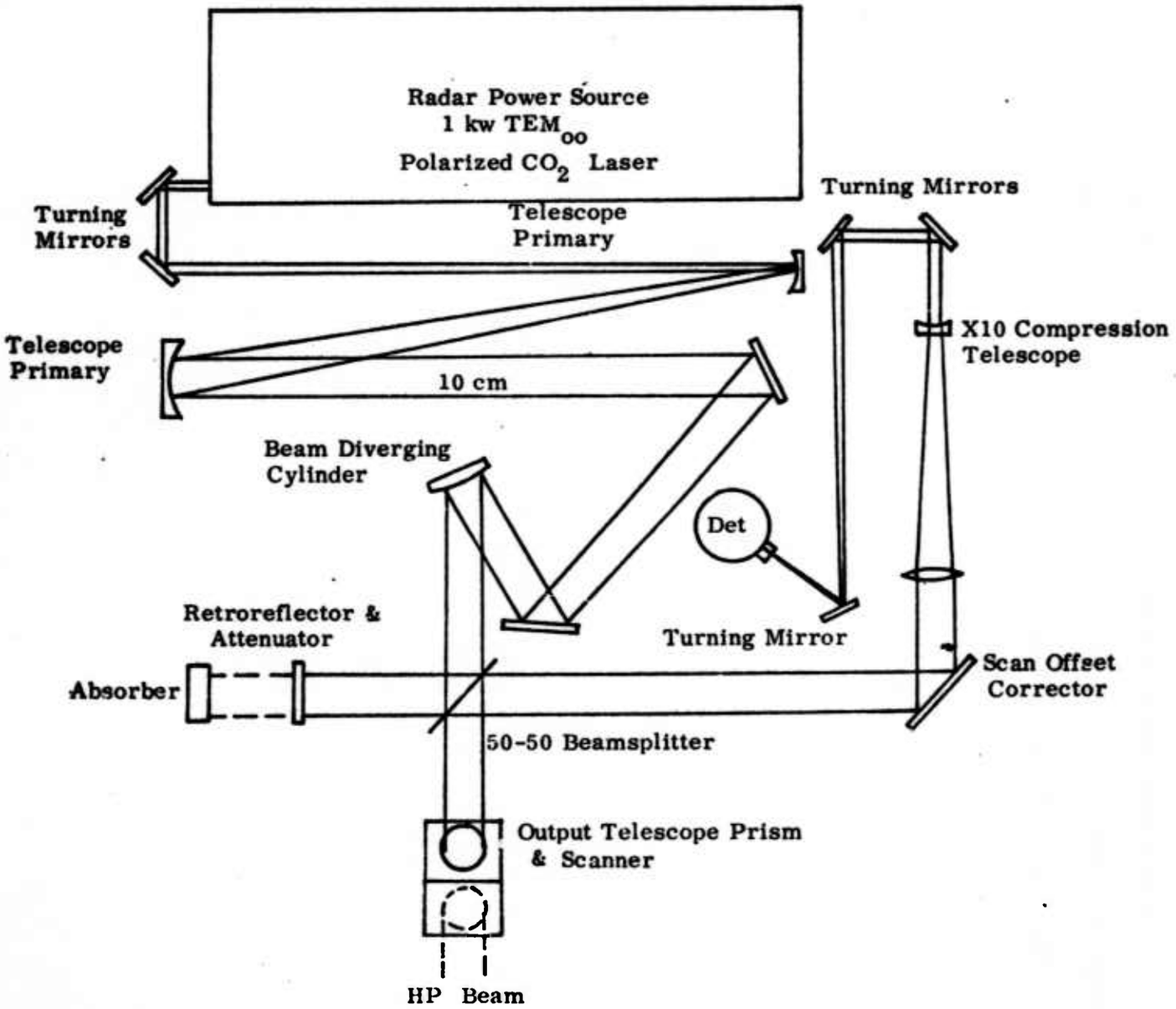

Figure VI-6: Geometrical Layout of the Fan Beam System

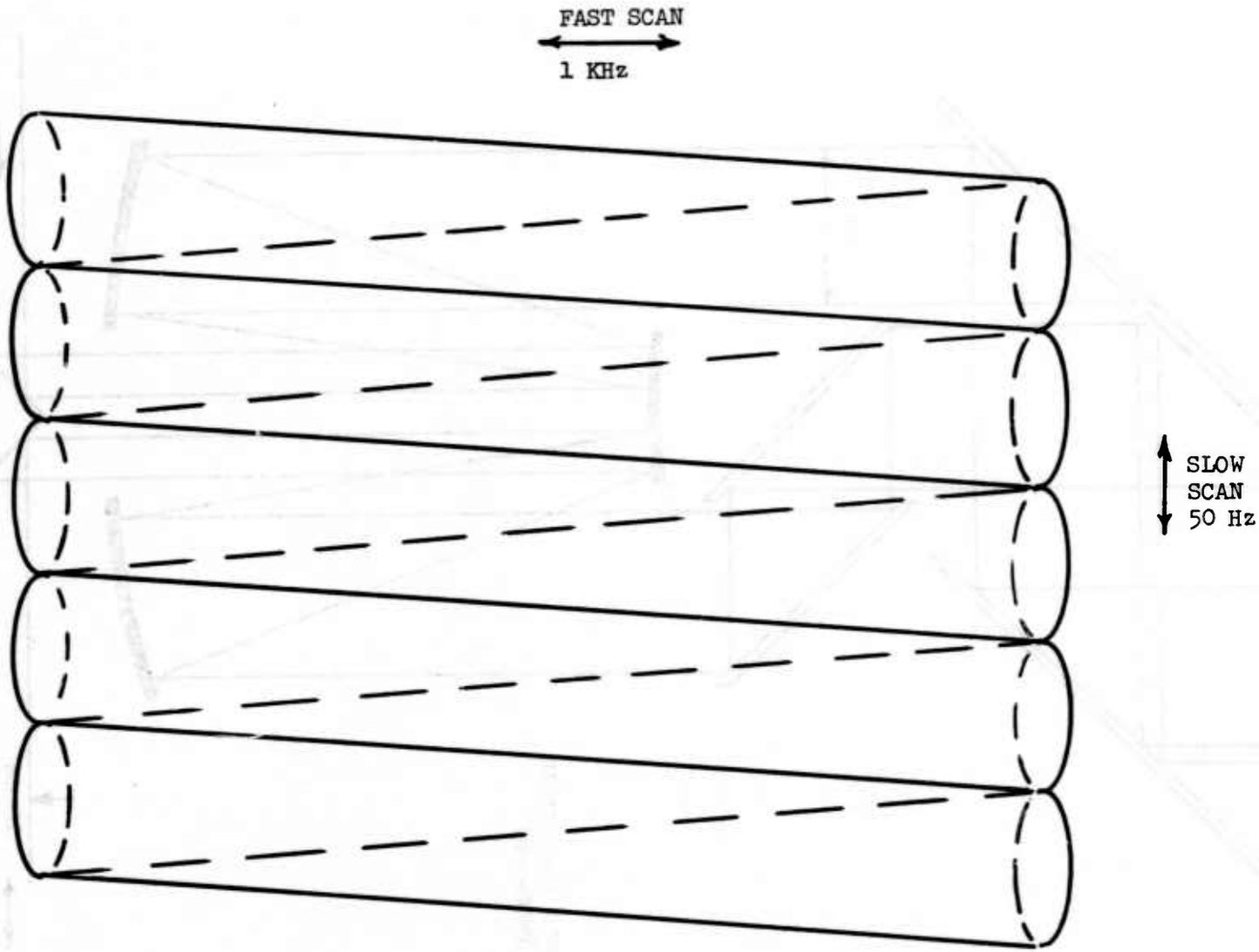

FIGURE VI-7: SINUSOIDAL SCAN PATTERN FOR 10-ELEMENT FAN BEAM

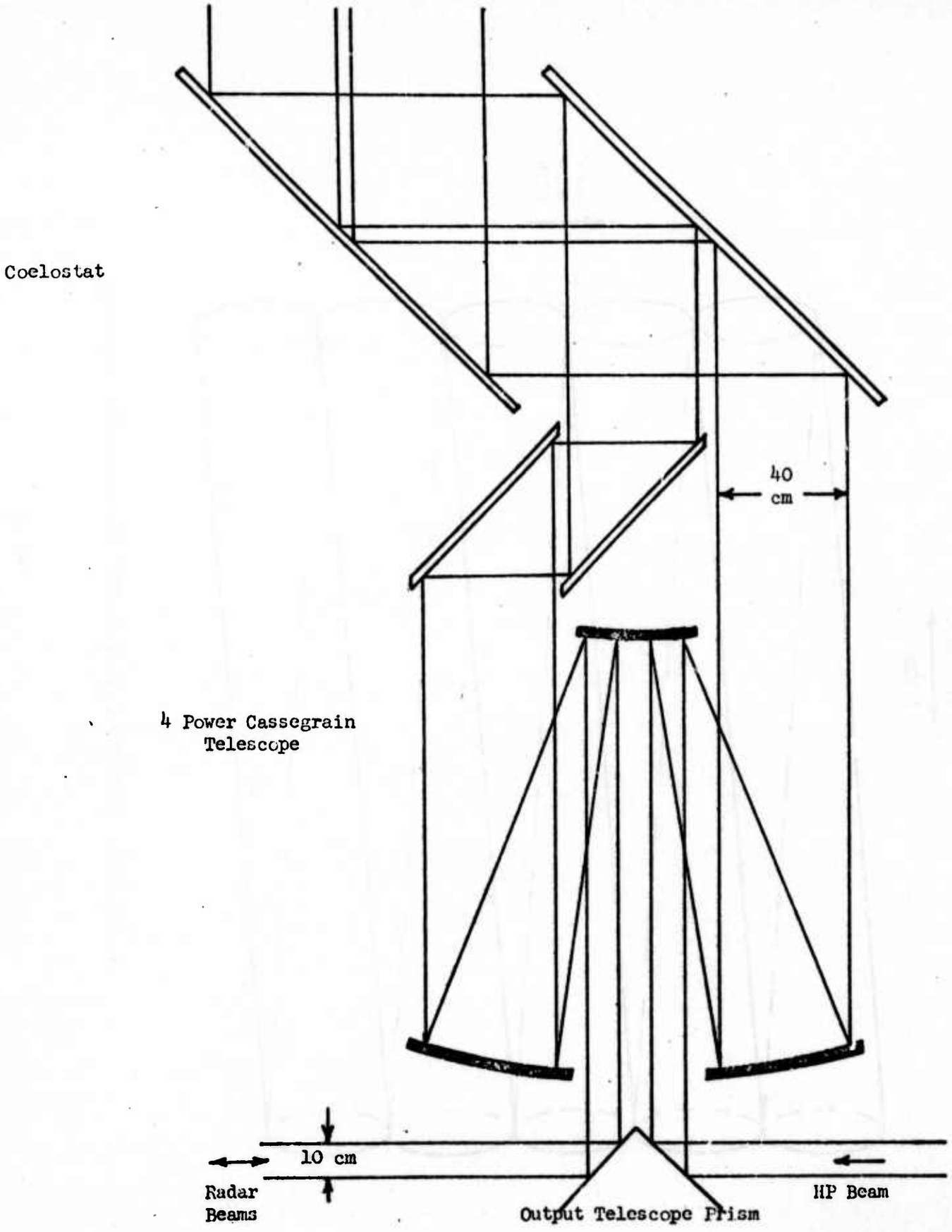

Figure VI-8: Output Telescope Configuration

VII. CONCLUSIONS AND RECOMMENDATIONS

A. CONCLUSIONS

The study effort has determined the utility of mechanical scanning techniques to a laser radar for fine-grained target imaging and tracking of aircraft targets with velocities of Mach 2. The laser radar system is to operate in conjunction with a high energy laser system. The base line requirement is for a high efficiency system with 100 x 100 diffraction-limited resolution elements operating at 100 frames per second with an output aperture of 1 meter and 5 KW of laser radar transmitting power at 10.6 microns using either a single detector element or a linear array.

The base line requirement of 100 x 100 diffraction-limited resolution elements operating at 100 frames per second can be met with either of two types of scanning systems: (1) the multifaceted rotating scanner; or (2) the torsional oscillating scanner.

In order to operate diffraction-limited over the field of 100 x 100 resolution elements, the multifaceted rotating scanner is limited to either a single beam system or a two beam system. Optical aberrations become too severe when more than two beams are used to scan the 100 x 100 resolution element field. The development of a single beam multifaceted scanner system is possible, but the range is limited to 10 KM without exceeding the distortion limits of the scanner using beryllium as the material. The use of tool steel as the multifaceted scanner material limits the range to 6.5 KM. (In the design of a multifaceted scanner, the radius of the scanner is related to

the maximum target range. An increase in range relates to an increase in scanner radius and thus an increase in scanner surface distortion.)

The development of a two beam multifaceted scanner system permits detection of target ranges up to 18 KM. This range limit is set by the manufacturer's scanner radius limit of 15 cm which is established by current fabrication facilities. Although the two beam system is feasible, the high speed multifaceted rotating scanner system presents extremely difficult offset angle correction problems. To correct for the offset angle cause by the transit time effect in a two beam system with a target at 18 KM range, the required offset angle corrector mirror size is approximately 60 cm. In addition to achieve optimum performance, this system requires accurate range information. The accuracy requirement in the range information is dictated by the average error in the offset corrector which results in signal loss. In the two beam multifaceted scanner system, a range accuracy of the order of $\pm$ 50 meters results in an effective loss in signal-to-noise of 30% relative to the peak signal-to-noise.

The torsional oscillating scanner is limited in its rate of operation. A rate of 1 KHz, however, is practical. Thus, the torsional oscillating scanner can be operated to scan a ten resolution element fan operating at 1 KHz or a 100 resolution element full fan operating at 100 Hz. To prevent distortion from limiting the operation of the torsional oscillating scanner, this scanner scans a 10 cm size beam. Thus, the torsional scanner is required to scan a field of 0.6° corresponding to 100 resolution elements; whereas, the multifaceted scanner which scans a 1 cm size beam is required to scan 6°

to cover the 100 resolution elements. (The beam size of 1 cm on the multifaceted scanner was selected to maintain as high an efficiency as reasonably possible for the scanner. (The beam size corresponds to the scanner "dead time" and affects the size and efficiency.)

The torsional oscillating scanner can be developed for a full fan system (100 resolution element fan) which sweeps across the field or for a ten resolution element fan which raster scans the field. The full fan systems require narrow Doppler bandwidth filters which present the problem of requiring extremely large numbers of filters to process targets with velocities up to Mach 2.

Thus, although any of four types of systems meet the base line requirement of scanning 100 x 100 diffraction-limited resolution elements operating at 100 frames per second; the four systems can be ordered in their degree of simplicity as follows:

1. The development of the ten resolution element fan system is the least complicated upon balancing the complexities of performing offset correction, designing the scanner, and processing the received signal.

2. The development of the two beam multifaceted scanner system requires the design and fabrication of a 15 cm radius multifaceted scanner, design and fabrication of complex optics to scan a 1 cm beam, and the design and fabrication of an extremely large offset angle corrector.

3. The development of a single beam multifaceted scanner system is approximately as complex as the two beam system and results in a range limitation of 10 KM.

4. The development of the full fan system simplifies the scanner mechanics at the expense of the requirement for an extremely large number of filter elements in the receiver processor.

In conclusion, the ten resolution element fan system appears to be an optimum compromise among the systems. This conclusion is reached for the following reasons:

1. The performance of the ten resolution element fan is not degraded by range accuracy requirements. This system operates near optimum performance with large tolerances in the range data. Even with range data that is only accurate to within $\pm$ 400 meters, the effective loss in signal-to-noise is less than 30% of the peak value.

2. A sinusoidal offset angle corrector which is servo controlled to the main scanner can be designed and implemented into the system.

3. The electronic processor requires only a reasonable number of filter elements to process the total Doppler bandwidth for a Mach 2 type target.

4. In comparison to a multifaceted scanning system, the optical design of the ten resolution element fan system is simpler and requires fewer components.

5. There appears to be no range limitation on the ten resolution fan system which is an advantage in future growth of the system. The two beam multifaceted scanner system is limited to approximately 18 KM range in its application; whereas, the ten resolution element fan beam system could be applied in fine-grained target imaging and tracking of satellites.

The ten resolution element fan beam system utilizes a ten element detector array in the receiver. The study has shown that the optimum size detector is the Airy disc size detector (2.44 λ/D). With such a detector array, the optical cross-talk can be reduced below 40 dB for detectors arrayed with a spacing of the order of 10% of the detector size. In addition, radiative cross-talk can be virtually eliminated by copper shielding the detectors from each other.

The base line requirement of a 1 meter output aperture requires that the high energy laser and the high performance laser radar share a common output aperture. A beam combiner is required in order to implement a shared aperture system. In the study, two types of beam combiners were investigated for application in combining the high energy laser beam and the laser radar beam. The two types studied were the Brewster angle beam combiner and the diffraction-grating beam combiner. Neither were considered within the present state-of-the-art for near term application. The Brewster angle beam combiner requires transmission of high energy densities through optical material. The absorption of current optical materials is not sufficiently small to permit operation at high energy densities. Thus, until adequate

transmissive materials are developed to operate at 10.6 microns, the Brewster angle beam combiner technique would not be suitable.

The diffraction grating beam combiner can be designed to operate at 95% efficiency. But to be acceptable, a beam combiner would have to operate near 100% efficiency with respect to the high energy beam without random scattering. A few percent scattering of the high energy beam uniformly over 2π steradians would be sufficient to damage the laser radar receiver detectors. Thus, the diffraction-grating beam combiner was also considered as not presently state-of-the-art.

As a result of the lack of a suitable beam combiner, the recommended system is based upon a dual aperture system consisting of two 40 cm apertures spaced approximately 10 cm (edge-to-edge). Each 40 cm aperture is part of a common 1 meter Cassegrain telescope such that both beams can be commonly focused by slightly motion of the secondary of the telescope.

The base line requirement of a 5 KW laser transmitter is approached by available current lasers. The GTE Sylvania Gas Transport Laser Model 971 is a high power, transverse flow laser with a continuous power output of 1 KW operating in TEM_{oo}. This laser has a beam diameter of approximately 13 millimeters measured across the $1/e^2$ intensity limits with a beam divergence of less than 1.3 mrad.

B. RECOMMENDATIONS

In the above discussion, it has been concluded that any of the four systems could be developed. The system which is recommended for

development is the ten resolution element fan beam system which is the simplest of the four systems. To initiate the development of this sytem, it is recommended tnat a design, fabrication and testing program be pursued on the critical components of the system. This includes the 1 KHz scanner which is required to scan a 10 cm beam through 100 resolution elements (approximately 0.6°), the offset corrector which is servo controlled to follow the main scanner, and the fan beam generator optics. This phase of tne program can be fully tested at reasonable ranges with a design which incorporates all of the laser radar design with the exception of the output telescope which expands the beam from 10 cm to 40 cm.

The current recommendation is for the development of a dual aperture system to direct the high energy laser on the target and operating in conjunction with the laser radar. However, because of the advantage of gaining an increase in power density and higher signal-to-noise with a 1 meter aperture (as compared to 40 cm dual apertures), it is also recommended that there be a development of an efficient beam combiner to permit the use of a shared aperture design. The efficiency of the beam combiner must approach 100% with respect to the high energy beam.

APPENDIX A: SIGNAL POWER IN HETERODYNE DETECTION WITH BEAM CENTER DISPLACEMENT AND DETECTOR SIZE VARIATIONS

Cathey[1] has shown that in heterodyne detection, the distribution of the signal amplitude over the detector varies as

$$A_o J_1(kaw)/(kaw)$$

where A_o is the amplitude of the reference beam, $J_1(kaw)$ is the Bessel function of the first kind and first order, $k = 2\pi/\lambda$, λ is the wavelength of illumination, a is the radius of the aperture, and w is a radial variable in the focal plane. Thus, to determine the resultant signal amplitude on a detector when the beam is displaced from the center of the detector requires a solution to

$$2A_o \iint \frac{J_1(kaw)}{kaw} \; w \, dw \, d\varphi \qquad (1)$$

with limits of integration defined by the detector size and position (see Figure 1).

For the special case where the beam is centered on the detector, Cathey has shown that the resultant amplitude is

$$A = C\left[1-J_o(kaw)\right] \qquad (2)$$

where C is a constant containing A_o and terms arising from integration. Thus, for the case of the beam centered on the detector, the heterodyne signal power is proportional to

---

[1] W. T. Cathey, "Signal Power in Heterodyne Detection as a Function of the Number of Airy Rings on the Detector," IEEE Proceedings, 56, 1968.

$$\left[1 - J_o(kaw)\right]^2 \qquad (3)$$

which is plotted in Figure 2 in normalized units $N = w/w_o$, where $w_o = 1.22\,\lambda/D$, the radius of the Airy disc in the Fraunhofer pattern.

For the general case in which the beam center is displaced from the detector center, the integral (1) cannot be determined except by numerical integration. Referring to Figure 3, the numerical integration was performed by summing the amplitudes of incremental areas of the detector, or

$$A = 2\sum_{n=1}^{N}\sum_{m=1}^{M}\Delta A_{nm} \qquad (4)$$

where

$$\Delta A_{nm} = \frac{J_1(R_{nm})}{R_{nm}}\; r_{nm}\,\Delta r\,\Delta\theta \qquad (5)$$

R = kaw, R_{nm} radius of the element from the beam center

r = kav, radius of the element from the detector center

θ = angle of the element measured with respect to the detector center.

$\Delta r = r_o/N$

$\Delta\theta = \pi/M$

r_o = radius of the detector

The resultant sum, equation (4), was then squared and normalized with respect to the corresponding value when the beam is centered on the detector. Figure 4 shows the behavior of the signal power on the detector as the beam is displaced from the center of the detector. The function

plotted in Figure 4 is

$$\left(\frac{A}{A_o}\right)^2\left[1 - J_o(kaw)\right]^2 \qquad (6)$$

where $\left[1 - J_o(kaw)\right]^2$ is the behavior of the signal power on the detector when the beam is centered on the detector.

The computer program is given in Table 1. An effective mesh size of 9000 elements was used in the program. To check the accuracy, the mesh size was increased by a factor of 4 with less than 0.1% change in value.

The radius of the element R_{nm} from the beam center is determined by

$$R_{nm}^2 = r_{nm}^2 + x^2 - 2r_{nm}x \cos \theta$$

where x = beam center displacement relative to the detector center.

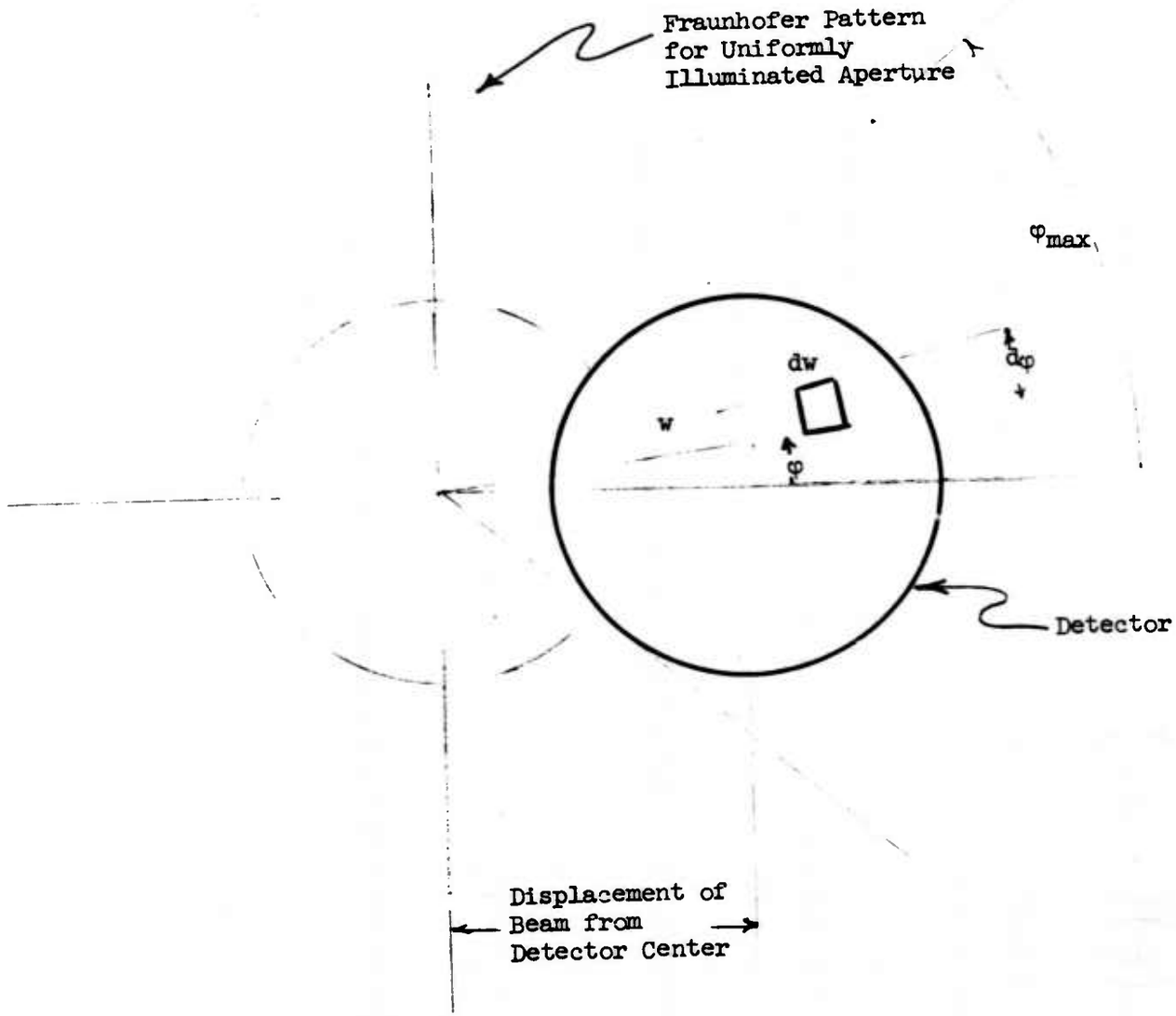

FIGURE 1: GEOMETRY OF $\iint \frac{J_1(kaw)}{(kaw)} w\, dw\, d\varphi$

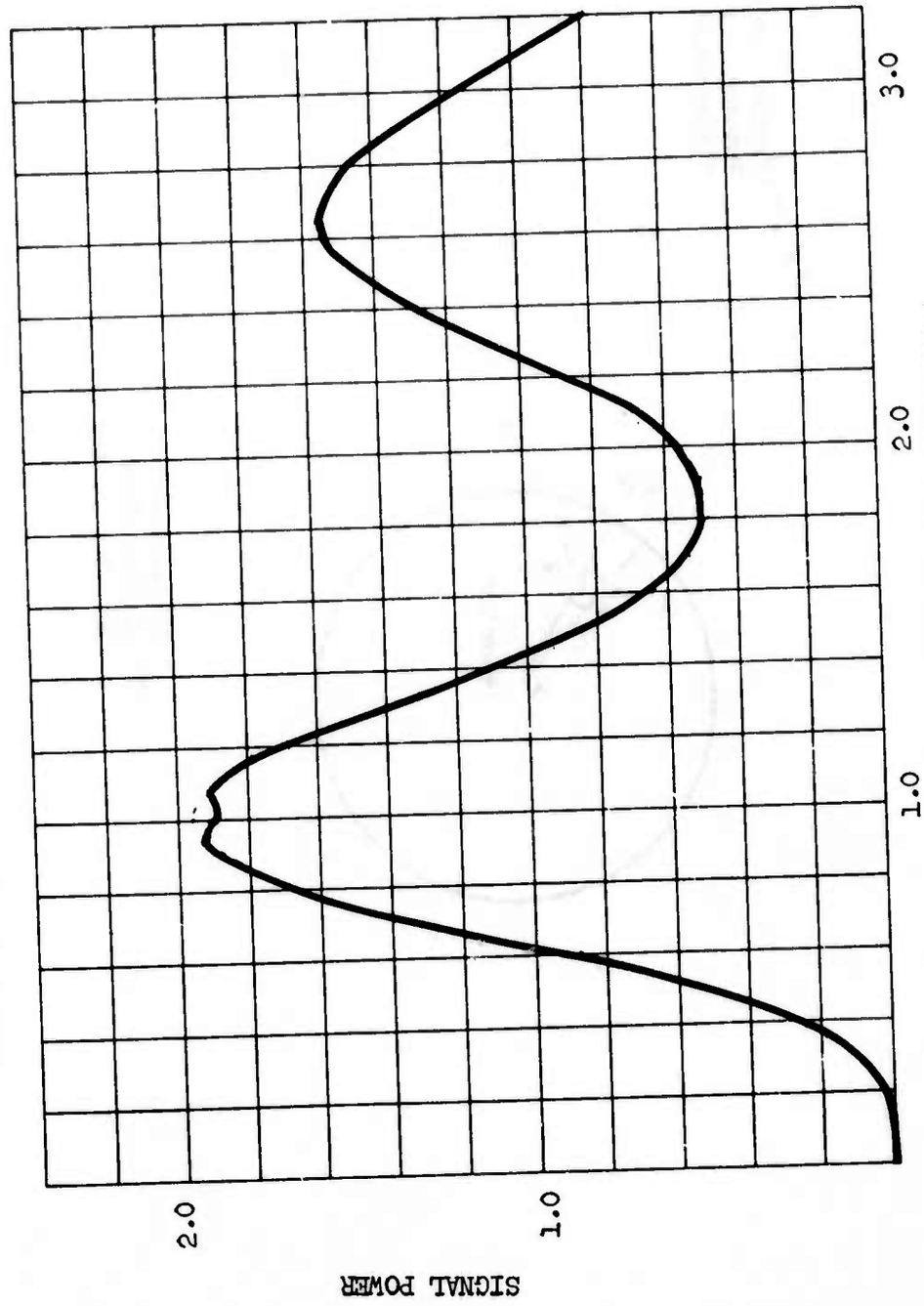

FIGURE 2: SIGNAL POWER ON DETECTOR WHEN COHERENT HETERODYNE DETECTION AND PLANE REFERENCE WAVE IS USED

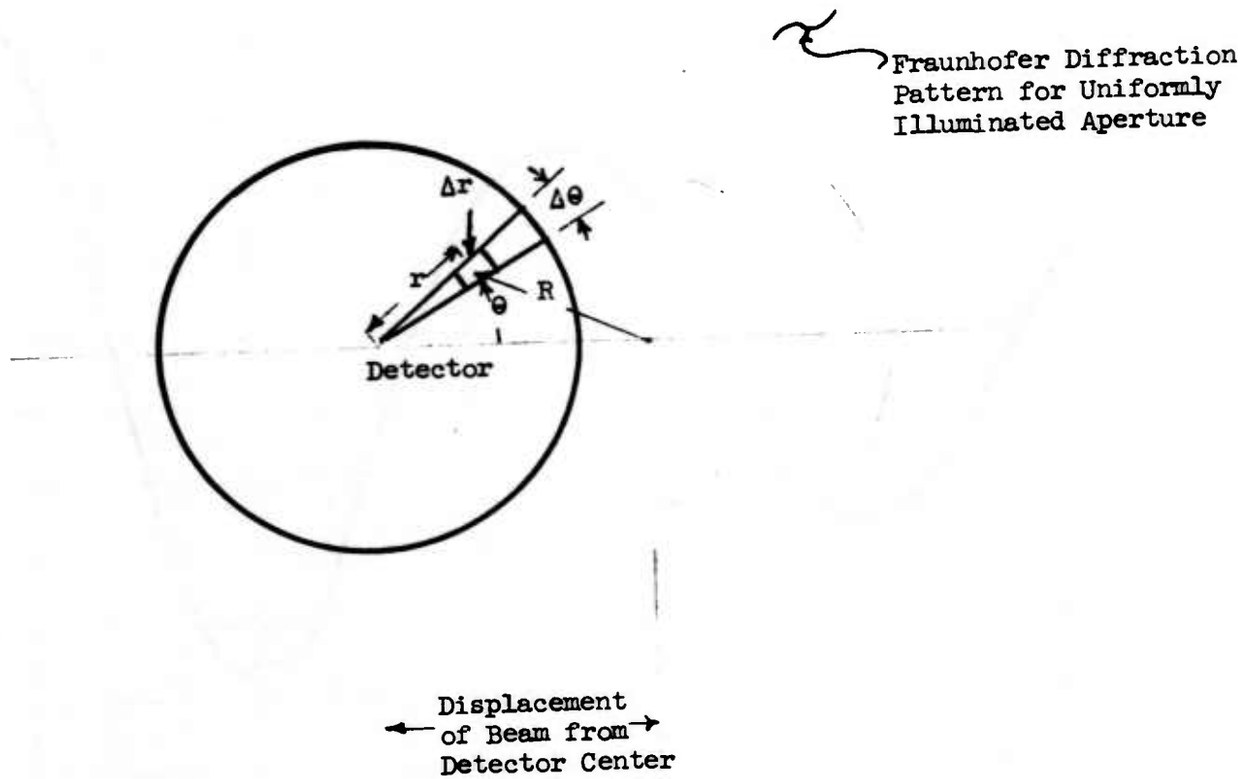

Figure 3: Geometry for Numberical Integration of the Heterodyne Signal Amplitude

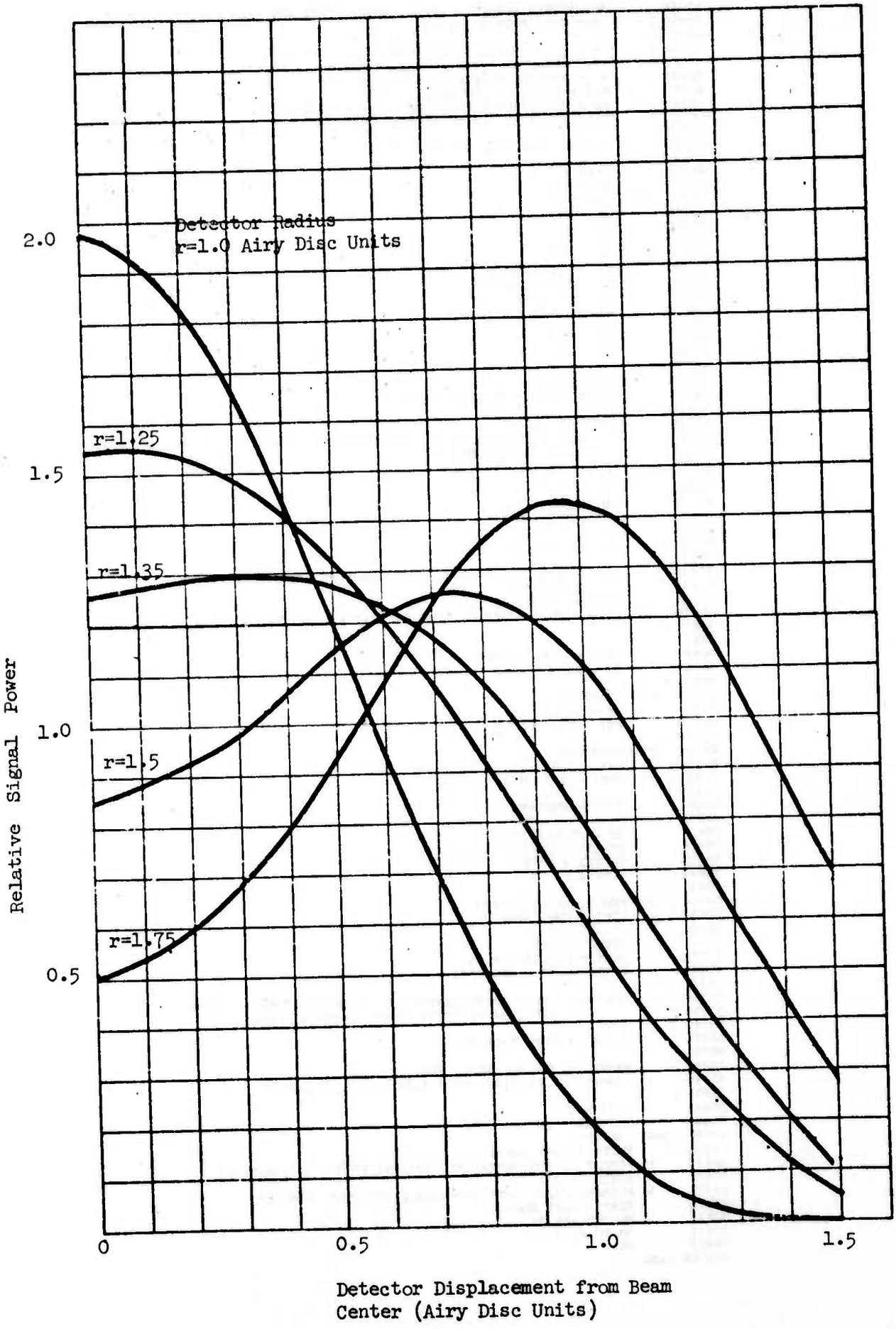

Figure 4: Signal Power in Heterodyne Detection with Beam Center Displacement

```
list
00010 C      NORMALIZED DETECTOR ENERGY WITH OFFSET WRT BEAM CENTER.
00020 C      DATA SET: DETECT FORTGI
00030 C
00050 C      RAD1 =  NORMALIZED DETECTOR RADIUS WRT 3.8317
00060 C      XD = DETECTOR OFFSET - NORMALIZED WRT 3.8317
00070 C      R  = RADIUS OF ELEMENT WRT BEAM CENTER
00080 C      PHI = ANGLE OF ELEMENT
00090 C      RX = RADIUS OF ELEMENT WRT DETECTOR CENTER
00100 C      RADJ = 3.8317 (FIRST ZERO OF J(X,1))
00110 C
00121        DOUBLE PRECISION RX, XD, RSQ, R
00130        DEL = 1.5
00140        RADJ = 3.8317
00150        RAD1 = 1.0
00151  4000 CONTINUE
00160        NP = 90
00170        NP = 50
00180        XD = 0.0
00190        DX = 0.05
00200        PHI = 1.0E-06
00210        PI = 3.141592654
00220        DELP = PI/NP
00230        DRX = RAD1 * RADJ/NP
00240        SUM1 = 0.0
00250        RX = DRX/2.0
00260        NX = DEL/DX + 2
00270 C
00290        WRITE (5,10) RAD1
00300     10 FORMAT (7X,'DETECTOR RADIUS =',F5.2/)
00310 C
00330        WRITE (5,15).
00340     15 FORMAT (7X,'DETECTOR',3X,'AMPLITUDE',5X,'AMP**2',6X, 'SIGNAL'/8X,
00350       % 'OFFSET',4X,'(NORMAL)'/)
00360        RAD1 = RAD1 * RADJ
00370        DO 1000 JX = 1, NX
00380 C
00390        XD = XD * RADJ
00400        DO 2000 JP = 1, NP
00410 C
00420        DO 3000 JR = 1, NR
00430 C
00440        RSQ = RX**2 +  XD**2 - (2.0 * RX * XD * COS(PHI))
00450        R = DSQRT(RSQ)
00460        DELS = BESJ(R,1)
00470        DELS = DELS * DRX *  DELP * RX/(R + 1.0E-06)
00471 C
00472 C
00480        SUM1 = SUM1 + DELS
00490        RX = RX + DRX
00500 C
00510  3000 CONTINUE
00520        RX = DRX/2.0
00530        PHI = PHI + DELP
00540 C
00550  2000 CONTINUE
00551        PHI = 1.0E-06
00560        SUM1 = 2 * SUM1
00570 C
00590        SUM2 = SUM1**2
00600 C
00610        XD = XD/RADJ
00620        IF (XD .GT. 0.0) GO TO 500
00630        SUMST2 = SUM2
00640        SUMST1 = SUM1
00650 C
00670   500 SUM 1 = SUM1/SUMST1
00680        SUM2 = SUM2/SUMST2
00690 C
00700        ARGUM = RAD1
00710        BES0 = BESJ(ARGUM,0)
00720        COHSIG = (1 - BES0)**2
00730 C
00740 C      COHSIG = VALUE OF THE INTENSITY OF RETURN SIGNAL OVER A
00750 C               CIRCULAR DETECTOR WHOSE RADIUS IS RAD1.
00760 C
00770        SIGNAL = SUM2 * COHSIG
00780 C
00800        WRITE (5,20) XD, SUM1, SUM2, SIGNAL
00810    20  FORMAT (7X,F6.3,4X,1PE10.3,3X,1PE9.3,3X,1PE9.3)
00820 C
00830        SUM1 = 0.0
00840        XD = XD + DX
00850  1000 CONTINUE
00860        WRITE (5,25) SUMST2
00870     25 FORMAT (/'NON-NORMALIZED INITIAL ENERGY = ',1PE9.3/)
00871        WRITE (5,30)
00872     30 FORMAT (////'INPUT NORMALIZED DETECTOR RADIUS:')
00873        READ (5,35) RAD1
00874     35 FORMAT (F6.3)
00875        GO TO 4000
00880        END
END OF DATA
```

TABLE 1: COMPUTER PROGRAM-SIGNAL POWER VARIATION IN HETERODYNE DETECTION WITH BEAM CENTER DISPLACEMENT

APPENDIX B: PROBLEMS ASSOCIATED WITH MULTIPLE REFLECTION SCAN AMPLIFIER

INTRODUCTION AND SUMMARY

The multiple reflection scan amplifier presents a possible way of amplifying the oscillations of a high frequency, small amplitude, vibrating mirror up to the magnitude required for a raster scanner in Contract N00014-72-C-0504. There are, however, four major problems which must be solved with such a scanner:

1) Heat dissipation,

2) Offset angle,

3) Aberrations, and

4) Amplification of extraneous modes in the vibrating mirrors.

The heat dissipation problem is insurmountable with a laser transmitter power of 500 watts, unless the vibrating mirrors have reflectivities of the order of 99.95 percent. This seems unlikely except in carefully controlled laboratory conditions.

Each of these four problems is very difficult and the design constraints imposed to solve one may interfere with a solution to the others. Although it may be possible, in principle, to solve any one or two of these problems, a simultaneous solution to all four seems unlikely. At the very best, a successful scan amplifier would require a lengthy, high risk development program. There are more direct methods of solving the scanning problem with much less cost and with much less risk.

BASIC CONCEPT FOR MULTIPLE REFLECTION SCAN AMPLIFIER

The basic optical structure for the scan amplifier designed and built by the Electronics Group over the period from 1966 to 1970 was, in principle, the absorption cell for spectroscopy of gases developed by J. U. White* in 1942. That basic cell, made famous by its description in Strong's "Concepts of Classical Optics", uses three spherical mirrors as shown in Figure 1. A beam of light focused on the entrance slit e is reflected back and forth through the system many times before being brought to focus on the exit slit x.

To make a scan amplifier from the White cell, it is only necessary to cause the two small mirrors on the left (M_1 and M_3) to oscillate in rotation about an axis through both mirrors lying in the plane of the paper. If this oscillation is to be at a very high frequency, the mirrors M_1 and M_2 must be quite small. A further complication arises because the beams no longer lie in the plane of the paper.

The Electronics Group design allowed the center of curvature of the two mirrors M_1 and M_3 to lie at the same point on the surface of M_2 (when the scan amplitude is zero). As a result, beams tend to walk, on successive passes, toward this center. A long slot or a strip mirror provides the exit aperture at the center.

With these four modifications:

1) Smaller mirrors M_1 and M_3
2) Common center for M_1 and M_3
3) Rotational oscillation of M_1 and M_3
4) Strip mirror for exit at center,

---

*J. U. White, J. Opt. Soc. Am. 32, p 285 (1942)

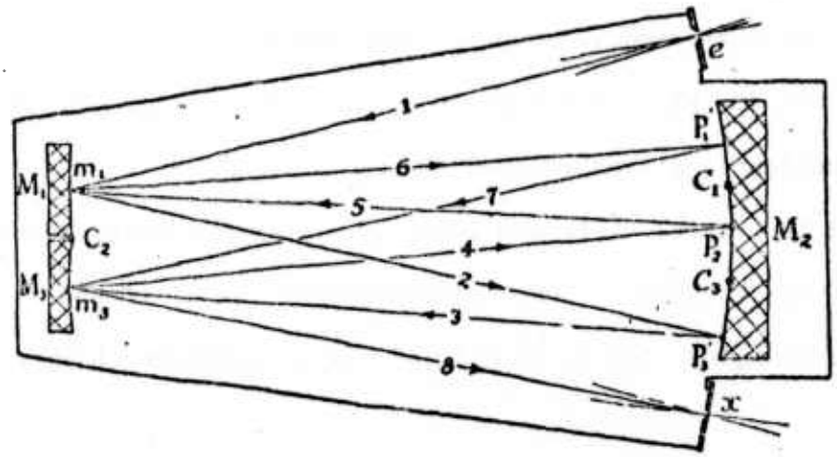
e
1
P'1
6
m1
M1
C1
5
7
M2
C2
P'2
4
2
C3
M3
m3
3
P'3
8
x

the White absorption cell becomes the Electronics Group Multiple Reflection Beam Scanner (MRBS).

GENERAL LIMITATIONS

By causing a beam to reflect several times from the same moving mirror, or from different mirrors appropriately phased, it is possible to cause the angular scan rates for the several reflections to add. At the same time, the total scan angle or amplitude is correspondingly increased. Consequently, a multiple reflection system can amplify angular scan rate and amplitude. It cannot, however, increase the scan frequency or cycling rate.

The inability of the scan amplifier to increase the scan frequency is a serious limitation. In the Phase I report on Contract No. N00014-72-C-0504, Line Array Imaging Techniques, it was pointed out on pages 28 and 29 that a beam can be redirected to several different faces of a rotating multifaceted mirror to obtain scan amplification. This is exceedingly useful if one desires to increase scan angles, but is no help at all in obtaining higher cycling frequencies.

The scan amplifier can help only if there is available a very high frequency system which is limited in angle below the scan angle desired. Devices with such high frequencies are tuning forks, piezo-electric blocks operating in the shear mode, and a few specially designed torsion bar suspension mirrors.

Invariably, mirrors oscillating at frequencies of the order of ten KHz are constrained to small size and small amplitude. For mirrors more than 1 cm across, the acceleration forces induce vibrations in the face of the mirror which cause distortions and deflections comparable to the primary deflection. Any attempt to enhance the primary deflection by multiple reflection will correspondingly increase distortions and deflections from these unwanted vibration modes.

MAJOR PROBLEMS WITH THE SCAN AMPLIFIER

The MRBS Scan Amplifier has four major problems when applied to the present laser radar problem. These are:

1) Heating of scanning mirrors due to multiple absorption;

2) Offset angle of return radar signal;

3) Additive aberrations due to off-axis focusing; and

4) Amplification of distortions due to extraneous vibration modes in scanning mirrors.

The first of these would appear to pose an almost insurmountable problem. The small high-frequency vibrating mirrors cannot be readily designed for heat dissipation when so much attention must be applied to designing for single mode vibration. The more one sacrifices in the vibrator design to achieve good heat dissipation, the greater the probability that problem #4 will prevent useful operation.

The aberration problem is difficult or impossible to calculate without selecting a specific design and doing a complete ray tracing computation. Even if the design succeeds in making aberrations on successive reflections cancel in part, the problem is not negligible.

The offset angle of the returned beam poses a serious problem in that the offset angle depends in a complicated way on the range and the point in the scan cycle which the target is reached. The resonant scanners are sinusoidal in time.

Each of these problems is discussed in more detail below.

POWER HANDLING PROBLEMS

Power handling problems arise at two critical points in the scan amplifier: on the small vibrating mirrors and at the first reflection from the large mirror. The vibrating mirror surfaces pose a problem because on each of the many reflections the absorption losses are additive. The first reflection from the large mirror is critical because the beam comes to a focus on that mirror and after only one reflection, the scan angle is only a few milliradians so that absorption losses are concentrated on an extremely small area of the large mirror.

The vibrating mirrors are of the order of one centimeter or less. Twenty-five reflections from each mirror would not be unreasonable. Even with mirrors having only a few tenths of one percent absorption, about five percent of the input power would be absorbed on each vibrating mirror. This requires heat dissipation of 0.05 P watts from the mirror surface of less than one square centimeter, where P is the laser power. This is 25 watts for a laser power P of 500 watts.

The laser spot size on the large mirror is approximately $(\frac{2.4 \lambda R}{w})$ where R is the radius of curvature of the mirrors, λ is the wavelength and w is the size of the small mirrors. After the first reflection from the scanning mirror the beam will be moving through an angle about twice the diffraction angle. Therefore, the laser beam will be focused on and scanned over a small area about $(\frac{5 \lambda R}{w})$ in diameter. If the absorption on reflection is two-tenths of one percent, then $(2 \times 10^{-3} P)$ watts will be dissipated in this small area. If the laser radar transmitter power is 500 watts, the vibrating mirrors are one centimeter wide (w = 1) and the radius of curvature is 30 cms, then the

hot spot on the large retroreflecting mirror must dissipate one watt from a spot about three square millimeters in size.

The vibrating mirror poses the more troublesome problem. Those mirrors must be designed optimally for vibration at frequencies of the order of 10^4 Hz. This does not allow the use of extensive cooling apparatus required to dissipate the 25 watts discussed above. If the vibrating mirror were a one cm cube of piezoelectric material with one surface bonded to an ambient heat sink while vibrating in a shear mode, the front surface temperature would be nearly two thousand degrees centigrade.

If the vibrating mirror were the end of a vibrating rod (tuning fork) with the other end bonded to an ambient heat sink, its dimensions would be approximately (2.5 cm x 0.7 cm x 0.7 cm) and its front surface temperature would be about two hundred degrees centigrade.

Although it is possible to design mirrors with less than two-tenths of one percent absorption at ten microns wavelength, such low absorptions can be maintained only under ideal laboratory conditions. Conditions in field equipment will involve mirrors with even higher absorption.

ABERRATIONS

The bundle of rays entering through the entrance aperture fills the mirror M_1. Ideally, the bundle would be brought to a focus again on the surface of M_2 at a point on the other side of the center of curvature of M_1 from the entrance aperture. Unfortunately, a spherical mirror will not focus perfectly a bundle of off-axis rays and the new focus (ignoring diffraction) will not be a point. It will have a size of the order of $w\left(\frac{L}{R}\right)^2$, where w is the size of the illuminated spot on M_1, R is the radius of curvature of M_1 and L

is the distance from the entrance aperture to the center of curvature of M_3. If the system is properly designed, some of this aberration will be cancelled by the next reflection from M_3. However, perfect cancellation is not possible and a gradual accumulation of the aberrations will prevent the bundle exiting the system from being a perfect spherical wave. These aberrations will lead to a focal spot size a few times larger than $w\left(\frac{L}{R}\right)^2$. This must be small compared to the diffraction-limited spot size $\left(\frac{2.4\ \lambda\ R}{w}\right)$ if aberrations are to be no problem.

The resulting criterion is

$$g\ \frac{2.4\ \lambda\ R^3}{w^2\ L^2} \gg 1$$

where the factor g is an unknown number which measures the accumulation of aberrations after the many reflections in the scan amplifier. If one notes that (L/R) must be about equal to the scan angle which is one hundred times the diffraction angle, this criterion reduces to

$$g\ R \gg 4\ \text{cm}$$

which is not unreasonable if g is small. This would be the case if the sequential aberrations tend to cancel rather than accumulate. But g could be as large as the number of reflections in the MRBS.

It should be emphasized however that the calculations carried out here are at best approximate and a true measure of the aberrations could be determined only by extensive ray tracing techniques with specific geometries.

OSCILLATING MIRROR DISTORTIONS

As pointed out in the discussion of general limitations on scan amplifiers, the oscillating mirrors must have a frequency as high as that desired. Only the amplitude and angular rate are amplified.

The problem of oscillating a mirror at ten thousand cycles per second is not trivial even if the mirror is small and one accepts a sinusoidal scan of small amplitude. Three methods that have been successfully used are:

1) Piezoelectric cube in a shear mode;

2) End of tuning fork; and

3) Mirror on torsion bar.

Each of these must be very carefully designed so that the desired mode can be driven without exciting any other mode. In addition to weak coupling between the modes, it is important that the preferred mode be the lowest frequency vibration mode of the system. Parametric down-conversion to drive lower modes is usually easier than up-conversion.

Bulova makes a resonant torsion bar with one end clamped and the other free but loaded with a small mirror. Very little power is required to drive and sustain the resonant mode. However, lateral bending vibrations of the torsion bar can easily be induced by any imbalance of the mirror or any asymmetry in the drive. The mirror is quite small (about 0.6 cm) and the amplitude is small (a few degrees) because the mirror is driven along its center line and bending modes in the mirror itself can be excited.

Tuning forks are merely bars with one end clamped and the other free in which bending modes are excited. The two-pronged fork is used with out-of-phase vibrations in the prongs so that their forces on the base (clamped end)

cancel. The bending modes of clamped-free bars are well understood and the analyses of Lord Rayleigh are still adequate. He gave the approximate formula that frequency in Hertz is given by

$$85{,}000\ t/\ell^2$$

where t is the thickness of a rectangular iron bar and ℓ is its length (in cm). This is still a good approximation except that the coefficient can be varied considerably either way with modern alloys. A clamped-free bar has two bending modes orthogonal to one another. In the tuning fork, this degeneracy is lifted by the interaction of the two prongs. Even so, the slightest excitation of the other mode will be amplified by the multiple reflections to sizable distortion of the scan patterns.

The shear cubes developed by the Electronics Group are by no means free of undesirable extraneous modes. A properly cut piezoelectric crystal can, in principle, have no other modes coupled to the shear mode. But the slightest imperfection in the cut angles causes coupling. Again these undesirable modes are amplified by multiple reflection.

The heating problems described in a previous section cause distortions of the geometry of the vibrators so that coupling between modes change. This can cause a nearly perfect oscillator to go bad, in that undesirable modes are excited when the thermal gradients build up.

OFFSET ANGLE DUE TO SIGNAL TRANSIT TIME

As discussed in the earlier report on scanners, the return signal from the target finds the scanner at a new angle, offset by an amount

$$\Delta\theta = \int_0^{\frac{2R}{C}} \dot{\theta}\,(t)\,dt$$

where R is the range to the target, C is the velocity of light and $\dot{\theta}$ is the angular scan rate which is a function of the time t. Since most high-frequency scanners run in a resonant sinusoidal mode, $\dot{\theta}$ will be approximately sin $(2\pi \nu t)$.

For a target at a range of 20 kilometers and a scanner with an angular rate of 10^6 resolution elements per second, the offset angle is about 120 resolution elements. This corresponds to more than one full line of scan. The difficulty arises when the return signal tries to find a multiple reflection path back through the scan amplifier. The mirrors are at a different angle than when the signal went out in that direction so there is no simple reversibility of path argument. If the scanner is geometrically perfect, and not just fine tuned so that errors cancel on the paths of outgoing beams, the return beam will find its way back through the scan amplifier and come out at an angle offset from the entering transmitted beam.

With slower single reflection scanners, this offset can be compensated so that the signal hits the single element detector. This is done by separating the signal from the transmitted beam and passing it through a second scanner with the phase offset an amount corresponding to the range. Unfortunately, that scanner must be identical to the original scanner. It is by no means certain that two identical scan amplifiers can be built. They are designed and constructed as nearly as possible to optimum, but adjustments are made to fine tune for maximum scan angle and minimum loss. This may change the optical path and the number of reflections considerably, and when applied to two separate scan amplifiers may cause them to deviate from a matched pair. Again the problem is not insurmountable but poses great difficulty and uncertainty.

CONCLUSIONS

The multiple reflection scan amplifier has four major problems:

1) Heat dissipation;

2) Offset angle;

3) Aberrations; and

4) Amplification of extraneous modes in the vibrating mirrors.

Although it might be possible in principle to solve any one of these for a single system by elaborate design and engineering, solving all four simultaneously seems unlikely. The heat dissipation problem in particular seems prohibitive. In any case, a successful design would require a lengthy, high risk development program. There are more direct methods of solving the scanning problem at much less cost with much less risk.

APPENDIX C: MULTIPLE REFLECTION SCAN AMPLIFIER DEVELOPED UNDER CONTRACT

To the best of our knowledge, the idea of scan amplification was first conceived within Rockwell International Corporation before 1966 and was developed under contract with the Navy (Contract No. N61339-66-C-0147). The breadboard device developed was then called Multiple Reflection Beam Steerer (MRBS). (The final report, Lasers for Training Devices, dated October 1970, is identified by the Rockwell International Report No. C70-1310/301.)

The MRBS is a device that utilizes repetitive reflections from two active deflection elements to increase the total number of resolution elements available in a scan. As can be seen in Figure 1, this is accomplished by placing scanning mirrors at conjugate focal points of a large, spherical mirror. The conjugate foci permit the laser beam to be successively reflected in an alternating manner to the scanning mirrors, transferring an additional increment of deflection to the beam at each reflection from the scanning mirrors. The active scanning elements consist of two small piezo-electric shear cubes with 3/16 inch diameter spherical mirrors attached. Vertical scanning is accomplished by the use of a d'Arsonval galvanometer to drive a flat mirror. Special driving circuitry was used to generate a 60 Hz linear scan with a flyback time on the order of 1 millisecond.

Under the contract, the breadboard display system was fabricated using the MRBS as a horizontal scanner. Its performance, however, was found to be deficient in image quality, and the scanning was objectionably non-linear. A technique was subsequently devised that solved the linearity problem by increasing the time available for retrace. This, however, caused a reduction in vertical resolution, but made it possible to obtain a reasonably good image.

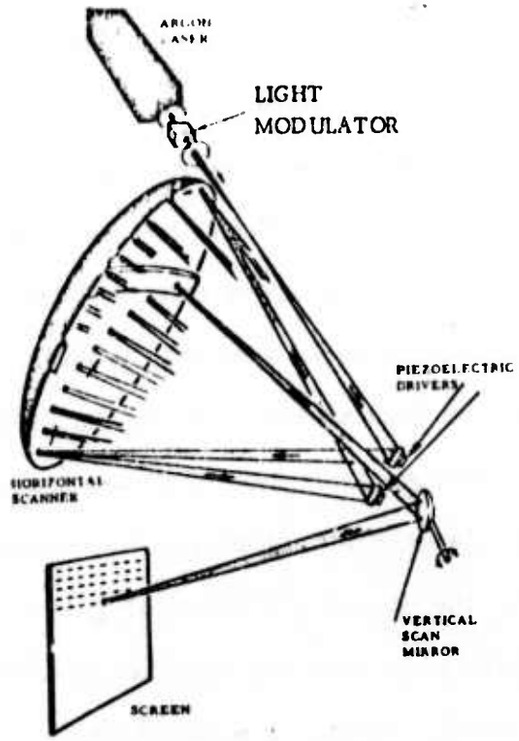

Figure 1. Multiple Reflection Beam Steerer (MRBS)/Vertical Scan

The MRBS consists of a main mirror, two small motor mirrors, and a strip mirror called the extractor. All have the same radius of curvature. The diameter of the main mirror is 4 inches, that of the motor mirrors is 3/16 inch, and the extractor mirror is 1/4 inch wide. Figure 2 is an optical diagram of the system. The laser beam is focused initially by a lens, L1, to a point, S, in space located just to the side of the main mirror, in the same geometric surface as the main mirror figure. The light diverges from this point to the first motor mirror, M1, which reflects it to and focuses it on the main mirror at a point, 1, located approximately as far from the main mirror center as the first focus, S. The main mirror then reflects the light to the second motor mirror, M2, which again returns it to and focuses it on the main mirror, this time to a point 2, just inside the original focus. The light continues to "walk" across the main mirror in this fashion, being displaced by the same increment each time it reflects through the system, until it falls on the extractor. The function of the extractor, as the name implies, is simply to remove the light from the system. It is normally tilted back slightly so that the emergent beam will pass over the motor mirrors. Since the extractor has the same curvature as the other mirrors, and since the other mirrors are working with foci at or very near their centers of curvature, the exit pupil for the scanner system is located at the center of curvature of the extractor, C3.

The motor mirrors, shown in Figure 2, are displayed in push-pull configuration at one limit of their normal scanning range. After reflection from the extractor, the output energy for this scan position would follow path A. As the motors are driven back to the other limit, the spot of light on the extractor moves from end A to end B, and the output light would then

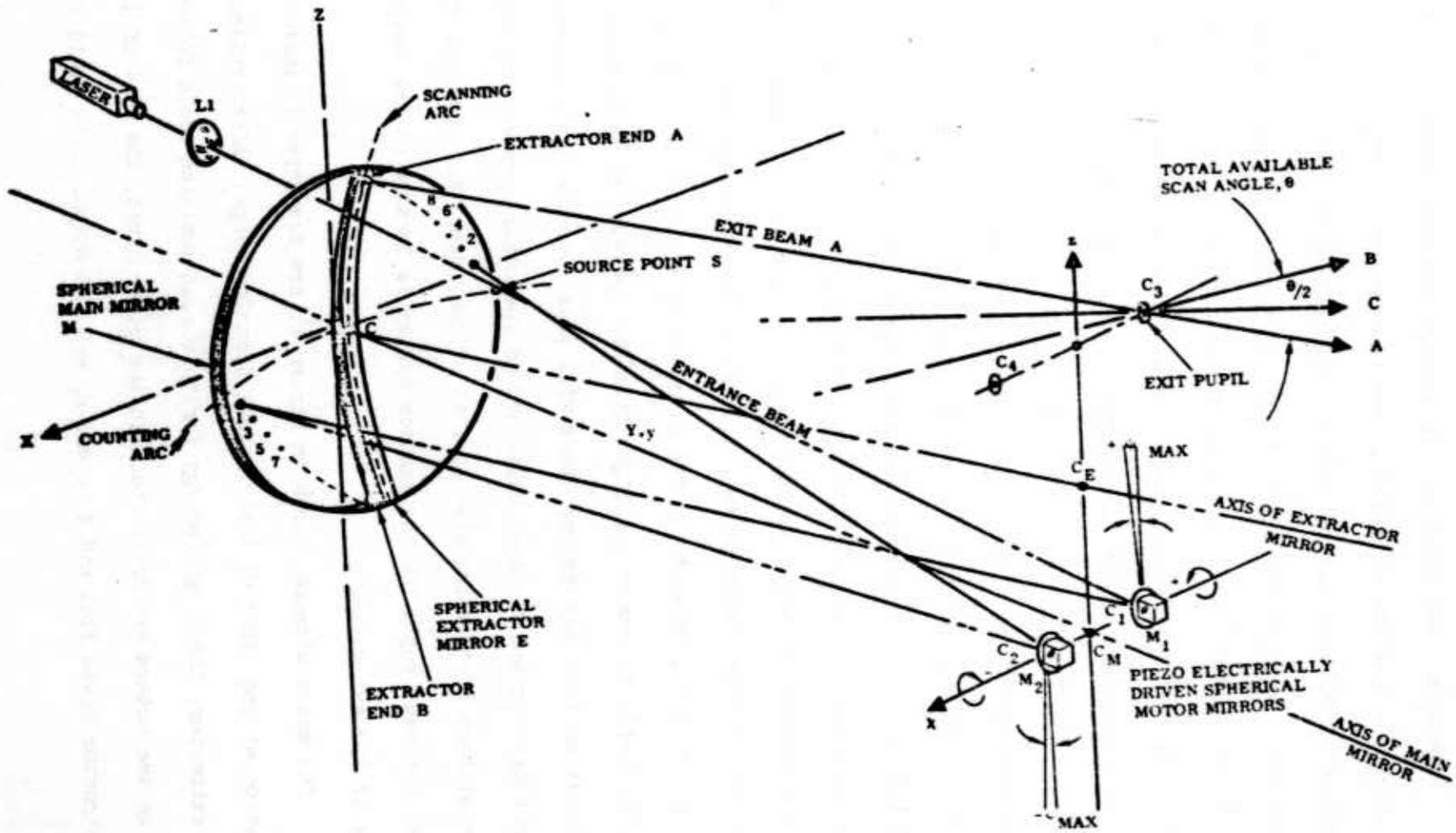

Figure 2. Multiple Reflection Beam Steerer System

follow path B out of the system. The angle between paths A and B represents the full output scan angle.

Each reflection from a motor mirror adds an additional angular increment to the output beam. Hence the angular displacement of the motor mirrors is multiplied by the number of motor mirror reflections.

The motor mirrors are bonded to 1/8 inch piezo-electric shear cubes (motors) which in turn are bonded to stainless steel mounting fixtures by conductive epoxy cement. These motor mirrors are then mounted into the MRBS assembly of the optical breadboard.

Adjustments are provided to rotate each of the motor mirrors about both the vertical and horizontal axes. The left motor-mirror (viewed from the rear) has a micrometer adjustment to provide fine adjustment of the distance to the main mirror. An adjustment is provided for varying the distance between the motor-mirror assembly and the main mirror. These adjustments are used to focus the beam during operation.

In order to obtain a linear horizontal sweep, the broadband saw-tooth approach was abandoned for a narrow bandwidth resonant system. This was found necessary due to the mechanical resonance that occurred in the piezo-electric shear cubes above 20 KHz. In this narrow band system, the shear cubes are driven with a sine wave of 7875 Hz, and every other line of video is blanked to allow the beam to return to the start of the following line. This concept, known as the alternate line scan, provides horizontal linearity with reduced vertical resolution.

The final system has a resolution of 100 spots per scan line. This is about half of what a typical consumer television receiver provides.

APPENDIX D: CONVECTIVE COOLING OF BEAMSPLITTERS FOR HIGH POWER LASER STRUCTURES

It is shown here that theoretically the beamsplitter problem for high power density systems is amenable to an engineering solution. The analysis, however, does not account for any nonuniformities in the material which could possibly result in extremely high localized heating problems resulting in material fracture or excessive beam deformation.

1. Material Choices

There are a number of candidate materials to choose from including germanium, silicon, tellurium, NaCl, KBr, AgCl, ZnSe CdTe, $Tl(Cl_x, Br_{1-x})$, GaAs and others. For reasons which include resistance to corrosion, absorption, mechanical strength, thermal conductivity, optical homogeneity and availability, we have selected as our prime candidate semi-insulating GaAs.

Gallium arsenide is an isotropic material with a band-gap of about 1.4 ev. When doped with iron or chromium, the residual carriers can be trapped into deep lying levels with an activation energy of 0.85 electron volts. J. Comly et al[1] found that the absorption of GaAs at 10.6 microns was independent of carrier concentration in the range from 10^4 to 10^9 ohm-cm. If a crystal were heated, the absorption coefficient would be slowly varying until a temperature were reached such that $\rho \simeq 10^4 \Omega$-cm. For crystals we have been investigating ($\rho_{300} \simeq 10^7 \Omega$-cm); this temperature is about 424°K or 151°C.

---

[1] J. Comly, E. Garmire and A. Yariv, J. Appl. Phys., 38, 4091 (1967).

Figure II-7 and Table II-I show the general results. $T_{critical}$ is the temperature at which "thermal runaway" would begin.

Room Temp Resistivity (ohm cm)	T_{max} Critical (deg Centigrade)
10^6	123
10^7	151
10^8	227

Table II-I. Critical Temp. VS Resistivity for Gallium Arsenide Beamsplitters

2. Heat Transfer from Windows

A good synopsis of gaseous heat transfer can be found in the American Institute of Physics Handbook, Section 2Y, "Laminar and Turbulent Flow of Gasses" by R. C. Roberts of the Naval Ordnance Laboratory. Referring to various authors, he shows that the heat transfer coefficient h is related to the thermal conductivity of the gas k and a characteristic dimension D (which depends on the case) through the "Nusselt" number K_N where

$$K_n = \frac{hD}{k} .$$

For the case of gasses inside of round tubes, an imperical relationship (which quite closely agrees with a theory due to Prandtl) can be derived which fits the data from a multitude of investigators.

This is (for air)

$$K_n = \frac{R_n^{0.778}}{39.81} ,$$

when R_n is the classical Reynolds number $\rho vD/\mu$.

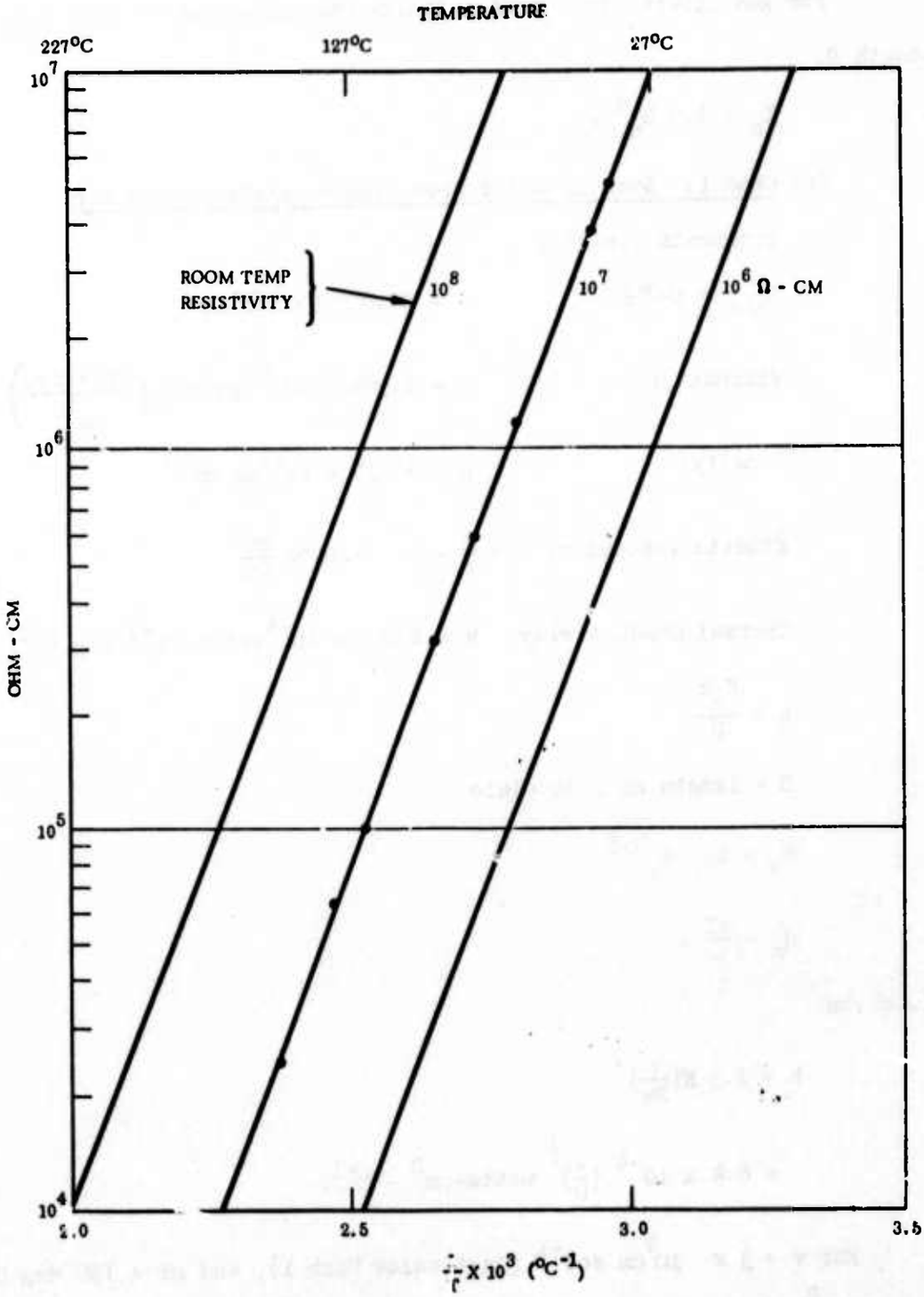

Figure II-7. Resistivity vs Temperature for Chromium-Doped GaAs Crystals

For gas flowing in a semi-infinite channel across a flat plate of length D,

$$K_n = 1.5\, R_n^{\frac{1}{2}} .$$

(a) Case I. Semi-Infinite Free Stream Constants for Air

Constants for air:

$T_{air} = 100°F = 37.8°C\ (318.8°K)$

Viscosity: $\mu = 1.904 \times 10^{-4}$ poises $\left(\frac{\text{dyne-sec}}{\text{cm}^2}\right)$

Density: $\rho = 1.135 \times 10^{-3}$ gm cm^{-3}

Kinetic Viscosity: $\nu = \frac{\mu}{\rho} = 0.1679\ \frac{\text{cm}^2}{\text{sec}}$

Thermal Conductivity: $k = 2.295 \times 10^{-4}$ watts cm^{-1} deg C^{-1}

$$h = \frac{K_n k}{D}$$

D = length of flat plate

$$K_n = 1.5\, R_n^{0.5}$$

$$R_n = \frac{vD}{\nu} .$$

This gives

$$h = 1.5\, K\left(\frac{v}{D\nu}\right)^{\frac{1}{2}}$$

$$= 8.4 \times 10^{-4} \left(\frac{v}{D}\right)^{\frac{1}{2}} \text{ watts-cm}^2\text{-°C}^{-1}.$$

For $v = 3 \times 10^4$ cm sec^{-1} (just below Mach 1), and $\Delta T = 190$ deg C ($\rho_{GaAs} = 10^8$ Ω-cm Room), and a 6-centimeter window, the heat power taken away by the gas $p_h = h\Delta T = 11.3$ watts cm^{-2}. For a GaAs window T cm thick, this would take care of the heat (ignoring conduction to the frame) from a beam

of density ($\alpha = 0.006\ cm^{-1}$).

$$p_b = \frac{p_h}{\alpha T}$$

$$= 1900\ watts/cm^2.$$

A better way to do it is shown in Case II.

(b) Case II. Thin Sheet Flow (see Figure II-8)

The "hydraulic diameter" for this case in Figure II-8 is

$$D_e = \frac{2DW}{W-D}.$$

However, if $D \ll W$ this becomes $D_e = 2D$. (W is the dimension of the channel into the paper.)

Using

$$K_n = \frac{R_n^{0.778}}{39.81}$$

and D = 0.025 cm, v = 335 meters/sec, with air as the fluid,

$$R_n = \frac{vD_e}{\nu} = \frac{2vD}{\nu} = 1.0 \times 10^4.$$

The corresponding value of $K_n = 32.5$. This gives a value of

$$h = \frac{kK_n}{D} = 0.298\ watts\ cm^{-2}\ {}^{\circ}C^{-1}.$$

(c) Comparison with Experiment

A block of copper was produced with a thin (0.010 inch) slot through it, through which air could be forced (see Figure II-9). A resistance heater was attached thermally to the block. The experiment consisted of running air through the block and reading steady-state temperatures as a function of the heater off and on. The heat transfer coefficient h is defined by the equation

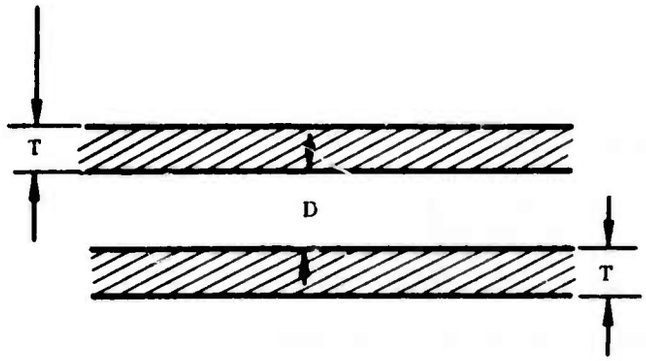

Figure II-8. Case II, Thin Sheet Flow

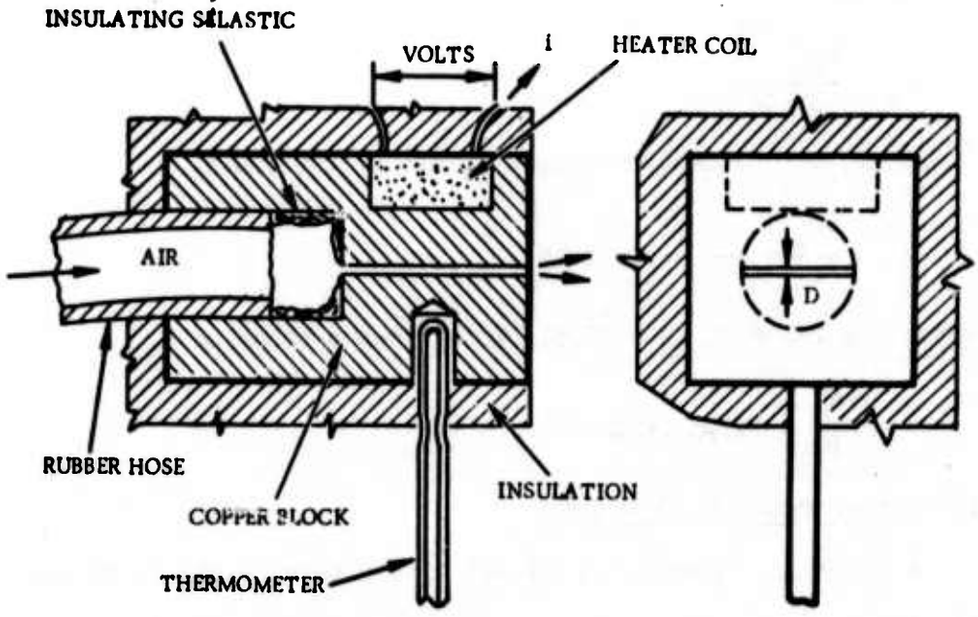

Figure II-9. Experimental Arrangement

$$h = \frac{P}{A\Delta T}$$

here P is the heat power, A the area of the heat transfer interface and ΔT the difference in temperature across the boundary.

Using air as the cooling medium, Figure II-10 shows the flow velocity vs gage pressure applied for a channel 0.010 inch thick, 1 inch long, and 0.5 inches wide. (The flow was measured experimentally.) Table II-II lists the results.

Flow Velocity $\frac{\text{meter}}{\text{sec}}$	Reynolds Number	Experimental h $\frac{\text{watts}}{\text{cm}^2\,^\circ\text{C}}$	Calculated h $\frac{\text{watts}}{\text{cm}^2\,^\circ\text{C}}$
300	8.8×10^3	0.194	0.230
340	1.0×10^4	0.242	0.298

Table II-II. Flow Measurement Results

3. Conclusions

The thin channel case can, for a temperature differential of 190°C take away (190)(0.242) = 46 watts per cm^2 vs the 11.3 watts/cm^2 for free-stream flow past the window. The resulting power capacity of the 1-cm thick window then comes up to 7660 watts per cm^2 of beam power, ignoring heat transfer by conduction altogether.

For a 10 cm diameter beam incident at Brewster's angle on a GaAs beam-splitter, the heat transfer area A_L is given by

$$A_L \sin\left(\frac{\pi}{2} - \theta_B\right) = A_b$$

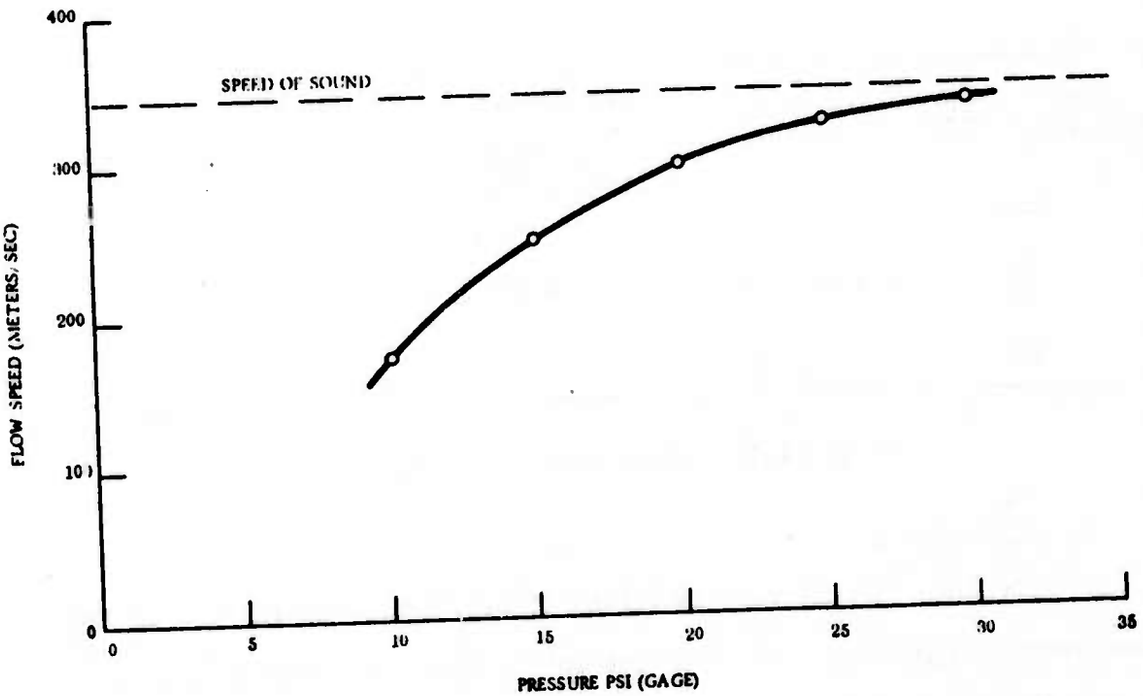

Figure II-10. Air Flow vs Pressure Applied

where A_b is the beam area and θ_B is Brewster's angle. Thus

$$A_L = \frac{A_b}{\cos \theta_b} = \frac{A_b}{\cos \tan^{-1} n}$$

$$= A_b \sqrt{n^2 + 1}$$

$$= \frac{\pi(10)^2}{4} \sqrt{(3.3)^2 + 1}$$

$$= 271 \text{ cm}^2.$$

The total power which could be transmitted would then be

$$(7660)(271) = 2.08 \times 10^6 \text{ watts}$$

which should be enough for many applications.